



Influence of a Wall-Embedded Phononic Crystal on Tollmien-Schlichting Waves

by

Angka Bayu Putranto - 4538811

A Master's thesis submitted to Delft University of Technology

Track - Aerodynamics and Wind Energy
Faculty of Aerospace Engineering

Under the supervisions of

Dr. ir. Marios Kotsonis and Dr. ir. Theodoros Michelis

Date of Defence: 17th of December 2021

Contents

Preface	iii
List of Figures	iv
List of Tables	ix
Abbreviations	x
Symbols	xi
Abstract	xiii
1 Introduction	1
2 Literature study	3
2.1 Flow transition	3
2.2 Acoustic metamaterials	10
2.2.1 Helmholtz resonator type	10
2.2.2 Membrane type	20
2.2.3 Phononic crystal (PC)	25
2.2.3.1 Motivation for the use of phononic crystal	26
2.2.3.2 Methods for phononic crystal analysis	28
2.2.4 Choice of metamaterial	34
3 Methodology	37
3.1 Design of simulation conditions	37
3.2 Design of the phononic crystal	41
3.2.1 Dispersion relation of the phononic crystal	42
3.2.2 Band gap eigenfrequency of the phononic crystal	47
3.2.3 Chosen design of the phononic crystal's unit cell	51
3.3 Simulation method	53
3.3.1 Structural analysis simulation	53
3.3.2 Steady-State Fluid-Structure Interaction (FSI) simulation	55
3.3.3 Frequency Domain Fluid-Structure Interaction (FSI) Simulation	56
3.4 Verification and Validation	58
3.4.1 Verification	58
3.4.2 Validation	59

4	Results and Discussions	60
4.1	Structural Analysis Simulation	60
4.1.1	Set-up of the Structural Analysis Simulation	60
4.1.2	Effect of boundary conditions on eigenfrequencies	61
4.1.3	Comparison of frequency domain surface displacement	63
4.2	Steady-State Fluid-Structure Interaction (FSI) Simulation	65
4.2.1	Set-up of the Steady-State FSI Simulation	66
4.2.2	Results of the Steady-State FSI Simulation	68
4.3	Frequency Domain Fluid-Structure Interaction (FSI) Simulation	70
4.3.1	Set-up of the Frequency Domain FSI Simulation	70
4.3.2	Results of the Frequency Domain FSI Simulation	71
4.3.2.1	Overall quantities	72
4.3.2.2	x -varying quantities	76
4.3.2.3	Summary and further remarks	81
5	Conclusions and Recommendations	84
5.1	Conclusions	84
5.2	Recommendations	87
	Appendix A	88
	Appendix B	89
	Appendix C	90
	Appendix D	91
	Appendix E	92
	Bibliography	95

Preface

We begin with Allah's name (The One God), The Most Compassionate, The Most Merciful. We praise him as he is the Lord of the universe. We pray for peace and blessings on all of his messengers, and in particular for the last prophet: Prophet Muhammad, and for his families and companions.

We live in a time where injustice dominates the world, presenting itself as justice. It is most certainly the world order of the one-eyed *Al-Masih Ad-Dajjal* (others are familiar with the name Anti-Christ), as implied by The Qur'an and by the prophecies of Prophet Muhammad (may peace and blessings be upon him). It is such a dangerous time that every single prophet heave prophesied about this one-eyed entity (hence, no doubt the pious Jews and Christians who follow The Torah and The Gospel are aware of this subject). Yet, hope is there (as hope is always there before what is decreed arrives) for those who are faithful and righteous in deeds, as the ending of this world order ultimately starts when Nabi 'Isa, *Al-Masih* (others know him as Jesus, the Christ) (may peace be upon him) kills the one-eyed *Al-Masih Ad-Dajjal*.

However, several other things must occur before that can happen. Indeed, we are living in a time of *transition*, where the stage of history is changing. Just like how the stage of history was changing during the period between World War I and World War II.

On a lighter note, the topic of my thesis is also on transition. However, it is on the transition of flows, as flows turn from laminar to turbulent. I came to the realization of the importance of transition towards the end of my thesis. As I reflect upon my choice, I did have interest in other thesis topics in mind (dealing with modeling of turbulence and propeller-wing interactions). The final choice on transition was purely coincidental, which perhaps also allows me to begin with such an introduction.

I would like to use this chance to say that I am truly impressed at how vast the subject of aerodynamics is. Different practical cases need to be considered in their own: flows over a wing, over a rotor, in a wind tunnel, jet flows, etc. (not to aeroelasticity and aeroacoustics); each with their own simplifications and methods of analysis. My thesis could only touch upon only a little from this very vast subject.

Moving on, we are living in such an interesting time that I am completing my thesis fully away from campus. This came into being when my plans on coming back to the Netherlands were cancelled. I only met with my supervisors once before the beginning of my thesis. This also resulted in me having to change the nature of the thesis.

While I tried maximizing interaction with my supervisors with regular online meetings, ultimately the experience of physical meetings cannot be replaced by virtual meetings. It is to my regret that I cannot have the joy of having more interactive discussions with my supervisors, formally or informally. It seems that this is once-in-a-lifetime opportunity taken away. Though at the end, I always believe that things are always for the better. Nevertheless, my supervisors were very kind and helpful in facilitating my thesis within this situation. Hence, appreciation comes from the bottom of my heart for Dr. ir. Marios Kotsonis and Dr. ir. Theodoros Michelis. Perhaps I may meet them again in the future on a different occasion.

It is always a nice thing to look back at the roads that I have crossed in reaching this stage of time, completing this thesis work. Ultimately this is the highest point of my education at the time of writing. I should not forget the educations that I have received throughout my life, from my time in Jakarta, Balikpapan, and a major change in my life as I went to Paris, and finally, my time in Delft. I would like to thank all of my teachers for all the knowledge that they have taught me. I would also like to use this opportunity to thank my family, as always.

I pray that any knowledge obtained from this thesis work may prove to be useful for the good of things.

Angka Bayu Putranto

South Tangerang, Indonesia

Jummadil-Awwal, 1443 or December, 2021

List of Figures

2.1	The different phases of flow transition, illustrated for a flow over a flat plate (figure from [34])	4
2.2	Example of a stability diagram comparing the result from O-S equation (solid line), experimental data (white circles) and lower branch of asymptotic theory (dashed and dotted lines)[26]. The experimental data was obtained from [51].	7
2.3	Comparison between experimental (square[55] and circles[51]) and theoretical neutral curves. Figure from reference [53]. In the figure, F is a dimensionless frequency and R is the Reynolds number.	8
2.4	Comparison of non-dimensionalized basic and disturbance velocity profile between OS equation and experimental data for flow over a flat plate. Figure from [48], and the data is from [49].	9
2.5	Ultrasonic metamaterial studied in reference [15]. Figure adapted from the same reference	11
2.6	Plot of E_{eff} as a function of sound frequency. Figure adapted from [15]	12
2.7	Theoretical and experimental dispersion curves of the HR type metamaterial studied in [15]. Figure adapted from the same reference	12
2.8	Transmission spectrum of the metamaterial studied in reference [15]. Figure adapted from the same reference.	13
2.9	Geometry of the HR-grafted tunnel studied in reference [59]	13
2.10	Geometry of a single and a series of HRs studied in reference [66]	15
2.11	Experimental set-up studied in reference [16] for a single HR	16
2.12	Transmission spectra of the experimental (a) and analytical formulation (b) studied in reference [16]	16
2.13	Experimental set-up (a) and transmission spectrum (b) of the HR array studied in reference [41]	17
2.14	Comparison of analytically and numerically predicted resonance frequencies in reference [41]	17
2.15	Geometry of the HR studied in reference [24]; (a) unit cell, (b) inductor-capacitor circuit analogy and (c) array of HRs. Here, two necks can be seen in the unit cell	18
2.16	Band structure of the HR array studied in reference [24]	18
2.17	Transmission spectrum of the HR array studied in reference [24]	18
2.18	Geometry of the HR series studied in reference [39]	19
2.19	Transmission loss spectrum of the HR series filled with air and water, studied in reference [39]	19
2.20	Experimental (top) and numerical (bottom) transmission spectrum of the membrane metamaterial studied in reference [70]	21
2.21	Effective mass of the membrane type metamaterial studied in reference [70]	21

2.22	Transmission spectrum of a single and panel membrane-type metamaterial (top) and displacement amplitude profile at the transmission dip frequency (bottom) of reference [69]	22
2.23	Transmission spectrum of different panels of membrane-type metamaterial [69]	22
2.24	Dynamic responses at transmission dip frequency of the membrane metamaterial studied in reference [46]. (a): at the centre of the structure and (b): 0.8 mm from the centre	23
2.25	(a) Sample A and (b) its absorption spectrum for the metamaterial studied in reference [43] (figure adapted from the reference)	23
2.26	(a) Sample B and (b) its absorption spectrum for the metamaterial studied in reference [43] (figure adapted from the reference)	23
2.27	Metamaterial configuration studied in reference [2] (figure adapted from the reference)	24
2.28	Numerically (top) and experimentally (bottom) obtained transmission spectrum of the metamaterial studied in reference [2] (figure adapted from the reference)	24
2.29	An example of a one-dimensional phononic crystal. In this example, there are four repeating unit cells where a unit cell is composed of two layers of different materials. The layer material may be solid or fluid.	26
2.30	Geometry of PC-embedded channel flow studied in reference [30] (figure adapted from the reference)	27
2.31	Development of disturbance flow kinetic energy along the streamwise direction [30] (figure adapted from the reference)	27
2.32	Transmission spectra of phononic crystal structures with different number of unit cells (defined as the maximum displacement at the opposite end of the applied force). The darker area shows the band gaps of the unit cell, as predicted by transfer matrix method. [31]	31
2.33	Natural frequencies of a one-dimensional phononic crystal structure, fixed at one end (given by the + symbol) [31]	32
2.34	Sample of the phononic crystal studied in reference [28], also showing the experimental set-up	32
2.35	Experimentally (a) and numerically (b) obtained transmission spectra of a phononic crystal studied in reference [28]	32
2.36	Phononic crystal structure studied in reference [21]. The unit cell (figure (a)) was used to find the band structure/dispersion relation, while the finite structure (figure (b)) was used to perform the frequency response study	33
2.37	Band structure (a), transmission (b), reflection (c) and surface-to-bulk losses spectra of the phononic crystal studied in reference [21]. The resulting spectra for the phononic crystal structure are given by the blue curves.	33
2.38	Sample of the phononic crystal studied in reference [22]	34
2.39	Experimentally (circles) and numerically (solid lines) obtained dispersion relation of the phononic crystal studied in reference [22]	34
3.1	Sketch of the FSI simulation set-up (not to scale). The rigid structure represents fixed boundary conditions	38
3.2	Stability diagram generated using the Orr-Sommerfeld equation for $V_\infty = 20$ m/s. A TS wave which have a combination of frequency and position within the "thumb-like" curve is unstable (in other words, the imaginary part of its wavenumber is negative).	39

3.3	Wavelength of TS wave (λ_{TS}) over the streamwise direction (x) for $V_\infty = 20 \text{ m/s}$ and $f_{\text{TS}} = 300 \text{ Hz}$	40
3.4	Geometry of the PC	42
3.5	Design space of the two-layer unit cell phononic crystal	52
3.6	Design space of the three-layer unit cell phononic crystal	52
3.7	Dispersion curve of the two layer design (44 mm rubber and 6 mm aluminium)	53
3.8	Dispersion curve of the three layer design (35 mm rubber, 3 mm aluminium and 5 mm steel)	53
4.1	Geometry of the two-layer one unit cell phononic crystal	61
4.2	Mesh of the two-layer one unit cell phononic crystal design	61
4.3	An example of bulk (left) and surface mode (right) of phononic crystal. (Three-layer unit cell design, $N_{\text{UC}} = 5$ and BC2 was used). The colored geometry represents the deformed configuration.	62
4.4	$\langle \phi_{u_y} \rangle$ for the three-layer unit cell, $N_{\text{UC}} = 5$ phononic crystal design	65
4.5	$\langle \tilde{u}_y \rangle$ for the three-layer unit cell, $N_{\text{UC}} = 5$ phononic crystal design	65
4.6	Geometry of the numerical simulation	66
4.7	Comparison of basic flow velocity V_x between the results obtained from (a) steady-state FSI simulation and (b) Blasius' solution.	69
4.8	Gauge pressure (Pa) near the leading edge of the flat plate.	69
4.9	Contour of the streamwise component of the velocity (V_x (m/s)) and the vertical displacement of the PC (u_y (m)).	70
4.10	Variation of ΔE_k with TS wave frequency	73
4.11	Variation of $\Delta \tilde{V}'_x$ and $\Delta \tilde{V}'_y$ with TS wave frequency	74
4.12	Overall amplitude response of the phononic crystal's x -displacement for various excitation response	75
4.13	Overall amplitude (blue curve) and phase (red curve) responses of the phononic crystal's x -displacement for various excitation response	75
4.14	$\int_0^H e_k \text{ dy}$ vs x for $f = 298$ ("in-phase"), 300.72 ("resonance") and 304 Hz ("out-of-phase") (subplot (a), (b) and (c) respectively). In each subplot, the location of the phononic crystal is given by the region shaded in magenta.	77
4.15	$\int_0^H \tilde{v}'_y \text{ dy}$ vs x for $f = 298$ ("in-phase"), 300.72 ("resonance") and 304 Hz ("out-of-phase") (subplot (a), (b) and (c) respectively). In each subplot, the location of the phononic crystal is given by the region shaded in magenta.	78
4.16	$\int_0^H \tilde{v}'_x \text{ dy}$ vs x for $f = 298$ ("in-phase"), 300.72 ("resonance") and 304 Hz ("out-of-phase") (subplot (a), (b) and (c) respectively). In each subplot, the location of the phononic crystal is given by the region shaded in magenta.	79
4.17	$\int_0^H (\tilde{v}'_x)^2 \text{ dy}$ vs x for $f = 298$ ("in-phase"), 300.72 ("resonance") and 304 Hz ("out-of-phase") (subplot (a), (b) and (c) respectively). In each subplot, the location of the phononic crystal is given by the region shaded in magenta.	80
4.18	Variation of the maximum decrease of the kinetic energy integral as a function of frequency	82
4.19	Variation of the maximum increase of the kinetic energy integral as a function of frequency	82
4.20	$\int_0^H \tilde{v}'_y \text{ dy}$ vs x for $f = 304 \text{ Hz}$ with five identical PCs	83
A.1	Narrow air gaps used to allow for displacements at the top corners of the PC in the frequency domain FSI simulation. The widths are $5 \mu\text{m}$	88

B.1	Zoomed-out view of the mesh used to perform the steady-state and frequency domain FSI simulations	89
B.2	Zoomed-in view of the mesh used to perform the steady-state and frequency domain FSI simulations. The focus is on the refinement around the leading edge ($x = 0$ m), forcing domain ($x \approx 0.185$ m) and the phononic crystal region ($x \approx 0.65$ m).	89
C.1	An example of the contour plot of $\tilde{v}'_x e^{i\phi_{v'_x}}$	90
C.2	An example of the contour plot of $\tilde{v}'_y e^{i\phi_{v'_y}}$	90
D.1	Examples of distribution of \tilde{u}_x along the top boundary of the phononic crystal. In the plot, "abs(u4)" refers to \tilde{u}_x	91
D.2	Examples of distribution of \tilde{u}_y along the top boundary of the phononic crystal. In the plot, "abs(v4)" refers to \tilde{u}_y	91
D.3	Examples of distribution of ϕ_{u_y} along the top boundary of the phononic crystal. In the plot, "arg(v4)" refers to ϕ_{u_y}	91
E.3	Profiles of V_x for $x = 2 \times 10^{-4}$ m (subfigure (a)) and $x = 0.65$ m (subfigure (b)) for the different mesh refinement levels.	93
E.4	Profiles of V_y for $x = 2 \times 10^{-4}$ m (subfigure (a)) and $x = 0.65$ m (subfigure (b)) for the different mesh refinement levels.	93
E.5	Plots of v'_x profile for the different mesh levels at $f = 298$ (a), 300.72 (b) and 304 (c) Hz.	94
E.5	Plots of v'_y profile for the different mesh levels at $f = 298$ (a), 300.72 (b) and 304 (c) Hz.	94

List of Tables

3.1	Design flow and PC conditions	41
3.2	Non-dimensional quantities of the flow condition	41
3.3	Material properties for the two and three unit cell designs	51
3.4	Two- and three-layer design unit cell properties	52
4.1	Effect of boundary conditions on f_{SM} of the different phononic crystal designs . .	63
4.2	Average negative surface displacements of the different phononic crystal designs around the corresponding $f_{SM, BC2}$	64
E.2	Mesh refinement level specifications for the steady-state and frequency domain FSI simulations.	92

Abbreviations

FEM	F inite - E lements M ethod
FSI	F luid - S tructure I nteraction
HR	H elmholtz - R esonator
IRT	I nterface R esponse T heory
PC	P hononic C rystal
PML	P erfectly - M atched L ayer
PWE	P lane- W ave E xpansion
RQ	R esearch Q uestion
TM	T ransfer - M atrix
TS (wave)	T ollmien - S chlichting (wave)

Symbols

A	Elastic wave's amplitude	[m]
α_p	Coefficient of thermal expansion	[1/K]
\mathbf{C}	Generalized stiffness tensor	[Pa]
C_p	Specific heat of air at constant pressure	[J/(Kg K)]
c	Wave's phase speed	[m/s]
D	Length of a phononic crystal's unit cell	[m]
d	Length of phononic crystal's layer	[m]
δ	Boundary layer thickness	[m]
δ^*	Boundary layer displacement thickness	[m]
E	Young's modulus	[Pa]
\mathbf{E}	Green-Lagrange strain tensor	[-]
\mathbf{F}	Deformation gradient tensor	[-]
f	Frequency	[Hz]
Φ	Linearized viscous dissipation	[Pa/s]
ϕ	Phase of a complex amplitude	[rad]
ϕ_f	Disturbance flow amplitude function	[m ² /s]
g	Green's function	
\mathbf{I}	Identity matrix	[-]
i	Imaginary number ($\sqrt{-1}$)	[-]
k	Wavenumber	[rad/m]
k_a	Thermal conductivity of air	[W/ (m K)]
l_{PC}	Length of the phononic crystal	[mm]
λ	Lame's first coefficient	[Pa]
μ	Lame's second coefficient	[Pa]
μ_a	Dynamic viscosity of air	[Pa s]
N	Number of phononic crystal's unit cell	[-]
P	Basic air pressure	[Pa]
p	Total air pressure (basic + fluctuation)	[Pa]
p'	Pressure fluctuation	[Pa]
ψ	Disturbance flow streamfunction	[m ² /s]
q	Bloch's wavenumber	[1/m]
Re	Reynold's number	[-]
ρ	Mass density	[kg/m ³]
\mathbf{S}	Second Piola-Kirchoff stress tensor	[Pa]
σ	First Piola-Kirchoff stress tensor	[Pa]

T	Temperature	[K]
\mathbf{T}	Unit cell's transfer matrix	
t	Time	[s]
τ	Cauchy's stress tensor	[Pa]
τ_v	Viscous part of the Cauchy's stress tensor for air	[Pa]
u_x, u_y	x - and y -component of the solid displacement field	[m]
V_e	Boundary layer edge velocity	[m/s]
V_∞	Freestream velocity	[m/s]
V_x, V_y	x - and y -components of the basic flow velocity	[m/s]
\mathbf{v}	Flow velocity vector	[m/s]
v_x, v_y	x - and y -components of the total flow velocity	[m/s]
v'_x, v'_y	x - and y -components of the disturbance flow velocity	[m/s]
ν_a	Kinematic viscosity of air	[m ² /s]
ν	Poisson's ratio	[-]
ω	Angular frequency	[rad/s]
w_{PC}	Width of the phononic crystal	[mm]
x	Streamwise or horizontal coordinate	[m]
y	Wall-normal or vertical coordinate	[m]
Z	Characteristic impedance	[kg m ⁴ /s]

Abstract

This thesis concerns a numerical investigation for the stabilization (delay of laminar-to-turbulent transition) of flows over a flat plate with a meta-unit of a possible metamaterial. The type of instability studied is that due to small disturbances in an incompressible, two-dimensional boundary layer. The linear growth of the disturbance in the form of a wave (also called the Tollmien-Schlichting wave) was of particular interest.

There is a newly emerging class of structures called "metamaterials" which are capable of controlling the properties of classical waves (electromagnetic/optical/acoustic). This thesis investigates whether or not one of these materials are capable of attenuating TS waves.

A literature review was conducted on three types of metamaterials, namely those based on Helmholtz-resonators, membranes structures and phononic crystals. The mechanisms for which the three aforementioned metamaterials attenuate acoustic waves are resonance, anti-resonance and Bragg's scattering respectively. Based on the likelihood of successfully achieving damping of TS waves, the phononic crystal was chosen to be further studied.

The interaction between the flow and phononic crystal was simulated in COMSOL Multiphysics® version 5.6. The flow conditions were chosen with results from the Orr-Sommerfeld equation. The phononic crystal was designed accordingly with analytical results derived from the Transfer Matrix method and Interface Response Theory. This design was verified and finalized with a Structural analysis simulation, whereby the governing equations for an isotropic solid were solved numerically.

It was found that the response of the phononic crystal was not governed by the Bragg's scattering mechanism, but rather by resonance. Very small damping of the TS wave could be found for frequencies above the resonance in the vicinity of the phononic crystal. In this frequency range, the wall-normal disturbance flow was found to increase. Consequently, to follow conservation of mass, the streamwise disturbance flow had to decrease. Overall, the decrease of the streamwise disturbance flow was more significant than its wall-normal counterpart and therefore the kinetic energy was found to decrease. Further downstream, destabilization occurs. However, it was also found that this destabilization can be shifted downstream by placing multiple phononic crystals while also enhancing stabilization.

Chapter 1

Introduction

Efficiency is key in engineering design. In the field of aerospace engineering, a well-designed aircraft should have as low drag as possible. There are various ways in which this can be achieved. One way is to have a majority of the flow over the vehicle's body parts (such as the wings) to be laminar instead of turbulent, assuming that there are no flow separations. This is because the skin friction within a laminar flow is much lower than within the turbulent counterpart [1][54]. As the skin friction decreases, the total drag of the vehicle also decreases. In turn, this translates into lower fuel consumption which further results in decrease in costs and possible environmental damages. Hence, researches in the areas of ensuring the laminarity of flows are of paramount interest.

Laminar-to-turbulent transition is of interest to various flows found in engineering, such as pipe and jet flows. In this thesis, the flow that shall be considered is the boundary layer flow.

Two different mechanisms of transition can be identified: amplification of small disturbances and bypass transition[34]. This thesis deals with the former case. Three stages can be identified within this class of transition, namely the problem of disturbance reception by the boundary layer, linear growth of the disturbances and non-linear breakdown into turbulence [34]. Of interest is the second stage, where the development of the disturbance is described by linear equations. In particular, a wave-form can be assumed in order to describe the disturbance. This wave has been observed experimentally and is also known as the Tollmien-Schlichting (TS) waves [54][67].

If one is able to control the growth of the disturbance, then one is also able to control the transition process. As the disturbance is initially in described by wave-like characteristics, this thesis aims at investigating whether or not the so-called "metamaterials" are able to affect the growth of TS waves. Metamaterials are structures that are specifically designed to alter the characteristics of propagating waves [10]. Typically, the building blocks of the metamaterials have dimensions that are much smaller than the wavelength of interest. Hence the accumulation of these building blocks give rise to effective material properties.

The wave dealt with these metamaterials have been the classical waves (i.e. electromagnetic/optic/acoustic waves)[42]. Unlike TS waves, these classical waves are not convective in nature:

they propagate even within a quiescent medium. Thus, the study of the interaction between metamaterials and TS waves would be a new subject of research.

With this in mind, the following main research question is posed:

Can TS waves in a laminar boundary layer flow be attenuated using a metamaterial?

In the above research question, the specific metamaterial to be used is not yet defined. It is to be determined with a literature study of different types of metamaterials (chapter 2). The metamaterials to be investigated are the **acoustic metamaterials** (instead of those dealing with electromagnetics or optics), as mechanical systems are being considered.

Sub-research questions are formed on the basis of the main research question and the desire to understand the physics behind the interaction between metamaterial and TS waves. These are given in the following list:

1. **What are the changes imparted on the TS waves when approaching a metamaterial unit?**
2. **What is the physical mechanism that drives the attenuation of the TS waves (if any attenuation takes place)?**
3. **How large is the attenuation (if any)? What is the sensitivity of the attenuation with respect to the TS wave's characteristics?**

This thesis aims at answering the above questions with **numerical simulations**.

Having formulated the research questions, this report is structured as follows. In chapter 2, a literature study is given on the two aspects of this thesis: stability analysis of flows and metamaterials. This chapter concludes with choosing a metamaterial type. The following chapter (chapter 3) is also divided in two parts. In the first part, conditions of the numerical simulation are chosen. This implies choosing the flow condition and designing the metamaterial, both with relatively simple methods. In the second part, the method for the numerical simulation is explained. Chapter 4 presents and discusses the results of the numerical simulation. Finally, chapter 5 gives the conclusion to this thesis in which the research questions are answered, and assesses the limitation of the current study in order to recommend improvement for the future.

While it is not yet known whether or not the chosen metamaterial is capable of damping TS waves, it is the objective of this thesis to successfully achieve stabilization.

Chapter 2

Literature study

The literature study is divided in two parts: a research on flow stability theory and acoustic metamaterials. For the study of flow stability, emphasis will be put on the "wave-like" behaviour. Unlike traditional waves which contains purely the propagation of a certain information (e.g. in the case of acoustic waves, either pressure or mass density fluctuation), the "wave-like" characteristic in the flow stability problem includes mass transfer. This shall be further corroborated in section 2.1.

The motivation for the study on acoustic metamaterials is the existence of a band gap (amongst other properties) - a range of sound wave frequencies where the sound amplitude is attenuated. The focus of the study is on understanding the mechanism for the creation of the band gaps, and the corresponding prediction methods. This shall be done in section 2.2.

This thesis investigates whether the concept of band gap of an acoustic metamaterial, which is traditionally designed for acoustic waves, could be applied to the convective waves within a flow stability problem.

2.1 Flow transition

The nature of flow can be divided into two categories: laminar and turbulent. In the case of laminar flow, the streamlines are well-ordered like layers. Patterns within the flow can be identified with ease. In the case of turbulent flow, the flow becomes chaotic. A large range of scales of eddies can be observed. This categorization of flow went back as far as the 19th century, where O. Reynolds [50] observed the flow within a pipe.

However, within a flow itself, it may be that part of the flow is laminar and the rest is turbulent. It may also be that the flow is initially laminar, and, after some changes in the flow conditions, the flow become turbulent. This change from laminar to turbulent is referred to as "transition". Two mechanisms of flow transition were identified. One deals with the transition by small disturbances, and the other looks at the transition due to large disturbances (also called "bypass") [34][45].

There are different stages that can be identified within the transition by small disturbances: the problem of receptivity/generation of instability waves from external disturbances, linear growth of the unstable waves and non-linear breakdown into turbulence[34]. This is illustrated in figure 2.1 for a flow over a flat plate.

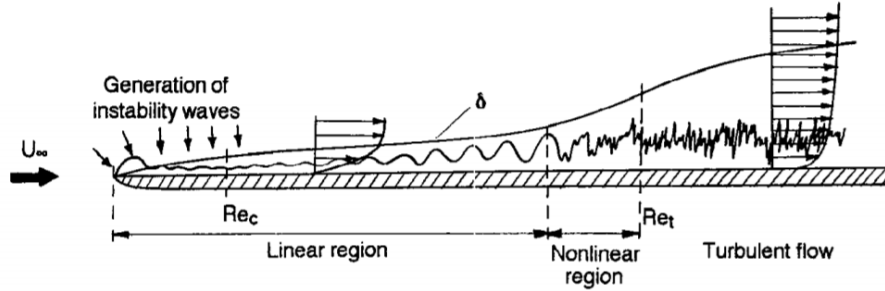


FIGURE 2.1: The different phases of flow transition, illustrated for a flow over a flat plate (figure from [34])

Hence, the initial behaviour of the small disturbances can be described with linearized equations.

Within transition due to small disturbances, different mechanisms could be observed such as two-dimensional disturbances, cross-flow disturbances (inherent in swept-wings) and supersonic disturbances [48]. This thesis treats the problem of transition by two-dimensional disturbances.

A "wave-like" behaviour can be observed within the two-dimensional disturbances, as indicated through the term "instability waves". These instability waves are also known as "Tollmien-Schlichting waves" [67] (shortened as "TS waves" in this report). However, this "wave-like" characteristic is different from traditional waves, such as acoustic or electromagnetic waves. In the instability waves in flow transition problem, the wave includes mass transfer (hence convective) whereas in traditional waves, no mass transfers occur. This can be illustrated mathematically through the Orr-Sommerfeld (OS) equation [47][57]. To further emphasize the difference between a traditional wave and an instability wave, the derivation of the OS equation shall be presented, using the steps laid down by Schlichting [54].

The OS equation assumes two-dimensional incompressible flow. Hence, the governing equations are the continuity of mass and momentum in two directions. They are given in equation 2.1a, 2.1b and 2.1c.

$$\frac{\partial v_x}{\partial x} + \frac{\partial v_y}{\partial y} = 0 \quad (2.1a)$$

$$\frac{\partial v_x}{\partial t} + v_x \frac{\partial v_x}{\partial x} + v_y \frac{\partial v_x}{\partial y} = -\frac{1}{\rho} \frac{\partial p}{\partial x} + \nu_a \left(\frac{\partial^2 v_x}{\partial x^2} + \frac{\partial^2 v_x}{\partial y^2} \right) \quad (2.1b)$$

$$\frac{\partial v_y}{\partial t} + v_x \frac{\partial v_y}{\partial x} + v_y \frac{\partial v_y}{\partial y} = -\frac{1}{\rho} \frac{\partial p}{\partial y} + \nu_a \left(\frac{\partial^2 v_y}{\partial x^2} + \frac{\partial^2 v_y}{\partial y^2} \right) \quad (2.1c)$$

where t is time, v_x and v_y are the x - and y -component of flow velocity respectively, ρ is the fluid density, p is the static pressure and ν_a is the fluid's kinematic viscosity. In this thesis, the

context of the flow problem is airflow over a flat plate. Hence, the x - and y -directions are the streamwise and wall-normal directions respectively.

Now, as mentioned before, the problem deals with transition due to small disturbances. To this end, the flow is decomposed into two parts: a (steady) basic flow solution and a disturbance component. In OS equation, the velocity of the basic flow is assumed to be parallel with no cross-flow component. This means that the basic flow is only a function of y . Thus, the total flow field is written as follows:

$$v_x = V_x(y) + v'_x(x, y, t) \quad (2.2a)$$

$$v_y = v'_y(x, y, t) \quad (2.2b)$$

$$p = P(x, y) + p'(x, y, t) \quad (2.2c)$$

where the capitalized letters denote basic flow quantities and the apostrophes represent disturbances. It is further assumed that the basic flow and the total flow field satisfy continuity and momentum equations separately. Thus, the goal is to find the equation that governs the disturbances. This can be done by firstly substituting equations 2.2a, 2.2b and 2.2c into equations 2.1a, 2.1b and 2.1c. Furthermore, any non-linear terms (i.e. multiplications of the disturbance quantities or their derivatives) are neglected. This is consistent with the assumption of small disturbances. Applying the aforementioned procedure yields:

$$\frac{\partial v'_x}{\partial x} + \frac{\partial v'_y}{\partial y} = 0 \quad (2.3a)$$

$$\frac{\partial v'_x}{\partial t} + V_x \frac{\partial v'_x}{\partial x} + v'_y \frac{\partial V_x}{\partial y} = -\frac{1}{\rho} \left(\frac{\partial P}{\partial x} + \frac{\partial p'}{\partial x} \right) + \nu_a \left(\frac{\partial^2 v'_x}{\partial x^2} + \frac{\partial^2 V_x}{\partial y^2} + \frac{\partial^2 v'_x}{\partial y^2} \right) \quad (2.3b)$$

$$\frac{\partial v'_y}{\partial t} + V_x \frac{\partial v'_y}{\partial x} = -\frac{1}{\rho} \left(\frac{\partial P}{\partial y} + \frac{\partial p}{\partial y} \right) + \nu_a \left(\frac{\partial^2 v'_x}{\partial x^2} + \frac{\partial^2 v'_y}{\partial y^2} \right) \quad (2.3c)$$

As mentioned, the basic flow also satisfies the continuity and momentum equations. Therefore the following also holds:

$$0 = -\frac{1}{\rho} \frac{\partial P}{\partial x} + \nu_a \left(\frac{\partial^2 U}{\partial y^2} \right) \quad (2.4a)$$

$$0 = -\frac{1}{\rho} \frac{\partial P}{\partial y} \quad (2.4b)$$

It is noted that in fact, the continuity equations satisfies the trivial equation $0 = 0$ and that most of the terms in the momentum equations are zero due to the assumed form of the basic flow.

Subtracting 2.4a and 2.4b from 2.3b and 2.3c results in the set of linearized disturbance equations:

$$\frac{\partial v'_x}{\partial x} + \frac{\partial v'_y}{\partial y} = 0 \quad (2.5a)$$

$$\frac{\partial v'_x}{\partial t} + V_x \frac{\partial v'_x}{\partial x} + v'_y \frac{\partial V_x}{\partial y} = -\frac{1}{\rho} \frac{\partial p'}{\partial x} + \nu_a \left(\frac{\partial^2 v'_x}{\partial x^2} + \frac{\partial^2 v'_x}{\partial y^2} \right) \quad (2.5b)$$

$$\frac{\partial v'_y}{\partial t} + V_x \frac{\partial v'_y}{\partial x} = -\frac{1}{\rho} \frac{\partial p}{\partial y} + \nu_a \left(\frac{\partial^2 v'_y}{\partial x^2} + \frac{\partial^2 v'_y}{\partial y^2} \right) \quad (2.5c)$$

Now, the wave-like nature of the disturbances can be introduced into the equations. This is done by assuming a disturbance streamfunction that has the form of a wave propagating in the x -direction, given as follows:

$$\psi(x, y, t) = \phi_f(y) e^{i(k_{\text{TS}}x - \omega_{\text{TS}}t)} \quad (2.6)$$

where ψ is the streamfunction and ϕ_f is the amplitude distribution function. Furthermore, k_{TS} and ω_{TS} are the wavenumber and angular frequency of the TS waves. With the streamfunction defined, the disturbance flow velocities can be readily obtained:

$$v'_x = \frac{\partial \psi}{\partial y} = \frac{d\phi_f}{dy} e^{i(k_{\text{TS}}x - \omega_{\text{TS}}t)} \quad (2.7a)$$

$$v'_y = -\frac{\partial \psi}{\partial x} = -i k_{\text{TS}} \phi_f e^{i(k_{\text{TS}}x - \omega_{\text{TS}}t)} \quad (2.7b)$$

It is remarked that using a streamfunction directly satisfies the continuity equation. Hence, only the momentum equations are necessary to simplify the dynamics of the disturbance flow field. The disturbance flow velocities are substituted into equation 2.5b and 2.5c. The resulting two equations can be further simplified by eliminating pressure. This is done through differentiating the x - momentum with respect to y and the y - momentum equation with respect to x ; and further equating $\frac{\partial^2 p'}{\partial x \partial y}$ from the two equations. After re-arranging the terms, the OS equation is obtained:

$$\boxed{(V_x - c_{\text{TS}}) \left(\frac{d^2 \phi_f}{dy^2} - k_{\text{TS}}^2 \phi_f \right) - \phi_f \frac{d^2 V_x}{dy^2} + \frac{i\nu}{k_{\text{TS}}} \left(\frac{d^4 \phi_f}{dy^4} - 2k_{\text{TS}}^2 \frac{d^2 \phi_f}{dy^2} + k_{\text{TS}}^4 \phi_f \right) = 0} \quad (2.8)$$

It is now clear that the "wave-like" behaviour stems from the assumption that the disturbance flow velocity creates "wave-like" streamlines (equation 2.6). This disturbance is convected downstream, hence this "wave" includes mass transfer. In contrast, the medium of propagation traditional waves such as acoustic waves are allowed to be quiescent; the fluid oscillates about its equilibrium position and is not convected at all [35].

Equation 2.8 is a 4-th order ordinary differential equation for ϕ_f . In the equation, c_{TS} is introduced, replacing the angular frequency as the two are related by $c_{TS} = \omega_{TS}/k_{TS}$.

As stated, the basic flow is assumed to be parallel i.e. only a function of y . This contradicts the nature of boundary layer flow over a flat plate, where the flow velocity field also depends on x (which can be seen by the growth of the boundary layer thickness as one travels downstream the plate). This contradiction is tackled in a general boundary layer flow by simply solving equation 2.8 locally (i.e. at a given x -position). Alternatively, when a self-similar solution exists, the OS equation can be scaled appropriately. Scaling the velocities and the amplitude function ϕ_f with the boundary layer edge velocity V_e , the length (y and k_{TS}) by a characteristic length of boundary layer (such as the boundary layer thickness δ) and introducing a local Reynolds number $Re_\delta = \frac{V_e \delta}{\nu}$ yields the non-dimensionalized OS equation [54]:

$$(V_x^* - c_{TS}^*) \left(\frac{d^2 \phi_f^*}{dy^2} - k_{TS}^{*2} \phi_f^* \right) - \frac{d^2 V_x^*}{dy^2} \phi_f^* + \frac{i}{k_{TS}^* Re_\delta} \left(\frac{d^4 \phi_f^*}{dy^4} - 2k_{TS}^{*2} \frac{d^2 \phi_f^*}{dy^2} + k_{TS}^{*4} \phi_f^* \right) = 0 \quad (2.9)$$

From the above equation, it can be seen that the parameters of the differential equation are the local Reynolds number (representing viscosity and position), the basic velocity profile, the TS wavenumber and frequency (or phase speed). In fact, by setting the parameters, the differential equation becomes an eigenvalue problem. For a given velocity profile, streamwise position and fluid viscosity, the stability problem can be analyzed in two ways: either by giving a real TS frequency as input and solve for the complex wavenumber or by giving a real TS wavenumber and solve for the complex frequency. The former is referred to as temporal stability analysis, while the latter is called spatial stability analysis.

The result of a stability analysis is a stability diagram. An example of a temporal stability diagram is given in figure 2.2[26].

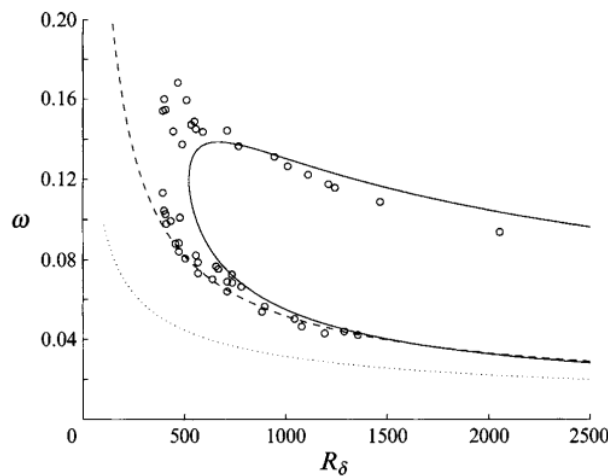


FIGURE 2.2: Example of a stability diagram comparing the result from O-S equation (solid line), experimental data (white circles) and lower branch of asymptotic theory (dashed and dotted lines)[26]. The experimental data was obtained from [51].

In this diagram, the local Reynolds number is in the abscissa and the input TS wave parameter (i.e. TS wave frequency) is in the ordinate. The plot (solid line) is a contour where the imaginary TS wavenumber equals zero, which defines neutral stability curve. As can be seen, this curve is characterized by an upper and lower branch. Inside, the imaginary part of the complex wavenumber is negative. This means that the amplitude of the wave grows, as can be observed by substituting a complex wavenumber into equation 2.6. In other words, the waves within the neutral stability curve are unstable.

Alternatives to the OS equation include asymptotic theory where the disturbances are expanded in terms of a parameter and an analytical expression is derived for the neutral curve [19][26][53][56], parabolized stability equations which accounts for variations in the streamwise and spanwise directions (hence accounts for non-parallel flow effects) [27] and direct numerical simulation of the disturbed flow [33]. Some results of the asymptotic theory have been presented by the dashed and dotted lines in figure 2.2[26].

The neutral curve between a stability analysis that includes non-parallel effects better fits experimental data than that which purely considers parallel flows. This can be seen from figure 2.3.

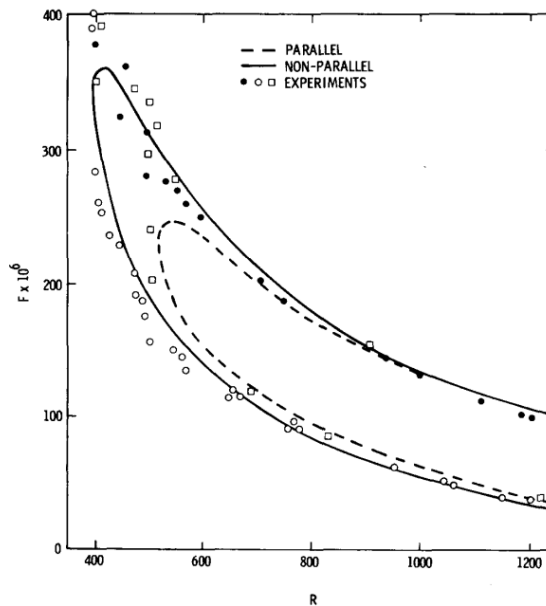


FIGURE 2.3: Comparison between experimental (square[55] and circles[51]) and theoretical neutral curves. Figure from reference [53]. In the figure, F is a dimensionless frequency and R is the Reynolds number.

The main discrepancies occur at low Reynolds numbers. However, the discrepancy is not purely due to non-parallel flow effects as can be argued by the results given in figure 2.4. There is a good agreement between the asymptotic theory which only includes parallel flow terms (dashed line) and experimental data (circles). Note that the asymptotic theory in the figure only predicts the lower branch of the neutral stability curve.

Nevertheless, the OS equation is deemed sufficiently good at predicting transition. This is already shown in figure 2.2 and 2.3 by the good agreement with experimental data at higher

Reynolds numbers. This is further supported by comparing the experimental and theoretical streamwise velocity profiles, as shown in figure 2.4.

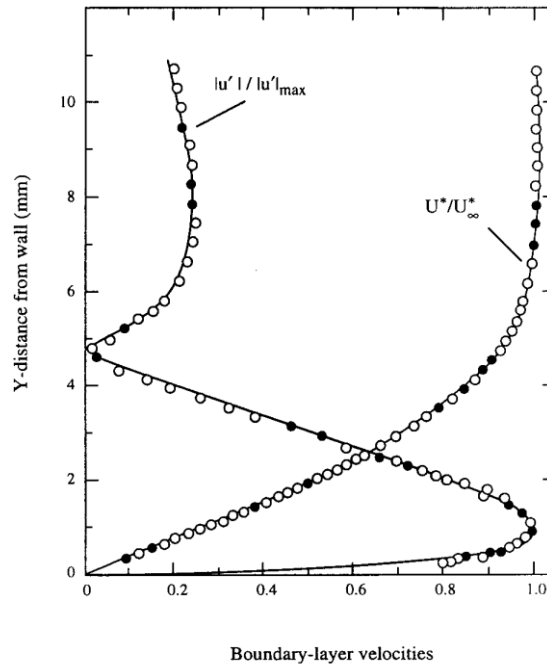


FIGURE 2.4: Comparison of non-dimensionalized basic and disturbance velocity profile between OS equation and experimental data for flow over a flat plate. Figure from [48], and the data is from [49].

All things considered, the wave-like behaviour of the disturbance which was introduced in the derivation of the OS equation is well supported by experimental result. Hence, if one is able to control the growth of these waves, then the stability of the flow may be enhanced.

A number of techniques employed to control the growth of TS waves exist in literature, which include the use of vibrating ribbon [44], vibrating plate [20], unsteady suction/blowing at the wall [64], wall heating [4], the use of plasma actuators [36] and compliant surfaces [8]. Significant reduction in the energy of the TS waves were successfully achieved with the aforementioned methods. The common disadvantages of these methods are the non-zero energy expenditure and the requirement of a potentially complex control system, except for the compliant surface method. Nevertheless, disadvantage also exists in this method, such as the rise of the TS wave energy around the leading edge of the compliant surface. Hence a control technique with zero energy expenditure (i.e. a passive control technique) with better response to TS wave is sought for.

This gives rise to the motivation for research on the interaction between TS waves and a class of structures called the "metamaterial". The speciality of this metamaterial is that it is built specifically for the purpose of manipulating the properties of a traditional wave (acoustic/electromagnetic/optics). Hence, the study of the effect of metamaterials on TS waves is a relatively new subject. A literature review on the current developments of metamaterial is given in the next section.

2.2 Acoustic metamaterials

Metamaterials are structures that are designed to manipulate the properties of a classical wave. The constituents of the metamaterials are orders of magnitude smaller than the wavelength of interest. Therefore, the structure that is built from these constituents give rise to effective material properties [42].

The metamaterials considered in this literature review will be only those that deal with acoustic waves, hence acoustic metamaterials (and not electromagnetic/optical metamaterials). This is because TS waves are ought to excite mechanical response to the metamaterial, rather than electromagnetic responses. As stated in the introduction, the main objective is to achieve stabilization of a flat plate boundary layer flow. The interest of using metamaterials stems from their use in attenuating acoustic waves at particular frequencies, as shall be corroborated in the following subsections. This literature review section aims at understanding the physical mechanisms of this acoustic wave attenuation and the models used in predicting the range of attenuated frequencies; and therefore serve as a basis for this thesis to extend the use of these metamaterials from classical acoustic waves to convective TS waves.

Metamaterials based on the following units are considered in this literature review: Helmholtz Resonator (HR) type (section 2.2.1), membrane type (section 2.2.2) and phononic crystals (PC) (section 2.2.3). The literature study concludes with section 2.2.4 which explains the choice of metamaterial based on the given researches.

2.2.1 Helmholtz resonator type

This section gives a literature review on the Helmholtz resonator (HR) type metamaterial. The discussion presented in the following paragraphs begins by introducing the Helmholtz resonators. Then, the focus shifts to the manner in which a collection of resonators constructs a metamaterial. As shall be seen, the most important concept in this metamaterial is the resonance of the HR structure. The subsequent paragraphs will therefore review the different theoretical methods for the prediction of HR resonance and experimental verification.

A Helmholtz resonator is a structure that consists of two main sections: a throat and a cavity [35]. The structure is arranged such that the neck is adjacent to a travelling acoustic wave. The acoustic wave impinges pressure on the neck, thereby creating motion of the air within the neck. This air within the neck further compresses the air within the cavity. In the classical modelling of the dynamics of a Helmholtz resonator, the air in the neck may be approximated as incompressible compared to the air in the cavity. This is because of the larger size of the cavity. Consequently, the neck-cavity system can be modelled as a forced mass-spring system; the mass being the neck and the spring being the cavity, while the forcing arises from the acoustic wave pressure. A dynamical analysis of this system gives rise to a resonance frequency, given by the following equation [10] [35]:

$$\omega_{\text{HR}} = c\sqrt{\frac{S_t}{Vl}} \quad (2.10)$$

where ω_{HR} is the angular resonance frequency, c is the speed of sound, S_t is the cross-sectional area of the throat, V is the volume of the cavity and l is the throat length. This length l may also be corrected with an "effective length" [15] [35][59]. The above equation does not take into account any losses. Nevertheless, the dynamical analysis shows that acoustic waves with frequencies close to the HR resonance are attenuated [35].

An HR type metamaterial was studied by N. Fang et al. [15]. The set-up is as follows. One side of a water-filled channel is attached by a series of identical Helmholtz resonators. The dimensions of the HR, as well as the periodic spacing between resonators, are much smaller than the relevant acoustic wavelength. Thus, a homogeneous response arises from this structure (hence the metamaterial). The experimental simulation of this system was realized with the help of two hydrophones: one upstream and the other downstream the channel, and one transducer upstream to generate the acoustic wave. The schematic of this problem is given in figure 2.5.

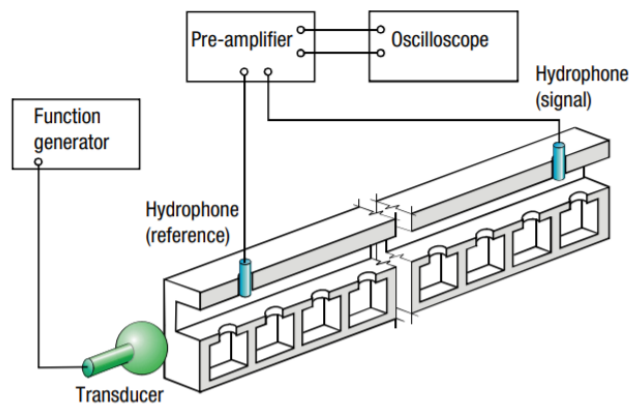


FIGURE 2.5: Ultrasonic metamaterial studied in reference [15]. Figure adapted from the same reference

In this HR metamaterial system, the material property of interest is the bulk modulus (E). As stated, due to the smallness of the HR dimensions and spacing with respect to the acoustic wavelength, there is an effectively homogeneous bulk modulus of the system (E_{eff}). This E_{eff} is different from the static E , and now depends on the frequency that excites the system (hence the sound wave frequency). By analogy with electrical circuits, E_{eff} of the system is plotted in the figure 2.6.

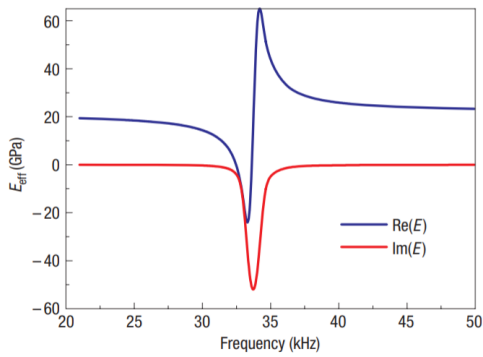


FIGURE 2.6: Plot of E_{eff} as a function of sound frequency. Figure adapted from [15]

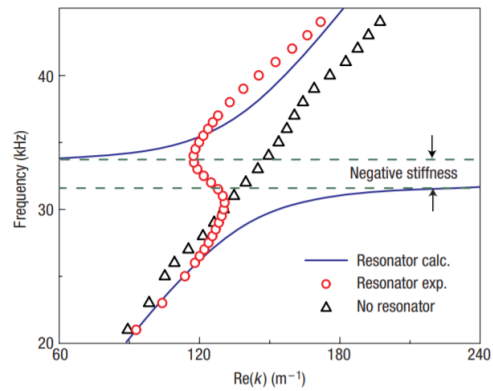


FIGURE 2.7: Theoretical and experimental dispersion curves of the HR type metamaterial studied in [15]. Figure adapted from the same reference

As seen in figure 2.6, there are negative and positive jumps for a certain range of frequencies. This range of frequency is near the resonance frequency of 32.5 kHz. In the lesser frequencies, the negative jump is large enough to cause $\text{Re}(E_{\text{eff}})$ to become lower than zero. Hence, the unusual property of negative bulk modulus.

Another property of the metamaterial that was analyzed in the study is the dispersion relation, which is the relation between the frequency and phase speed of wavenumber of the sound wave propagating in the system. This is given in figure 2.7 theoretically and experimentally. In the theoretical curve, there is a frequency range for which the curve forms a gap. This is called the "band gap". Acoustic waves that have frequencies within this band gap are evanescent in nature, hence attenuated and do not propagate [59]. In the experimental curve however, real wavenumbers within the band gap still exists. This is attributed to the fact that the theoretical calculation did not account for losses. The mechanism that forms the band gap is not dissipation of energy, rather it is the destructive interference due to the scattering of the acoustic wave within the structure, also known as Bragg's scattering [59].

Yet another analysis that can be performed on the metamaterial is the analysis of the transmission spectrum (variation of transmission coefficient with respect to the sound wave frequency). This is shown in figure 2.8

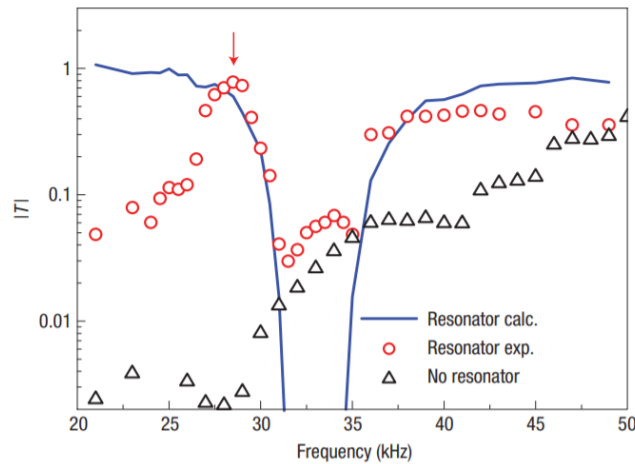


FIGURE 2.8: Transmission spectrum of the metamaterial studied in reference [15]. Figure adapted from the same reference.

The figure above shows the theoretical and experimental calculation of the transmission spectrum. As can be seen, there is a range of frequencies for which the transmission curve dips, both theoretically and experimentally (around 31 to 35 kHz). The frequency range that results in the transmission dip also corresponds to the band gap and negative bulk modulus, which are around the resonance frequency.

In 1994, N. Sugimoto and T. Horioka [59] analyzed the dynamics of a tunnel to which an infinite series of Helmholtz resonators was embedded. The geometry is given in figure 2.9. The analysis is two-fold: the first result deals with the partial differential equation governing acoustic waves, accounting for boundary layer displacement effects and dissipation of sound energy due to viscosity. Essentially this deals with acoustic motion within the section of the tunnel sandwiched between two Helmholtz resonators. The second part of the analysis resulted in the equation governing the dynamics of the resonator in response to the impinging acoustic pressure.

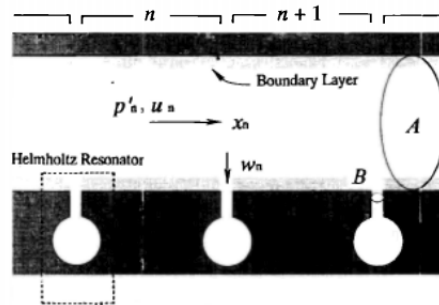


FIGURE 2.9: Geometry of the HR-grafted tunnel studied in reference [59]

The two analyses are then combined, along with continuity of acoustic impedance between tunnel sections, to create a transfer matrix which relates the acoustic pressure amplitudes of the n^{th} section of the tunnel to section $(n+1)^{\text{th}}$. Mathematically, this is written as:

$$\mathbf{X}_{n+1} = W\mathbf{X}_n \quad (2.11)$$

where the vector \mathbf{X} contains the pressure amplitudes and W is the transfer matrix.

The analysis is further advanced by considering a periodicity of the tunnel section, which enables the use of Bloch-Floquet's theorem. The dispersion equation that relates q (Bloch's wavenumber) with ω (acoustic wave angular frequency) was derived using the condition for non-trivial solution.

Band gaps in the dispersion relation (i.e. ω for which q becomes complex) are obtained through two mechanisms: resonance and Bragg scattering. The resonance frequencies are given in equation 2.12 and 2.13, the former being for a lossless case and the later being for a lossy case. The Bragg scattering frequencies are given in equation 2.14 and 2.15, with the same lossless/lossy ordering as the resonance frequency.

$$\omega_0 = \sqrt{\frac{Ba_0}{LV}} \quad (2.12)$$

$$\omega_{0\nu} = \omega_0 \left[1 - \frac{1}{\sqrt{2}r} \left(\frac{\nu}{\omega_0} \right)^{1/2} \right] \quad (2.13)$$

$$\omega_m = \frac{m\pi a_0}{d} \quad (2.14)$$

$$\omega_{m\nu} = \omega_m \left[1 - \frac{C}{\sqrt{2}R} \left(\frac{\nu}{\omega_m} \right)^{1/2} \right] \quad (2.15)$$

This paper shows several possible equations in predicting the band gap frequencies of a Helmholtz resonator series.

In the next decade, **Z. G. Wang et al.** [66] analyzed propagation of sound waves through a series of Helmholtz resonators with "Interface Response Theory". This is a method of analysis based on the Green's function of the system's dynamics. Such an analysis enables one to derive analytical expressions for the transmission spectrum and dispersion relation of the HR series. The geometry of the problem is given in figure 2.10.

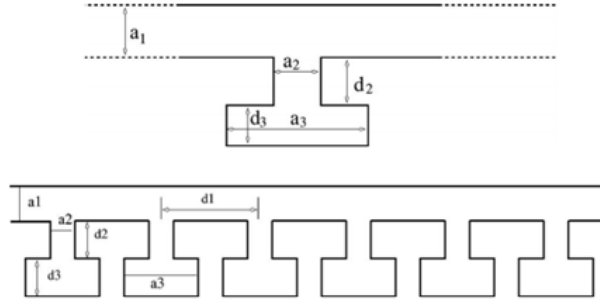


FIGURE 2.10: Geometry of a single and a series of HRs studied in reference [66]

Four cases were analyzed: (1) single HR, (1) an infinite series of HRs, (3) a finite series of HR with no defect and (4) a finite series of HR with defects. As mentioned, analytical expressions for the transmission spectrum and dispersion curve were derived. For instance, the transmission spectrum for a single HR is given by:

$$t = \frac{\cot(\alpha_2 d_2) - \frac{Z_2}{Z_3} \tan(\alpha_3 d_3)}{\left[\cot(\alpha_2 d_2) - \frac{Z_2}{Z_3} \tan(\alpha_3 d_3) \right] + \frac{i}{2} \frac{Z_1}{Z_2} \left[1 + \frac{Z_2}{Z_3} \cot(\alpha_2 d_2) \tan(\alpha_3 d_3) \right]} \quad (2.16)$$

where t is the transmission coefficient, α is the sound wavenumber ($= \omega/c$), d is the length of a given section, Z is the characteristic acoustic impedance, subscript 1 denotes the waveguide section, subscript 2 denotes the neck section and subscript 3 denotes the cavity section of the resonator.

The band gap appears for frequencies in which $t = 0$. These frequencies are given by:

$$\cot(\alpha_2 d_2) - \frac{Z_2}{Z_3} \tan(\alpha_3 d_3) = 0 \quad (2.17)$$

Compared to the previously derived resonance frequencies for lossless HRs (equation 2.10 and 2.12), equation 2.17 is applicable to a more general HR: the fluid in the neck and the cavity may differ, and there is no restriction on acoustic compactness of the geometry ($\alpha \ll 1$ is not necessary for the equation). In fact, it was easily shown that for an HR with homogeneous fluid and acoustically compact geometries, equation 2.17 reduces to equation 2.10 or 2.12, without any restriction on the relative size of the neck with respect to the cavity.

As for the other cases that were analyzed, dispersion relation was derived for the infinite case, whereas the transmission spectra were derived for the finite cases.

Several years later, **J. Fey and W. M. Robertson** [16] compared the analytical equation derived by Z. G. Wang et al. [66] with experimental results. In their analytical study, they extended the application of equation 2.16 to a series of non-identical resonators, by simply multiplying the transmission spectra for each individual resonators. In the experimental study, the

Helmholtz resonator(s) was attached to a waveguide; where one end of the waveguide is attached to a speaker (for acoustic signal generation) and the other end is attached to a microphone (for acoustic signal reception). This experimental set-up allows for the measurement of transmission spectrum, and is illustrated in figure 2.11. The comparison between experimental and analytical transmission spectra are given in figure 2.12.

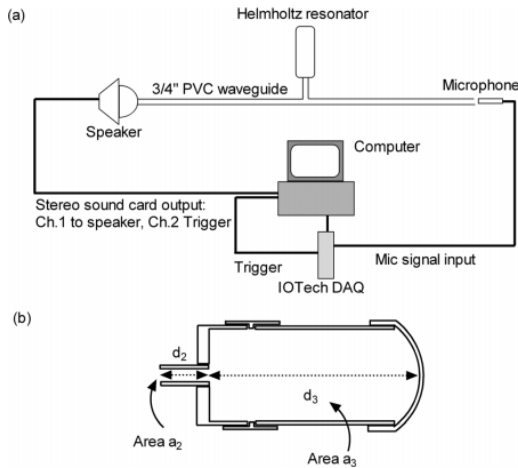


FIGURE 2.11: Experimental set-up studied in reference [16] for a single HR

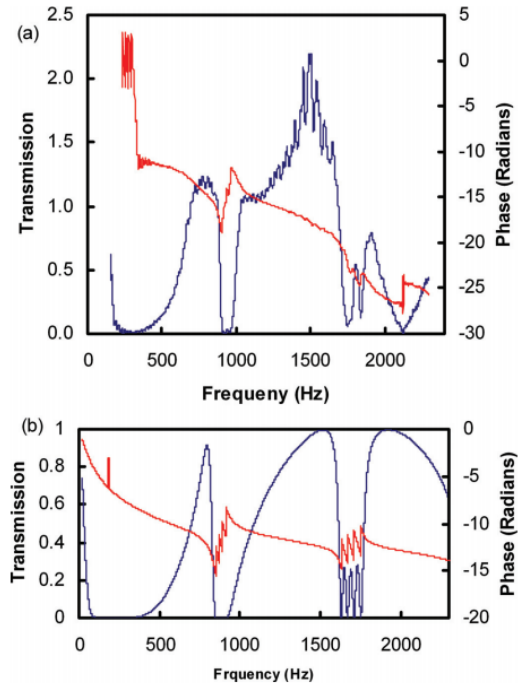


FIGURE 2.12: Transmission spectra of the experimental (a) and analytical formulation (b) studied in reference [16]

It is to be noted that in the figure 2.11, only one resonator was illustrated in the experimental set-up given by the authors. However, the transmission spectra of figure 2.12 were the results of four detuned resonators.

Upon comparing the resulting transmission spectra, it can be seen that the general trend of transmission dips is well-predicted with the proposed analytical equation. Discrepancies in the transmission magnitudes can be seen at the low and large frequency limits in particular.

In 2012, **J.H.Lu et al.** [41] also analyzed an array of water-filled Helmholtz resonators. The studied geometry is given at the top of figure 2.13.

The analysis were both numerical and experimental. The numerical analysis was performed using two-dimensional Finite-Difference Time-Domain (FDTD) methods, along with appropriate boundary conditions: periodic boundary condition in x and a boundary condition that minimizes reflection in y (referring to the geometry in figure 2.13). As for the experimental analysis, an "ultrasonic immersion transmission technique" was adopted. The aim of the two analysis is to study the transmission spectrum of the system.

The resulting transmission spectrum from both numerical analysis and experimental simulation is given at the bottom of figure 2.13. Relatively good agreement can be seen between the two analysis method, in particular for the prediction/measured transmission dips.

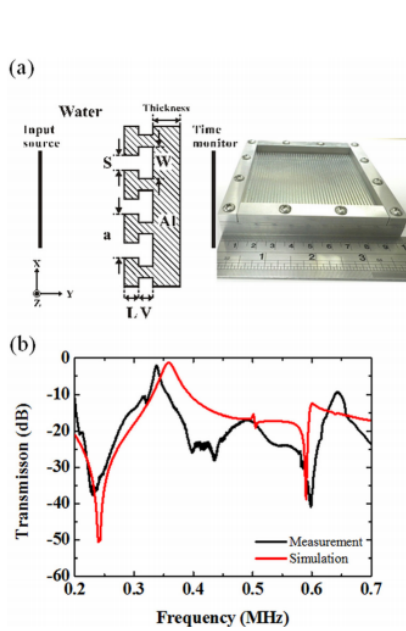


FIGURE 2.13: Experimental set-up (a) and transmission spectrum (b) of the HR array studied in reference [41]

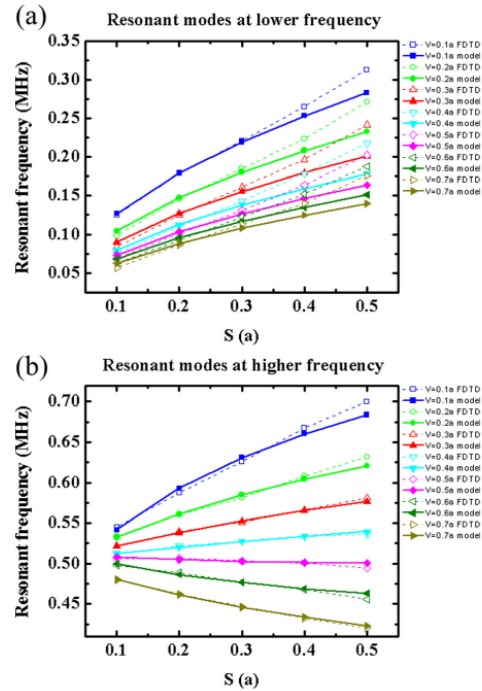


FIGURE 2.14: Comparison of analytically and numerically predicted resonance frequencies in reference [41]

Different from the classical HR models previously discussed, there is a higher orders resonance which gave rise to the second frequency transmission dip. This higher resonance frequency behaviour was captured when a numerical simulation is performed after discretizing the appropriate partial differential equation, whereas the single mass-spring analogy in the classical HR model (equation 2.10) only yields a single resonance frequency. The authors proposed a dual mass-spring system in order to analytically model the higher order resonances. A comparison between the analytical and numerical prediction of resonance for varying width of the neck is given in figure 2.14. Good agreement can be seen.

Compared to the previously discussed studies, this paper adds a new method for the prediction of HR-type metamaterial behaviour, namely a numerical method. Furthermore, higher order resonance was found, which increases the range of operating frequency for the metamaterial.

Another study of an array of Helmholtz resonators was performed by **D. Guan et al.** [24]. This time, however, a different geometry of the resonator was analyzed. The geometry consists of two necks and a cavity. This is illustrated in figure 2.15. The authors also considered an electric circuit analogy for the Helmholtz resonator, the same analogy as the one presented in reference [15].

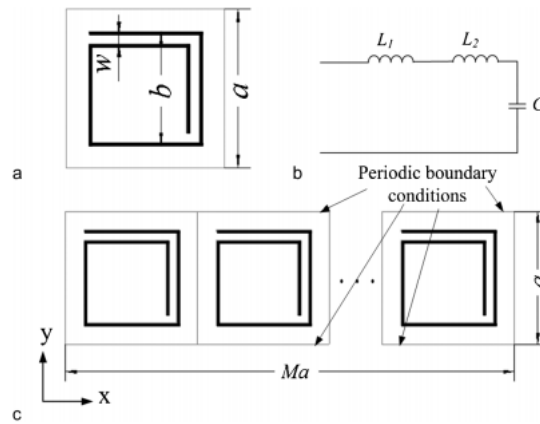


FIGURE 2.15: Geometry of the HR studied in reference [24]; (a) unit cell, (b) inductor-capacitor circuit analogy and (c) array of HRs. Here, two necks can be seen in the unit cell

A numerical analysis was performed, solving the two-dimensional Helmholtz equation which governs single frequency sound propagations with the finite elements method (FEM). Acoustic wave propagates in the $x - y$ plane. Periodic boundary condition was employed in the y boundaries, through the use of Bloch-Floquet's theorem. The band structure and the transmission spectrum of the system were computed. The results are shown in figure 2.16 and 2.17.

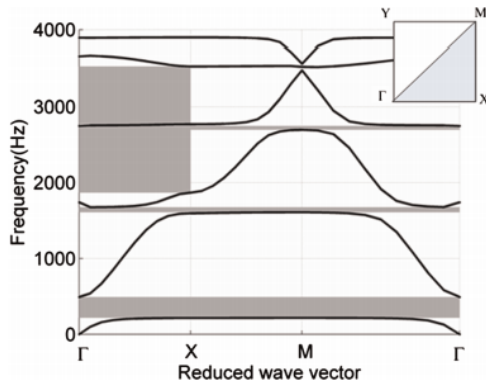


FIGURE 2.16: Band structure of the HR array studied in reference [24]

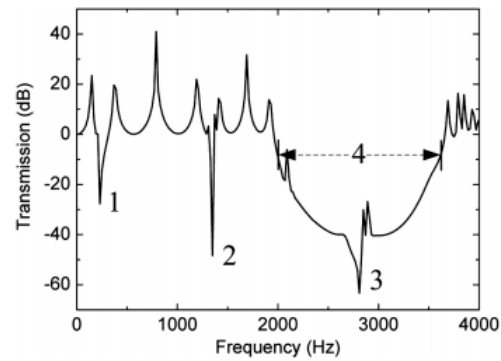


FIGURE 2.17: Transmission spectrum of the HR array studied in reference [24]

Unlike the band structure given in figure 2.7, the band structure of figure 2.16 is for a two-dimensional wave. The range of wave vectors within a 2D Brillouin zone was considered. As a result, a new phenomena appears: namely, a partial band gap. This partial band gap represents attenuation of sound for some angular direction of wave propagation only. Two partial band gaps are represented in the band structure by the shaded areas which do not span the whole horizontal (present in the frequency range of 1867 - 2746 Hz and 2769 - 3530 Hz). In addition to the partial band gaps, three complete band gaps are present.

In the transmission spectrum, frequency dip 1-3 corresponds to the band gap (although the authors commented that there may have been numerical errors around frequency dip 2) and frequency dip 4 corresponds to the partial band gap.

The reviewed papers, however, did not deal with interaction of flow and the dynamics of the Helmholtz resonators. Nevertheless, the methods and concepts present in the literatures discussed may serve as a basis for further analysis in taking into account flow over the resonator.

2.2.2 Membrane type

This section documents the findings on the membrane type metamaterial. The focus of the membrane metamaterial literature review is on *highlighting the results found in previous studies*. These results are then used to understand the physics and the methods of analysis used for describing the behaviour of the membrane type metamaterial are noted down, to serve as a starting point for the objective of attenuating TS waves.

The earliest membrane-type metamaterial was suggested by **Z. Yang et al.** [70], in which they proposed a new type of structure in order to overcome the inefficiency of attenuating sound at low frequencies with the use of mass-law. They proposed a rubber membrane, with a mass attached (steel disk) at the centre. This unit cell is fixed onto a rigid grid. Numerical simulation (using finite elements methods) and experimental analysis (using impedance tube measurements) were undertaken to study the transmission spectrum (of sound waves going through the structure) for this metamaterial. It was found that there was a transmission dip between two transmission peaks, as shown in figure 2.20. This dip was attributed to the superposition of two resonances at opposing phase, hence creating an anti-resonance (frequency for which displacement is minimum). Also it is noted that the numerical and experimental methods are in relatively good agreement for the prediction of sound transmission.

Another analysis based on the FEM simulation is the study of the spatially averaged mass density, defined as spatially averaged normal stress divided by the normal acceleration. It was found that this effective mass is negative near the frequency of the transmission dip as shown in figure 2.21.

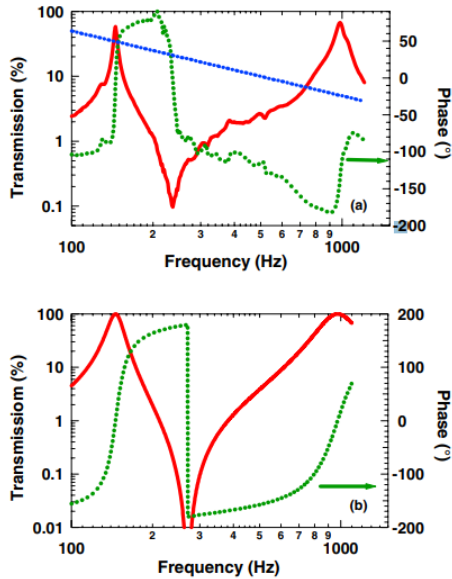


FIGURE 2.20: Experimental (top) and numerical (bottom) transmission spectrum of the membrane metamaterial studied in reference [70]

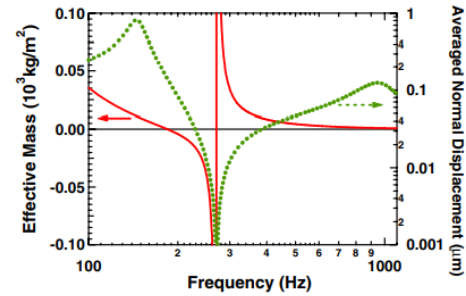


FIGURE 2.21: Effective mass of the membrane type metamaterial studied in reference [70]

Later on, **Z. Yang et al.** [69] extended the single-unit metamaterial to a panel, with the aim of achieving broadband attenuation rather than just for a narrow frequency range. The same behaviour in the transmission spectrum (i.e. a transmission dip between two transmission peaks) was found with the panel, as can be seen at the top of figure 2.22. A new analysis in this paper is the study of the normal displacement amplitude profile at the transmission dip frequency, measured using laser vibrometer. This can be seen at the bottom of figure 2.22. In the inset of the same figure, the average displacement for the different sound frequencies were plotted. It can be seen that the average displacement at the transmission dip frequency is approximately zero, for which the authors concluded to be the cause of the low transmission.

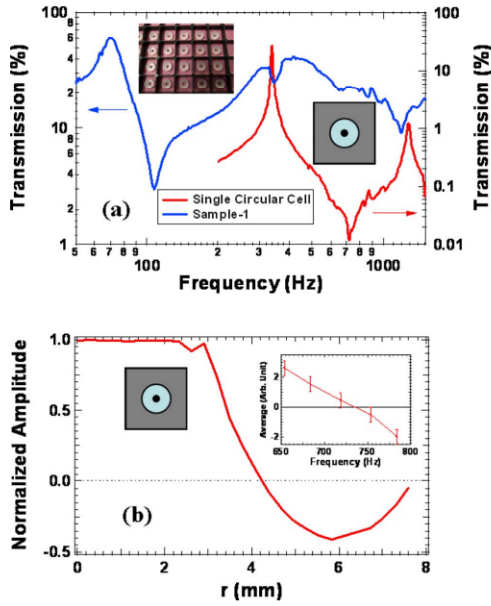


FIGURE 2.22: Transmission spectrum of a single and panel membrane-type metamaterial (top) and displacement amplitude profile at the transmission dip frequency (bottom) of reference [69]

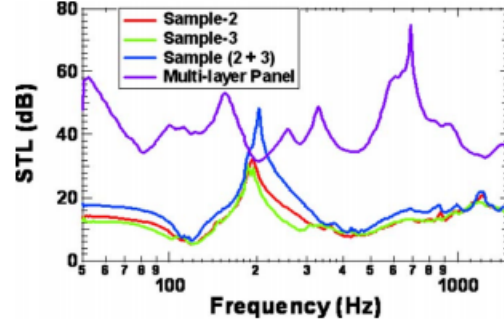


FIGURE 2.23: Transmission spectrum of different panels of membrane-type metamaterial [69]

Finally, in the study it was found that stacking panels with different transmission spectrum (which was done by varying the centre mass) made it possible to achieve broadband attenuation (figure 2.23).

C. J. Naify et al. [46] also investigated the same single unit mass-attached membrane configuration as reference [70]. They studied the effect of membrane tension and mass magnitude on the transmission dip frequency, both numerically (finite elements analysis) and experimentally (laser vibrometer measurements). Again, the numerical and experimental results are in relatively good agreement.

Furthermore, they investigated the displacement profile at the transmission dip, and found the same profile as the one found at the bottom of figure 2.22.

A new study that they conducted is the dynamic response of the mass-membrane structure at the transmission dip frequency. The plot of acoustic pressure and structural acceleration against time is given in figure 2.24. It can be seen that the acceleration and pressure are nearly out of phase at the centre of the structure. On the other hand, slightly away from the centre, the acceleration and the pressure are approximately in phase. *In fact, this means that on most of the structure, the pressure and displacements are nearly out-of-phase.* This is because the acceleration and displacement are out-of-phase of each other when a harmonic dependency is assumed. This may be of interest, for instance, for a possible destructive interference of Tollmien-Schlichting waves.

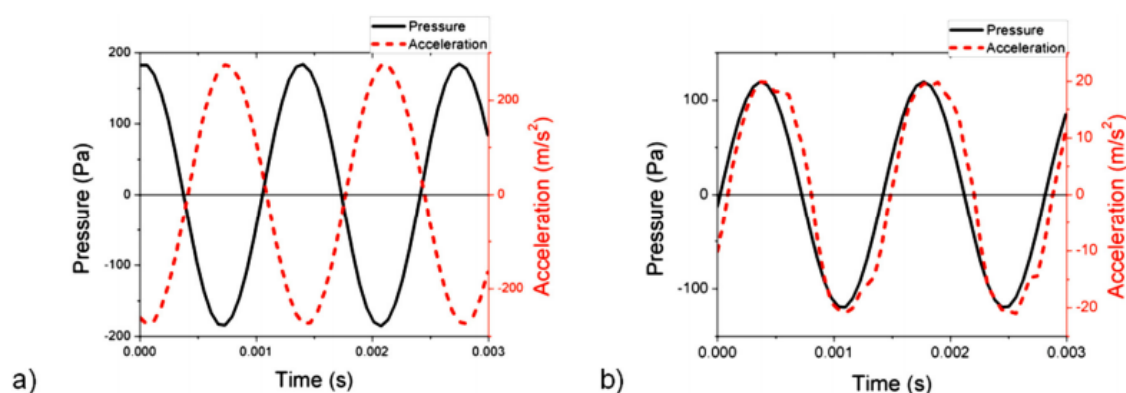


FIGURE 2.24: Dynamic responses at transmission dip frequency of the membrane metamaterial studied in reference [46]. (a): at the centre of the structure and (b): 0.8 mm from the centre

J. Mei et al. [43] studied a membrane type metamaterial with a different geometry: rectangular rubber membrane attached to semi-circular iron platelets. Two samples are studied, denoted as sample A and B, which are shown in figure 2.25 and 2.26 respectively. Several characteristics of this sample were investigated. Among others the studies are on the absorption spectrum (with respect to an incident sound wave), the normal displacement profiles (eigenmodes) at absorption peaks and the elastic energy density. The methods of studies are numerical (finite element simulation with COMSOL®) and experimental. Three absorption peaks were obtained for sample A (see the bottom of figure 2.26).

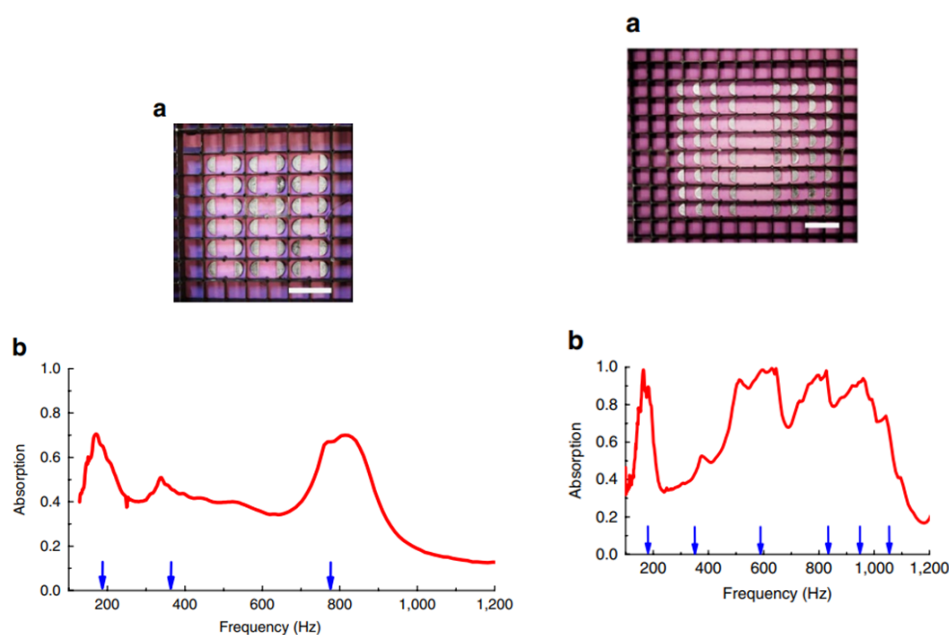


FIGURE 2.25: (a) Sample A and (b) its absorption spectrum for the metamaterial studied in reference [43] (figure adapted from the reference)

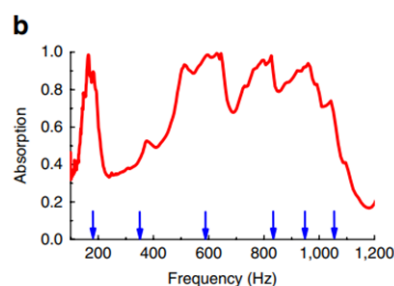
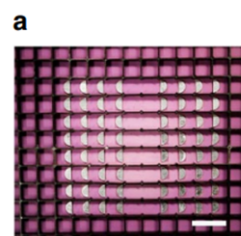


FIGURE 2.26: (a) Sample B and (b) its absorption spectrum for the metamaterial studied in reference [43] (figure adapted from the reference)

The lowest frequency for this absorption peak corresponds to flapping motion as corroborated by the displacement profile. It is also shown the magnitude of absorption at the lowest frequency is the largest (around 70% absorption). This absorption corresponds to a large elastic/flexural energy density which is attributed to the discontinuity in the first spatial derivative of the normal displacement near the iron platelets. Hence it is deduced that the energy of the acoustic wave has been converted into flapping motion. Sample B was constructed in order to improve the absorption by the flapping motion. Indeed, with sample B, the absorption was shown to be near unity (figure 2.26).

L. Y. L. Ang et al. [2] studied another variant of the membrane type metamaterial for broadband sound attenuation. They studied a relatively large panel, which consists of hollow tubes sandwiched by face sheets. Two cases were investigated: plain configuration as described before and an addition of membrane placed in between the hollow tubes. An illustration is given in figure 2.27. In particular, the transmission spectrum was studied using both numerical and experimental methods. The results are given in figure 2.28.

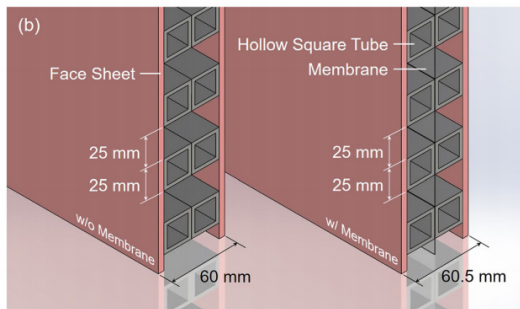


FIGURE 2.27: Metamaterial configuration studied in reference [2] (figure adapted from the reference)

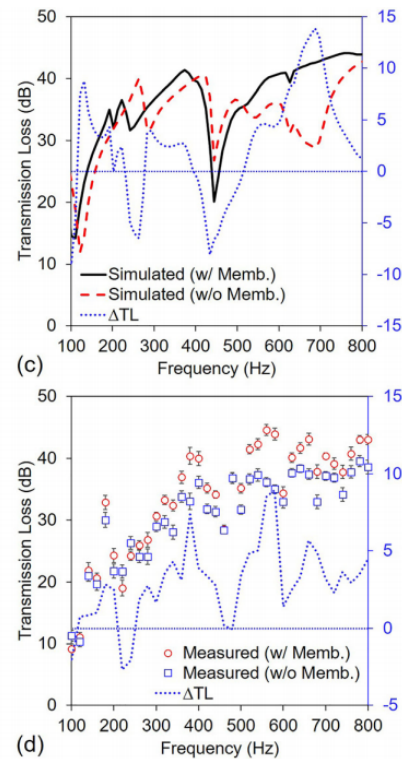


FIGURE 2.28: Numerically (top) and experimentally (bottom) obtained transmission spectrum of the metamaterial studied in reference [2] (figure adapted from the reference)

Upon closer inspection, there is a relatively large discrepancy between the numerical and experimental results. This discrepancy was attributed to the modelling of the numerical simulation:

the problem treated was sound propagation within a waveguide whereas the experiment was conducted in a reverberation chamber. Nevertheless, the general trends in the two results were deemed to be similar. The main finding is the increase in transmission loss over the higher frequencies (500-800 Hz) when membrane is added to the panel. This was attributed to one of the resonance mode of the membrane.

In conclusion, the membrane type metamaterial has been shown to be capable of attenuating sound considerably. There are numerous variations of this type of metamaterial. The most important concept in characterizing this metamaterial is the resonance/eigenmode. Initially, the metamaterial could only be used to attain attenuation for a narrow range of frequency. Upon further development, the metamaterial attenuation frequencies could be tuned, or a broadband attenuation could be achieved. For the interest of attenuating TS waves, two mechanisms of the metamaterial were deemed to be useful: namely the out-of-phase acceleration of the structure (which yields negative mass) and conversion of the incident flow energy into elastic energy (without prematurely triggering transition).

2.2.3 Phononic crystal (PC)

Phononic crystals (PC) are structures with a certain periodicity in the acoustic/elastic property (also known as superlattice [10]). The periodicity affects the propagation characteristics of acoustic waves within the structure. They are analogous to the electromagnetic counterpart, namely the photonic crystals [32]. The interest in these multi-layered structures stems from the existence of band gaps, in which acoustic waves are attenuated [9],[37]. Note that this is the same band gap discussed in the two previous metamaterials.

In the case of a one-dimensional phononic crystal, the periodicity is only along a single direction. The structure is built upon a repeating unit-cell. This unit cell is composed of several layers, two being the minimum [10][52]. The length of the period is equal to the length of the unit cell. Typically, this length is comparable to the wavelength of interest [42]. An illustration of this one-dimensional phononic crystal, along with the associated terminologies, is given in figure 2.29

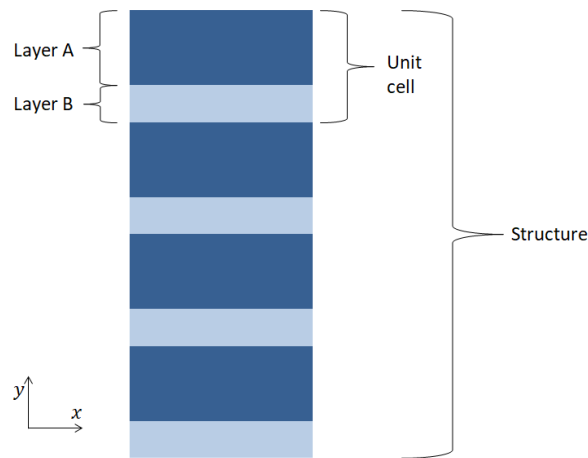


FIGURE 2.29: An example of a one-dimensional phononic crystal. In this example, there are four repeating unit cells where a unit cell is composed of two layers of different materials. The layer material may be solid or fluid.

As mentioned before, an important consequence of this layered material is the existence of band-gaps/stop bands due to the reflection/transmission which led to constructive and destructive interference of acoustic waves within the structure [10]. Traditionally, the analysis is on the wave that propagates within the structure and not for a wave that interacts at the interface of the structure. Hence, the study of the interaction between TS waves and phononic crystal is a relatively new area of research.

This subsection is divided as follows: first, the motivation for the use of phononic crystal shall be discussed in sub-sub-section 2.2.3.1. This sub-sub-section outlines the important properties of a PC that are relevant in the analysis of an interaction with TS waves. Then, different methods for analyzing a PC shall be discussed in section 2.2.3.2.

2.2.3.1 Motivation for the use of phononic crystal

The main motivation comes from a result of the research done in reference [30], in which instabilities within a water-filled channel flow interact with a one-dimensional phononic crystal embedded on the wall of the channel. The geometry of the problem is illustrated in figure 2.30. A full numerical fluid-structure interaction was performed, along with analyses of the isolated structure.

Three important results are stated here. Number one is that the displacement of the phononic crystal at the fluid-structure interface and the instability waves in the fluid are found to be out-of-phase for frequencies that lie within the bandgap of the phononic crystal.

Number two, the out-of-phase displacement correlates with a reduction of (temporally-averaged) kinetic energy of the disturbance flow field when compared to where there is no phononic crystal on the wall (rigid wall). This reduction in energy is illustrated in figure 2.31. It is remarked that the kinetic energy was integrated along the wall-normal and spanwise directions.

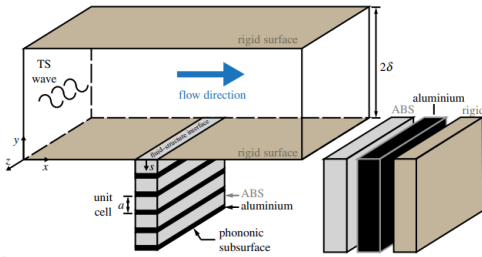


FIGURE 2.30: Geometry of PC-embedded channel flow studied in reference [30] (figure adapted from the reference)

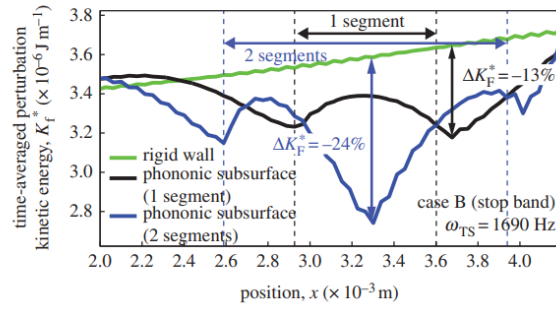


FIGURE 2.31: Development of disturbance flow kinetic energy along the streamwise direction [30] (figure adapted from the reference)

The third important result is that, the amplitude of the out-of-phase displacement is found to be largest closest to the "truncation frequency". This truncation frequency is a characteristic of the finite structure, and was found through a relatively simple one-dimensional forced-vibration problem. In fact, as shall be seen later on (see for instance, section 4.1), this truncation frequency is an eigenfrequency of the phononic crystal that lies within the band gap.

Hence, it is hypothesised that it may be possible to stabilize an amplifying disturbance where the pressure wave and the displacement are out-of-phase. It is noted that the integral disturbance flow kinetic energy integral has also been used in previous studies as a measure of stability[19] (among other variables such as the streamwise disturbance velocity[19][51][55], the square of the streamwise disturbance velocity [19] and the local kinetic energy (mentioned in [19] and [53])). Thus, a reduction in the kinetic energy may be considered as stabilization.

This stabilization occurs for frequencies within the bandgap of the phononic crystal, and the largest stabilization occurs for frequencies that are closest to the truncation frequency (due to a larger displacement, resulting in a greater effect on the flow).

This promising numerical result causes the choice of further studying the phononic crystal for stabilization of TS waves to be more appealing. Furthermore, compared to the Helmholtz resonators, the assumption of acoustic response within the metamaterial structure becomes less dangerous. Finally, compared to the membrane type metamaterial where the problem is either axisymmetric or fully three-dimensional, the phononic crystal can be analyzed in the two-dimensional space (as shall be seen in section 2.2.3.2) which matches that of the linear stability analysis of flows with no cross-flow.

The reference paper [30] did not provide analysis on the streamwise disturbance flow velocity. Furthermore, only a few number of TS wave frequencies were tested, rather than a frequency sweep. It is assumed that the simulation time was restricting a frequency sweep. Thus, there are still areas to be investigated in the study of stabilization of TS waves with the phononic crystal.

2.2.3.2 Methods for phononic crystal analysis

Currently, there are several methods available in literature in predicting the dispersion relation of a phononic crystal: transfer matrix method (TM), Green's function method (also called "Interface Response Theory" (IRT)), plane-wave expansion (PWE) method and finite elements (FEM) method. The following paragraphs discuss each method separately. While the main focus of the paragraph is on reviewing the method of analysis, a very brief introduction to the study of waves in layered media shall be given in the discussion of the TM method. Moreover, results of PC analyses will be shown in the discussion of the FEM method.

a. Transfer Matrix (TM) Method

The first method (transfer matrix) is attributed to Thomson [61] in solving the bulk waves within stratified solids and later improved by Haskell [25], allowing for surface waves (waves that attenuate as it propagates away from the surface). The main goal of the method is to relate the variables (either combination of displacement and stresses, or amplitudes) at one interface with another interface. Hence, this problem is applicable to a finite structure.

Where a one-dimensional infinitely-repeating unit cell is considered however, there is a relatively more simple formulation presented in numerous references for different problems as listed below:

1. Transverse waves [5] (also as waves with "out-of-plane modes" [65] or "shear horizontal modes" [29] because the displacement associated to the travelling wave is in the z direction (or in the direction perpendicular to the page), referring to the coordinates system of figure 2.29).
2. Sagittal waves [11] (also called as waves with "in-the-plane modes" [65] or "mixed modes" [29]. This is because the displacements attributed to the wave are in the x and y direction, referring to the coordinate system of figure 2.29)
3. Longitudinal and transverse waves propagating only in the direction perpendicular to the layers [14], [31], [58], [65]

The above classification of problems is applicable only if the layers are made of isotropic solids [11][29][65].

The steps taken in formulating a transfer matrix solution are given in the following list:

1. Set-up the equation of motion.
2. Remark that the solution to the partial differential equations (i.e. the solid displacements) can be built from wave modes
3. Relate the displacement and stresses to amplitudes of the wave function (the stress can be derived from the displacement from the constitutive relation).
4. Relate the displacement and stresses at one end of the layer, say the left-end, to the other end of the layer, say the right-end. This yields a transfer matrix for the j -th layer.

5. Apply continuity of stresses and displacement. The previous step is then repeated for all layers, and the resulting transfer matrix that relates the stresses and displacements at the beginning of the first layer to those at the end of the n -th layer is given by the product of consecutive transfer matrix of the j -th layer
6. In the case of an infinite system, apply periodic boundary condition through Bloch's theorem.

Returning to the interaction between TS waves and elastic waves within the PC, the fluctuating pressure and stress that is impinging on the PC at the fluid-structure boundary would excite sagittal wave responses. This means that there can be displacements in both x and y directions (referring to figure 2.29).

For the design of the PC, further assumptions are made: (1) the problem is 2-dimensional (spatial derivative in the direction normal to the screen is zero, referring to figure 2.29) and (2) the streamwise width of the PC will be very narrow (much smaller than the local wavelength of the TS waves). Furthermore, the PC is surrounded by rigid structure. The aim for these assumptions is to simplify the problem such that only longitudinal waves that propagate in the y direction should be considered; that there are no waves propagating in the x direction.

b. Green's Function Method/Interface Response Theory (IRT)

The second method is based on Green's function, the so-called "Interface Response Theory" (IRT) [10][12][13][60]. This method requires one to find the Green's function of the reference system (meaning that one needs to find the Green's function of each of the material that constitutes the layer). This reference Green's function is then related to the (finite) structure's Green's function (i.e. the Green's function of the finite layers) through the equation for Interface-Response Theory.

The eigenmodes are obtained by setting the determinant of the structure's inverse Green's function to zero (which, essentially finds the non-trivial solution of the dynamical problem). Alternatively, one can also find the eigenmodes by finding the poles of the Green's function of the finite structure [10].

Additionally, the IRT method can also be used to find the dispersion relation of an infinitely extending system. Here, it is sufficient to say that the dispersion relation obtained through the Green's function method (for a two-layered one-dimensional PC) is the same as the TM method (equation 3.20) An extra condition is imposed on the finite structure: the eigenmodes of the phononic crystal is quantized. Only the following are allowed within a branch of the passband:

$$qD = \frac{m\pi}{N} \quad (2.18)$$

where q is the global wavenumber (or the Bloch's wavenumber), D is the length of the unit cell, $m = 1, 2, \dots, N - 1$ and N being the number of the unit cell. Hence there are $N-1$ eigenmodes within a branch in the pass-band (i.e. frequencies outside the bandgap) and a single mode in the bandgap, N being the number of unit cells. This quantization of the wavenumber of the

finite structure is similar to the result in reference [5] for the study of transverse waves in a finite slab of layered structures.

c. Plane-Wave Expansion (PWE) Method

The following paragraphs briefly describes the findings on the plane-wave expansion (PWE) method for the analysis of phononic crystals. This method was initially proposed in reference [38]. The basis of the method is to express the displacements and elastic properties as a complex Fourier series with unknown coefficients. They are then substituted into the equation of motion of (linear, elastic, isotropic) solids which then sets up an eigenvalue problem. Band gaps may be predicted with this method.

A brief overview of the method and the resulting system of equations is also given in reference [29]. This is essentially a numerical method. Their validity have been compared with finite elements method as given in reference [68] and [18] (through comparison of the frequency ranges of the band gap in the dispersion curves and the dip in the transmission spectra).

d. Finite Elements Method (FEM)

Finite elements method (FEM) (meaning numerically analyze the governing partial differential equation with this discretization technique) can also be applied for the analysis of a phononic crystal. This has been done in several papers, as shall be corroborated in the following paragraphs. The starting point is the same as all the other methods, that is, the equations of motion (balance of linear momentum for linear, elastic, isotropic solids). The primary unknowns are the solid displacements. The equations are discretized and the solutions give information on the behaviours of the phononic crystal.

There are two types of studies that can be performed with FEM: namely, an eigenvalue analysis and a frequency response study. In both cases, a harmonic time dependency is assumed on the solid displacements. The eigenvalue analysis can be used to obtain the band structure of the phononic crystal, whereas the frequency response study can be performed to obtain the transmission spectra.

Hussein et al. [31] studied the propagation of longitudinal waves in the direction perpendicular to the layering using FEM. Essentially, the problem is one-dimensional; and the discrete equation for the frequency response study is given in the following form:

$$(-\omega^2\mathbf{M} + \mathbf{K})\mathbf{D} = \mathbf{F} \quad (2.19)$$

where ω is the angular frequency of the driving force, \mathbf{M} is the mass matrix, \mathbf{K} is the stiffness matrix, \mathbf{D} is the vector of displacement and \mathbf{F} is the force vector. The discretized system of equations is solved with appropriate boundary conditions. \mathbf{D} is solved given an ω , which yields the steady-state displacement field. As mentioned before, this strategy can be used to study the transmission of the PC structure. An example this study is given in figure 2.32.

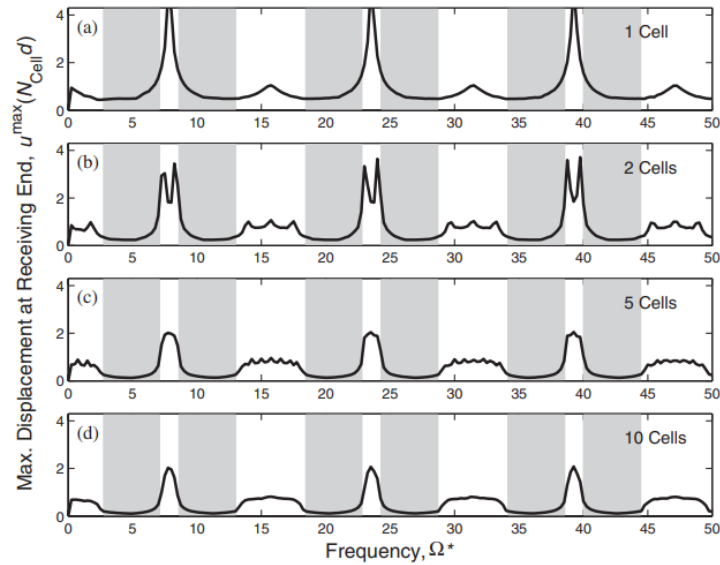


FIGURE 2.32: Transmission spectra of phononic crystal structures with different number of unit cells (defined as the maximum displacement at the opposite end of the applied force). The darker area shows the band gaps of the unit cell, as predicted by transfer matrix method. [31]

An important result shown in the figure above is the correlation between transmission spectrum and band gap: low transmissions happen inside the band gap. Hence, the band gap is a property of the unit cell which gives a good qualitative prediction of the transmission of the corresponding finite phononic crystal structure.

Furthermore, it is interesting to note that there are no transmission peaks in the band gap, as suggested by the result of the Green's function method (IRT) in the previous paragraph. This is because the unit cell of the phononic crystal structure (which produced figure 2.32) is symmetric [10]. Hence, it is imperative that we do not choose a symmetric unit cell for the TS wave attenuation problem.

As for the eigenvalue problem, the vector \mathbf{F} is set to 0 in equation 2.19 and \mathbf{D} becomes the eigenvector of the problem. Same as before, the problem is accompanied by appropriate boundary conditions. Solving the system for the eigenvalue yields the band structure of the phononic crystal. An example is given in figure 2.33.

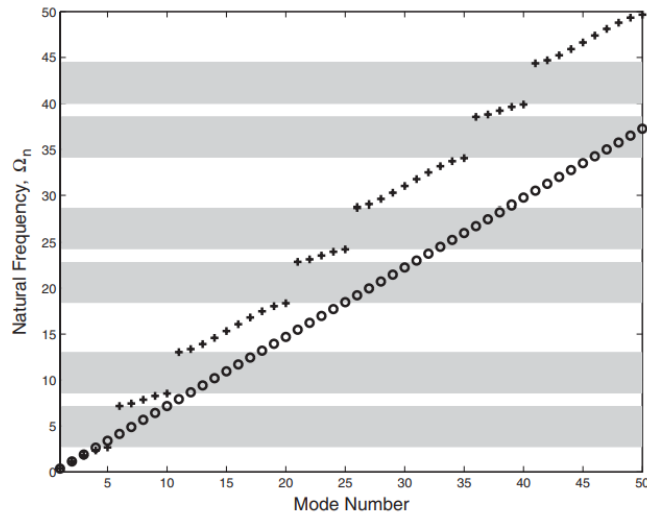


FIGURE 2.33: Natural frequencies of a one-dimensional phononic crystal structure, fixed at one end (given by the + symbol) [31]

Here, there are no eigenfrequencies in the band gap (as mentioned before, due to the symmetry of the unit cell [10]).

Hladky-Hennion and Billy [28] performed both an experimental and numerical (FEM) study of a type of phononic crystal consisting of beads with alternating masses. One sample is shown in figure 2.34. The study is on the transmission spectrum. A comparison between the experimental and numerical transmission spectra is given in figure 2.35.



FIGURE 2.34: Sample of the phononic crystal studied in reference [28], also showing the experimental set-up

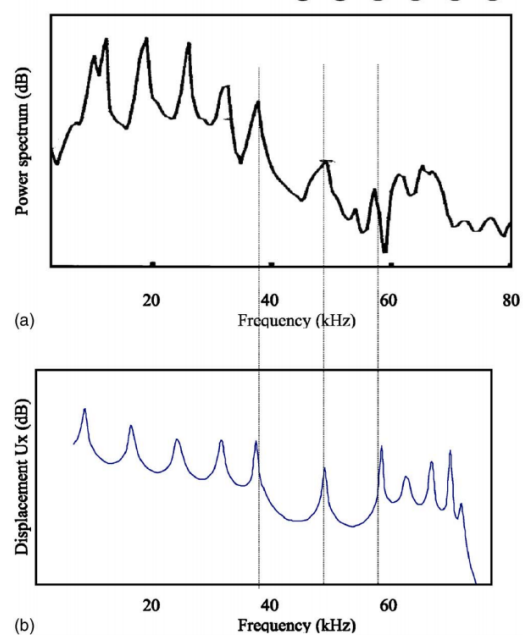


FIGURE 2.35: Experimentally (a) and numerically (b) obtained transmission spectra of a phononic crystal studied in reference [28]

The transmission spectra shows a localized resonance mode amid transmission dip. Furthermore, it can be seen the experimental and numerical value of this resonance frequency are in good agreement.

Graczykowski et al. [21] studied the dispersion and transmission of surface acoustic waves for a pillar-like phononic crystal using FEM. The geometry of the phononic crystal is given in figure 2.36.

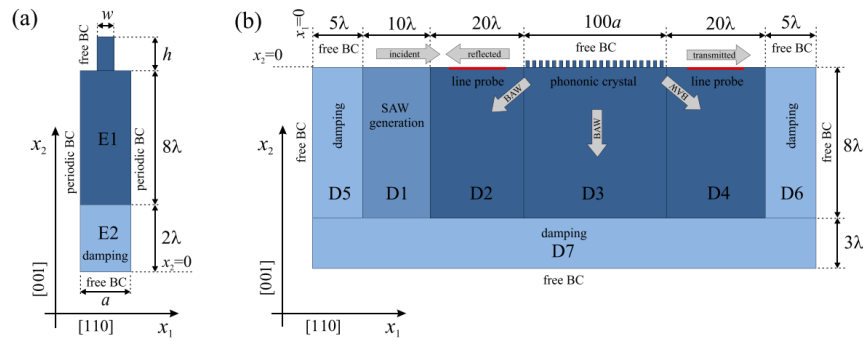


FIGURE 2.36: Phononic crystal structure studied in reference [21]. The unit cell (figure (a)) was used to find the band structure/dispersion relation, while the finite structure (figure (b)) was used to perform the frequency response study

The surface acoustic waves propagate in the x_1 direction, and evanescent in nature in the x_2 direction (referring to the coordinate system in figure 2.36).

The resulting band structure of surface acoustic waves (SAW), transmission, reflection and bulk-to-surface acoustic loss spectra are given in figure 2.37. As a side note, here, in the band structure, they have distinguished different types of SAW: the true SAW modes are shown by the red curves and the pseudo SAW modes are shown by the blue curves. The true and pseudo SAW are distinguished by the magnitude of decay of the wave amplitude as we move towards $-x_2$ direction (the true SAW having more decay, and the pseudo SAW having less decay).

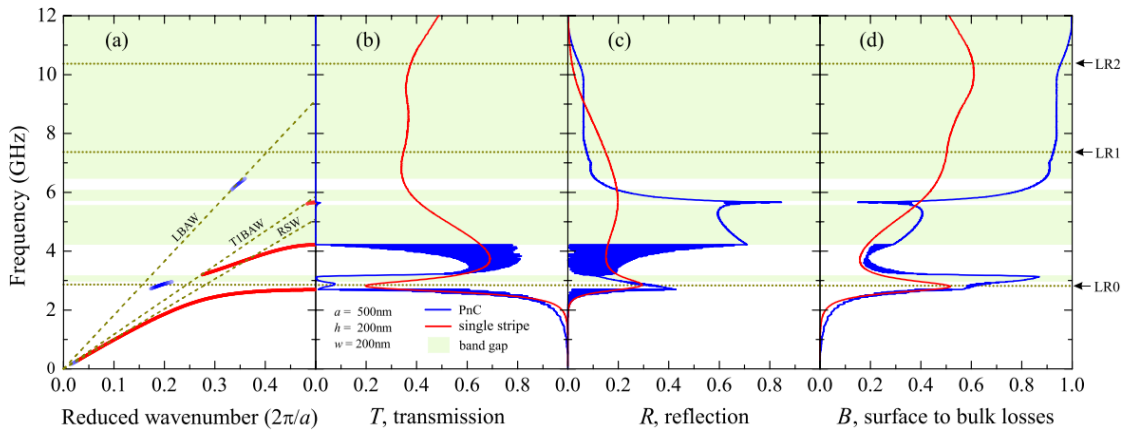


FIGURE 2.37: Band structure (a), transmission (b), reflection (c) and surface-to-bulk losses spectra of the phononic crystal studied in reference [21]. The resulting spectra for the phononic crystal structure are given by the blue curves.

Upon comparing the band gaps of the band structure and the dips in the transmission spectra (given by the blue curve); it can be that they correlate very well: band gaps results in low transmission.

One interesting observation of the band structure is the existence of local resonance in the band gap. This is denoted by a dotted line labelled "LR0" in figure 2.37. This corresponds to local transmission peak (amid the transmission dip) in the transmission spectrum.

The final result from FEM analysis that shall be shown in this section is the result of the study by **Graczykowski et al.** [22]. FEM analysis was performed on a surface phononic crystal (shown in figure 2.38). The band structure for the surface acoustic waves were obtained by FEM and experimental method (called "Brillouin Light Scattering" technique) and it is given in figure 2.39.

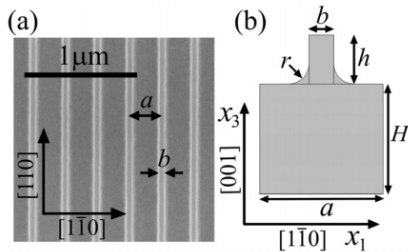


FIGURE 2.38: Sample of the phononic crystal studied in reference [22]

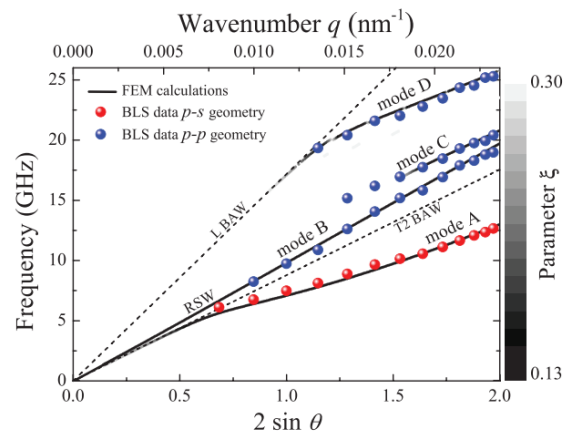


FIGURE 2.39: Experimentally (circles) and numerically (solid lines) obtained dispersion relation of the phononic crystal studied in reference [22]

This example is used to simply illustrate the accuracy of the FEM method; relatively good agreement was found between the FEM method and the experimental data. The general trend of the dispersion curves are in excellent agreement. Discrepancy is on the extent of the existence of the modes.

As a final remark, some of the FEM results were used to investigate waves that are more complicated (multiple wave vector components and direction of propagation/polarization); while in this report the main example of the transfer matrix method was used to tackle simpler problems (one wave vector, one displacement component).

2.2.4 Choice of metamaterial

In this literature study, three types of metamaterials were reviewed: the Helmholtz-resonator (HR) type, the membrane type and the phononic crystal. Studying the interaction of any of the aforementioned metamaterials with TS waves is a valid research area. However, in this thesis,

only one shall be further analyzed in order to answer the research question. The explanation of the choice is given in the subsequent paragraphs.

The discussion begins by considering the HR and membrane type metamaterials. The basis for the working of these metamaterials is resonance. However, in the practice of attenuating acoustic waves, differences exist. The resonance frequency of HR type metamaterial is the frequency in which acoustic waves are attenuated. Around this frequency, the displacement of air within the neck is the largest. In contrast, it is the frequency of anti-resonance (which lies somewhere between two resonance modes) where sound transmission is minimum in the membrane-type metamaterial. The displacements of the membrane structure are minimum around this frequency. In the context of utilizing these two metamaterials for the stabilization of TS waves, it is believed that the traditional working principle of HR type metamaterial is more prone to success. This is because it is necessary for the metamaterial system to have a larger response in order to interact with the TS wave. This is not the traditional working principle of the membrane-type metamaterial, where minimum displacement is sought for.

There are also differences in the geometrical orientation of the metamaterial when used to attenuate acoustic waves. In the case of HR metamaterial, the acoustic wave travels adjacent to it (for instance, see figure 2.5). As for the membrane type, the acoustic wave has to pass through the system. Therefore the orientation of HR type metamaterial is more suitable to dealing with the flow problem (see figure 2.1 for the orientation of flat plate (where a part of the surface would have to be replaced by a metamaterial eventually) in a boundary layer flow).

Finally, this thesis project aims at studying flow stabilization with metamaterials with simpler flow geometry. The HR type metamaterial can be analyzed in a two-dimensional framework, which fits with the two-dimensional boundary layer. On the other hand, the membrane type metamaterial has only been analyzed in the three-dimensional framework. With this, the metamaterial is dropped and further comparison shall be made between the two remaining metamaterials.

Consider the comparison between HR type metamaterial and the phononic crystal. In their interaction with acoustic waves, these materials work with different principles. The HR type metamaterial relies on resonance in attenuating sound as mentioned, whereas the phononic crystal relies on the band gap. This band gap is a result of analysis of (acoustic/elastic) wave propagating *within* the structure. Therefore, in theory there should be no relation with any wave *outside* of the phononic crystal (such as a possible TS wave). However, as highlighted in the literature study, one research showed that it is possible to achieve damping of TS wave's kinetic energy when its frequency lies within the band gap of the phononic crystal [30]. The cited research also highlighted the importance of the resonance frequency within the band gap: as the decrease of TS wave kinetic energy is largest near the resonance. Hence, in the context of TS wave stabilization, resonance is important in both HR type metamaterial and phononic crystal.

The orientation of the phononic crystal can also be made to fit in the geometry of the flat plate boundary layer, as is the case for the HR type metamaterial. Furthermore, a two-dimensional analysis has also been performed in this metamaterial. Hence, the downsides of the membrane type metamaterial are not present in the phononic crystal.

The advantage of phononic crystal over the HR type metamaterial is that there is no risk in assuming the governing physics within the metamaterial in the context of stabilizing TS waves. This shall be explained as follows. In the case of HR type metamaterial, the physics of the fluid is assumed to be governed by acoustic wave equation. The necessity of this assumption comes from the fact that both the air within the flow (i.e. the air on the flat plate) and the air within the HR type metamaterial are continuous (unless a liquid wants to be used to fill the HR).

On the other hand, one does not need to assume the governing physics within a phononic crystal: the classical structural mechanics model should be sufficient. This is because there is a clear difference between the media of flow and the metamaterial. One simply needs to choose the correct structural model.

On the basis of the discussion given in the previous paragraphs, the phononic crystal was chosen as the metamaterial to be further studied in this thesis. The promising numerical result of TS wave stabilization also motivates for the use of phononic crystal. Nevertheless, there are still objectives to fulfil, as given by the following list:

- Investigate if there exists a feasible design space of the phononic crystal for unstable TS wave frequencies with air as the medium.
- Use a more accurate model for the speed of sound in solids.
- Use a more complete PDE for the equation of motion: include displacements in multiple directions.
- Design a shorter phononic crystal
- Perform a frequency-sweep in the FSI simulation
- Investigate other physical properties in the resulting flow domain other than the kinetic energy (such as the disturbance velocity components and/or pressure)

The next chapters shall present the work done in the thesis project. The goal is to simulate the fluid-structure interaction problem with a high degree accuracy numerical simulation. Before that, the condition of this higher accuracy simulation should be chosen properly. This includes choosing the flow conditions (such as freestream velocity and choosing the correct TS waves in which instability exist) and designing the phononic crystal. Chapter 3 treat these problems, as well as explaining the method for the higher accuracy simulation. Chapter 4 presents and discusses the results of the numerical simulation. Finally, chapter 5 concludes this thesis by answering the research questions and giving recommendation in which the present simulation can be improved, which can be used for future studies.

Chapter 3

Methodology

This chapter explains the method used to study of stabilization of TS waves with a metamaterial. As mentioned in section 2.2.4, the chosen metamaterial unit is the **phononic crystal**. The type of the study performed in this thesis is **two-dimensional numerical simulation**.

The methodology is divided into four parts. In the first part (section 3.1), a relatively simple technique of analysis is discussed and employed in order to identify a set of flow conditions which will be studied with high accuracy simulations. In the second part (section 3.2), the phononic crystal is designed with analytical equations according to the chosen simulation conditions. In third part (section 3.3), the method used to simulate the FSI problem shall be explained in detail. Finally, in the last part (section 3.4), the verification and validation procedures shall be described.

3.1 Design of simulation conditions

In this thesis study, the problem of instabilities will be tested on the flow over a flat plate. Part of the flat plate will be replaced by a phononic crystal. An illustration of the problem is given in figure 3.1.

Figure 3.1 shows how the phononic crystal structure should be implemented in practice: a substrate, which is ideally rigid, should support the phononic crystal. However, in the numerical simulation, the supporting structures will be replaced by appropriate boundary conditions. As a remark, the intention is to lubricate the right and left sides of the phononic crystal. The motivation for this is to ensure there is as much displacement of the phononic crystal as possible, in order to obtain larger effects on the flow.

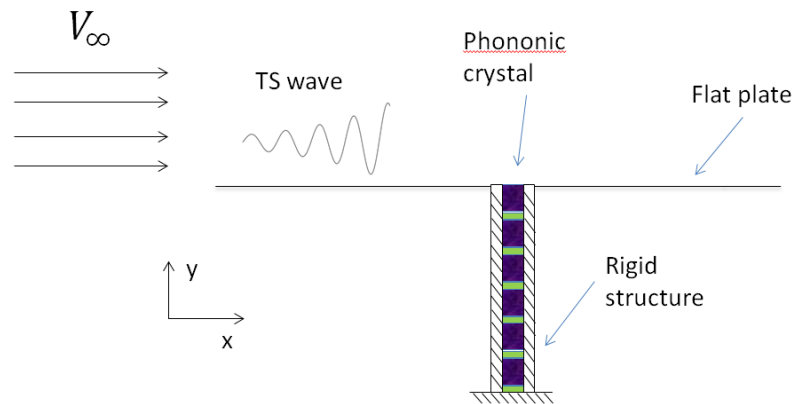


FIGURE 3.1: Sketch of the FSI simulation set-up (not to scale). The rigid structure represents fixed boundary conditions

The choice of the flow conditions stem from three main reasons: (1) the conditions should be attainable with TU Delft's A-Tunnel¹ for future experimental studies, (2) the flow should not violate the incompressible assumption of Orr-Sommerfeld equation and (3) the conditions are used to design the phonic crystal.

As indicated above, the stability analysis for the design of flow conditions was performed using the Orr-Sommerfeld equations (equation 2.8). In the equation, the following variables are important in describing the flow conditions:

1. Freestream velocity V_∞
2. Basic flow field \mathbf{V}
3. Frequency of the TS wave f_{TS}
4. Wavenumber of the TS wave k_{TS}
5. A measure of the amplitude, the so-called N -factor [62]

Two types of stability analysis can be performed, namely a spatial and temporal stability analysis. The former shall be chosen considering the first reason. In experimental conditions, TS waves are typically excited with either a vibrating ribbon (from [55] as mentioned in [54]) or wire [44], acoustics (i.e. with a loudspeaker such as those found in reference [20] and [23]) and plasma actuator [7]. With TU Delft's equipment, it is possible to specify the frequency of the TS wave rather than the wavenumber. This is done with the help of a plasma actuator.

Furthermore, it is known that the incompressible approximation is a reasonable approximation for Mach number below 0.3 as a rule of thumb [1]. Under standard sea-level conditions, a freestream velocity of 20 m/s is below this threshold. Hence, this value of freestream velocity shall be chosen. This velocity is indeed attainable by the A-Tunnel.

As for the basic flow field, this is specified by the geometry of the solid that produces boundary layer: a one-metre flat plate at zero angle of attack. This means that the flow over the body

¹<https://www.tudelft.nl/lr/organisatie/afdelingen/aerodynamics-wind-energy-flight-performance-and-propulsion/facilities/low-speed-wind-tunnels/a-tunnel>

has zero pressure gradient, for which a computation of the velocity profile yields the Blasius velocity profile [3].

A spatial stability diagram is produced using the aforementioned V_∞ and \mathbf{V} with Orr-Sommerfeld equation shown in figure 3.2.

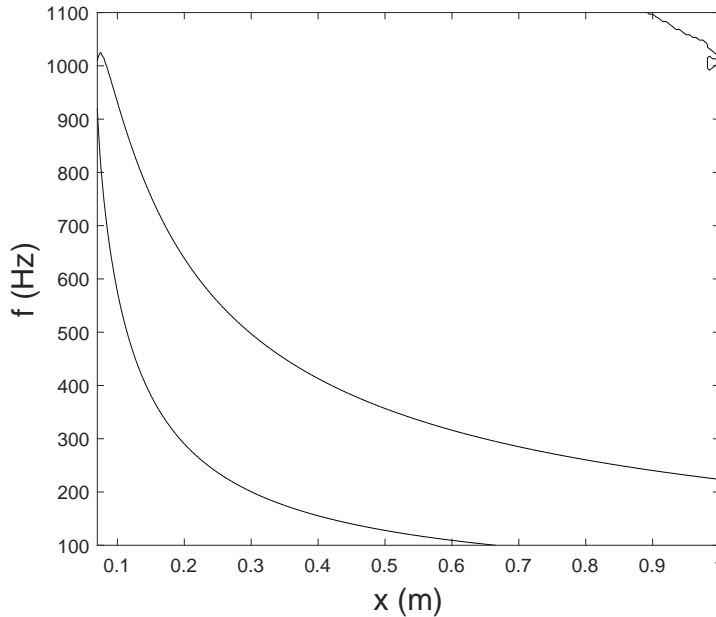


FIGURE 3.2: Stability diagram generated using the Orr-Sommerfeld equation for $V_\infty = 20 \text{ m/s}$. A TS wave which have a combination of frequency and position within the "thumb-like" curve is unstable (in other words, the imaginary part of its wavenumber is negative).

As mentioned in section 2.1, the waves with negative $k_{\text{TS},i}$ have a growing amplitude i.e. unstable. A point shall be chosen inside the thumb-shaped curve (neutral stability line) for the more-detailed stabilization problem with phononic crystal. This point specifies the frequency of the TS wave and the streamwise location of the phononic crystal.

Ideally, the chosen frequency should be close to the eigenfrequency of the phononic crystal (to be elaborated in section 3.2). The process is therefore iterative: starting with an initial choice of frequency, a phononic crystal shall be designed. If the phononic crystal does not have an eigenfrequency close to the initially chosen frequency, then another frequency shall be chosen to accommodate the phononic crystal. At this stage, the initial choice of frequency is 300 Hz. This frequency is also within the frequency range that the plasma actuator can generate.

With the choice of frequency, the other variables that were given in the beginning of this subsection can now be considered. $k_{\text{TS},r}$ and N -factor were also computed along with $k_{\text{TS},i}$, although not shown.

As stated, N -factor is a measure of amplitude. In fact, it is the exponent of the amplitude ratio between the amplitude at a point of instability (lying on the neutral curve) and another point

downstream. It is also equivalent to the integration of the growth rate (in reference [62], the symbol σ was used). Hence, a larger N -factor denotes a larger amplitude. A sufficiently large N -factor is desirable since for future experimental studies, the TS waves have to be properly distinguished from possibly noisy measurements. For the chosen frequency of 300 Hz, the largest N -factor was found to be 2.9244 which is the case at the station $x = 0.65$ m. Hence, this station shall be chosen as the mid-point of the phononic crystal. At this location, $k_{\text{TS},i} \approx 2.73$ rad/m and $\lambda_{\text{TS}} \approx 2.30$ cm.

Finally, an investigation was performed on the wavelength of the TS wave (λ_{TS}) using the computed wavenumber ($\lambda_{\text{TS}} = 2\pi/k_{\text{TS},r}$). For the chosen frequency of 300 Hz, the plot of λ_{TS} against the streamwise coordinate x is given in figure 3.3.

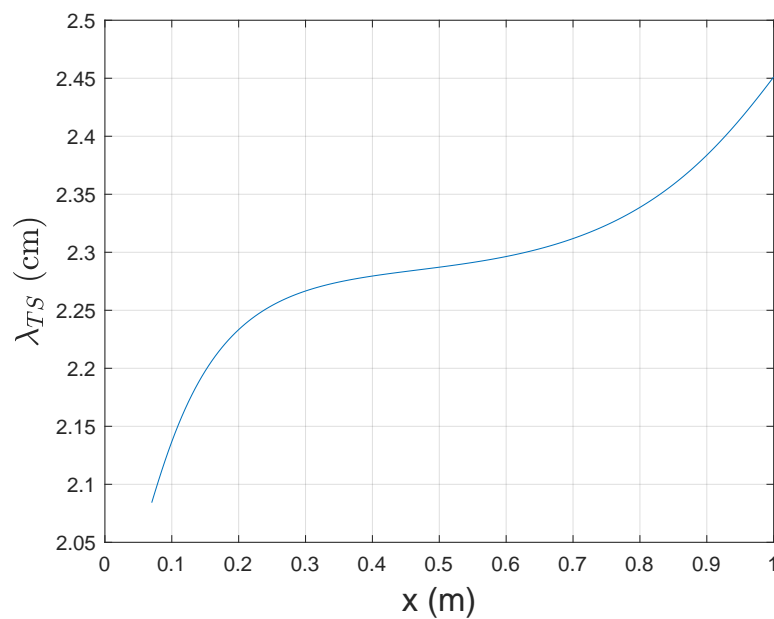


FIGURE 3.3: Wavelength of TS wave (λ_{TS}) over the streamwise direction (x) for $V_\infty = 20$ m/s and $f_{\text{TS}} = 300$ Hz

As can be seen from figure 3.3, the wavelength of the TS wave is in the order of centimetres. Therefore, the width of the phononic crystal (w_{PC}) shall be in the order of millimetres. The advantage of this difference in the order of magnitude of the dimensions is that the fluid-structure interface of the phononic crystal does not experience a large streamwise variation of the pressure. This implies that for the modelling of the load-response of the phononic crystal, a uniform load can be used (instead of a streamwise-varying load). To this end, the width of the phononic crystal is chosen to be 1 mm.

The flow conditions (and some PC specifications) are summarised in table 3.1.

Variable	Value	Unit
V_∞	20	m/s
f_{TS}	300	Hz
N factor at PC	2.92	-
$k_{TS,r}$ at PC	2.73	rad/m
λ_{TS} at PC	2.30	cm
x_{PC}	0.65	m
w_{PC}	1	mm

TABLE 3.1: Design flow and PC conditions

In addition, table 3.2 gives non-dimensionalized quantities of several quantities given in the above table to three significant figures.

Non-dimensional variables	Value
w_{PC}/λ_{TS}	4.35×10^{-2}
$V_\infty x_{PC}/\nu$	8.58×10^5
$V_\infty \delta_{PC}^*/\nu$	1.59×10^3
$f_{TS} \nu/V_\infty^2$	1.14×10^{-5}

TABLE 3.2: Non-dimensional quantities of the flow condition

3.2 Design of the phononic crystal

Two properties of the phononic crystal are investigated: the band structure/dispersion relation and the eigenfrequency that lies within the band structure. The first property is desirable in order to find the band gap frequencies of the phononic crystal, which, according to the result of reference [30], correlates with an out-of-phase response. On the other hand, the second property (eigenfrequency) is desirable to find the forcing frequency that yields a large displacement. Overall, the aim is to have an out-of-phase displacement (with respect to the harmonic pressure load that is imposed by the TS wave) with as large displacement as possible. This aim was also described in reference [30].

To obtain the aforementioned properties, analytical results from two methods of analysis shall be used. The dispersion curve of the phononic crystal can be obtained from the analytical result given by the Transfer Matrix Method and Interface Response theory. This shall be discussed in more detail in section 3.2.1. The eigenfrequency that lies within the band gap can be obtained using the analytical result given by the Interface Response Theory, which shall be discussed in detail in section 3.2.2. Final, the results of applying the two aforementioned methods are shown by giving the chosen unit cell (in section 3.2.3).

3.2.1 Dispersion relation of the phononic crystal

The Transfer Matrix method for the analysis of multilayered media has been discussed in several papers, as given in the literature study (section 2.2.3). Analytical results of the dispersion relation have been derived in previous papers for specific cases. However, it is thought to be beneficial to outline the method again in this report, in order to be able to reflect upon the assumptions used on the modelling of the phononic crystal.

The outline of the Transfer Matrix method shall follow closely the one given in reference [31]. However, the starting point is different: in this thesis report, the equation of motion is given by the full three-dimensional equation for a linearly elastic, isotropic solids: [40]:

$$\rho \frac{\partial^2 \mathbf{u}}{\partial t^2} = (\lambda + \mu) \nabla (\nabla \cdot \mathbf{u}) + \mu \nabla^2 \mathbf{u} \quad (3.1)$$

where ρ is the solid mass density, $\mathbf{u} = [u_x \ u_y \ u_z]^T$ is the displacement field, t is time, and λ and μ are Lamé's constants. It is noted that the material properties (λ and μ) are out of the spatial derivatives, as is the case in the general equation of motion for any solids (see, for instance, reference [21] where the material properties are embedded in the elements of the generalized stiffness tensor). This is because the equation of motion will be applied to each layer separately, where the layer is homogeneous.

The phononic crystal geometry for the analysis is given in the following figure.

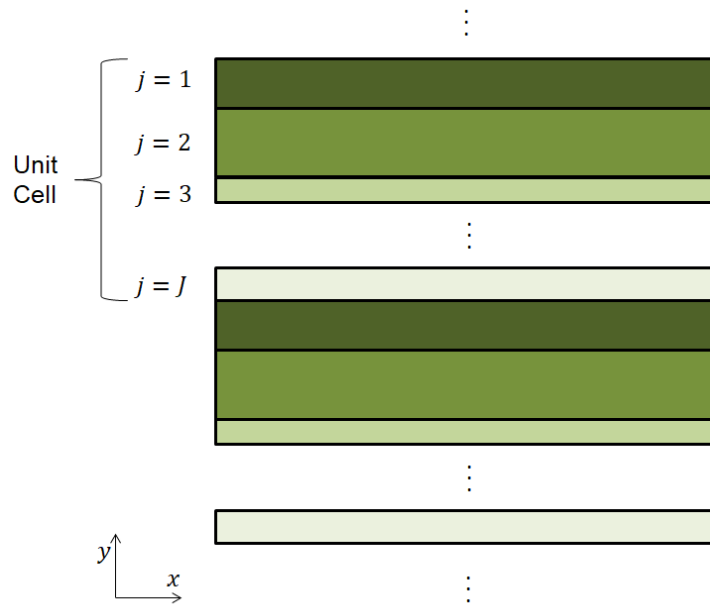


FIGURE 3.4: Geometry of the PC

The phononic crystal has infinitely repeating unit cells, and within a unit cell there are J layers. Later on, this infinite number of unit cells is represented by a periodic boundary condition.

Important properties that define the j^{th} layer are ρ_j , λ_j , μ_j , and d_j (layer thickness or length of the layer in the y direction). As a side note, λ_j and μ_j shall be replaced by engineering constants E_j (Young's modulus) and ν_j (Poisson's ratio), which are also enough to describe the displacement field of a linearly elastic, isotropic solids.

It is also remarked that the orientation of the phononic crystal is vertical, as is the case for the fluid-structure interaction problem (figure 3.3). Consequently, the direction parallel (x) and perpendicular to the layers (y) of figure 3.4 are aligned with the streamwise and wall-normal direction respectively.

Returning to the equations of motion, the following simplifications were made in order to reduce the problem into being one-dimensional: spatial derivatives in the x and z directions are zero (where z is the direction normal to the page). Furthermore, considering the context of the FSI problem, it is assumed that the phononic crystal primarily deforms in the y direction as the pressure wave (due to pressure fluctuation from TS waves) imposes much greater stress onto the structure than the shear-stress wave due to fluctuation in the flow velocities (this assumption is applied only for the design of the phononic crystal; in the full FSI simulation, this assumption was dropped). Hence, the equations for the displacement in y is considered, whereas the equation for the displacement in x is disregarded.

The equation for the displacement of structure in the y direction is given as follows:

$$\rho \frac{\partial^2 u_y}{\partial t^2} = (\lambda + 2\mu) \frac{\partial^2 u_y}{\partial x^2} \quad (3.2)$$

Upon closer observation, this equation is in fact a one-dimensional wave equation with the following wave speed:

$$c = \sqrt{\frac{\lambda + 2\mu}{\rho}} \quad (3.3)$$

This wave speed is in fact the same as the one derived for a three-dimensional problem [40]. Furthermore, the wave speed can be expressed in terms of Young's modulus (E) and Poisson's ratio (ν) [40] as follows:

$$c = \sqrt{\frac{E(1 - \nu)}{\rho(1 + \nu)(1 - 2\nu)}} \quad (3.4)$$

From here on, the steps to derive a Transfer Matrix formulation of the structural problem follows from reference [31]. This is outlined as follows:

1. Starting from the first layer of the unit cell (see figure 3.4), take travelling waves as the solution of equation 3.2. Explicitly, this is given by:

$$u_{y,1}(y, t) = (A_{+,1}e^{ik_1y} + A_{-,1}e^{-ik_1y})e^{-i\omega t} \quad (3.5)$$

where with $e^{-i\omega t}$ time dependence, $A_{+,1}$ and $A_{-,1}$ represent the amplitude of the wave travelling in the positive and negative y direction respectively. The subscript 1 denotes quantities that belong to the first layer. Furthermore, k_1 is the wavenumber and ω is the angular frequency. This wavenumber is given by $k_1 = \omega/c_1$.

2. Derive the stress (σ) from u_y using the following equation:

$$\sigma_1 = (\lambda_1 + \mu_1) \frac{\partial u_{y,1}}{\partial y} \quad (3.6)$$

3. Collect $u_{y,1}$ and σ_1 in a vector, say, vector \mathbf{y}_1 . Similarly, collect $A_{+,1}$ and $A_{-,1}$ in another vector, say, vector \mathbf{b} . The two are related by a matrix, say, matrix \mathbf{A} , as follows:

$$\mathbf{y}_1 = \mathbf{A}_1 \mathbf{b}_1 \quad (3.7)$$

The elements of the matrix are easily derived from equation 3.5 and 3.6. It is noted that the above equation relates \mathbf{a} to \mathbf{y} at any point in the layer, including the interfaces.

4. Relate \mathbf{y} at the top interface of a layer to the bottom interface of the same layer. This yields another matrix, say, matrix \mathbf{B}_1 :

$$\mathbf{y}_1^{\text{bottom}} = \mathbf{A}_1 \mathbf{B}_1 \mathbf{b}_1^{\text{top}} \quad (3.8)$$

The elements of matrix \mathbf{B}_1 are easily derived using equation 3.5, 3.6, and noting that there is a shift of d_j between the two interfaces.

5. Use equation 3.7 to express $\mathbf{a}_1^{\text{top}}$ in terms of $\mathbf{y}_1^{\text{top}}$, and substitute this into equation 3.8:

$$\mathbf{y}_1^{\text{bottom}} = \mathbf{A}_1 \mathbf{B}_1 \mathbf{A}_1^{-1} \mathbf{y}_1^{\text{top}} \quad (3.9)$$

6. Apply continuity of displacement and stress at the layer interface: $\mathbf{y}_2^{\text{top}} = \mathbf{y}_1^{\text{bottom}}$. Upon closer observation, this means that $\mathbf{A}_1 \mathbf{B}_1 \mathbf{A}_1^{-1}$ is the Transfer Matrix that relates $\mathbf{y}_2^{\text{top}}$ with $\mathbf{y}_1^{\text{top}}$. Therefore, denote $\mathbf{T}_1 = \mathbf{A}_1 \mathbf{B}_1 \mathbf{A}_1^{-1}$ and this yields:

$$\mathbf{y}_2^{\text{top}} = \mathbf{T}_1 \mathbf{y}_1^{\text{top}} \quad (3.10)$$

7. It can be seen that this process can be repeated multiple times going through successive layers to relate $\mathbf{y}_J^{\text{bottom}}$ with $\mathbf{y}_1^{\text{top}}$. One would then find a multiplication of Transfer Matrices as one travels through the layers:

$$\mathbf{y}_J^{\text{bottom}} = \mathbf{T}_J \mathbf{T}_{J-1} \dots \mathbf{T}_1 \mathbf{y}_1^{\text{top}} \quad (3.11)$$

The multiplication of Transfer Matrices yields the Transfer Matrix of the unit cell, denoted as \mathbf{T} :

$$\mathbf{T} = \mathbf{T}_J \mathbf{T}_{J-1} \dots \mathbf{T}_1 \quad (3.12)$$

8. An infinitely repeating unit cells is considered to find the dispersion relation. Applying Bloch's [59][65] (or Floquet's [31][58]) theorem to account for the periodicity of the top and the bottom of the unit cell yields:

$$\mathbf{y}_J^{\text{bottom}} = e^{iqD} \mathbf{y}_1^{\text{top}} \quad (3.13)$$

where q is the Bloch's (or Floquet's) wavenumber and $D = \sum_{j=1}^J d_j$ is the thickness of the unit cell.

9. Use equation 3.11 and 3.13 to eliminate $\mathbf{y}_j^{\text{bottom}}$. Furthermore, drop the subscript and superscript in $\mathbf{y}_1^{\text{top}}$. This results in:

$$\mathbf{T}\mathbf{y} = e^{iqD}\mathbf{y} \quad (3.14)$$

The condition for the non-trivial solutions yields the dispersion relation (relation between ω and q) of the phononic crystal:

$$\det(\mathbf{T} - \mathbf{I}e^{iqD}) = 0 \quad (3.15)$$

In this thesis, designs of two- and three-layer unit cells are investigated ($J = 2$ and $J = 3$ respectively). The motivation for investigating a three-layer unit cell in addition to the two-layer unit cell is to see if the three-layer unit cell can yield a shorter unit cell given the chosen f_{TS} ; as the problem of lengthy unit cell was prevalent in reference [30].

The dispersion relation for the two-layer unit cell shall be derived in detail in the following paragraphs. The dispersion relation for the three-layer unit cell follows the same steps, and only the result will be shown.

The elements of T_j has been computed explicitly by Hussein et al. and shown in reference [31]. This is given in equation 3.16.

$$\mathbf{T}_j = \begin{bmatrix} C_j & \frac{1}{Z_j}S_j \\ -Z_jS_j & C_j \end{bmatrix} \quad (3.16)$$

where $C_j = \cos\left(\frac{\omega d_j}{c_j}\right)$, $S_j = \sin\left(\frac{\omega d_j}{c_j}\right)$, and $Z_j = \rho_j c_j \omega$. For brevity, the elements of \mathbf{T}_j will be shortened as follows:

$$\mathbf{T}_j = \begin{bmatrix} a_j & b_j \\ c_j & a_j \end{bmatrix} \quad (3.17)$$

The Transfer Matrix of the two-layer unit cell is therefore given by:

$$\begin{aligned} \mathbf{T} &= \begin{bmatrix} a_1 & b_1 \\ c_1 & a_1 \end{bmatrix} \begin{bmatrix} a_2 & b_2 \\ c_2 & a_2 \end{bmatrix} \\ &= \begin{bmatrix} a_1a_2 + b_1c_2 & a_1b_2 + b_1a_2 \\ c_1a_2 + a_1c_2 & c_1b_2 + a_1a_2 \end{bmatrix} \end{aligned} \quad (3.18)$$

Substituting the above into equation 3.15 yields:

$$\det \left(\begin{bmatrix} a_1 a_2 + b_1 c_2 - e^{iqD} & a_1 b_2 + b_1 a_2 \\ c_1 a_2 + a_1 c_2 & c_1 b_2 + a_1 a_2 - e^{iqD} \end{bmatrix} \right) = 0 \quad (3.19)$$

This determinant can be expanded and simplified as follows:

$$(a_1 a_2 + b_1 c_2 - e^{iqD})(c_1 b_2 + a_1 a_2 - e^{iqD}) - (a_1 b_2 + b_1 a_2)(c_1 a_2 + a_1 c_2) = 0$$

$$\begin{aligned} a_1 a_2 c_1 b_2 + (a_1 a_2)^2 - a_1 a_2 e^{iqD} + b_1 c_2 c_1 b_2 + b_1 c_2 a_1 a_2 - b_1 c_2 e^{iqD} - c_1 b_2 e^{iqD} - a_1 a_2 e^{iqD} \\ + (e^{iqD})^2 - a_1 b_2 c_1 a_2 - a_1^2 b_2 c_2 - b_1 c_1 a_2^2 - b_1 a_2 a_1 c_2 = 0 \end{aligned}$$

Next, group terms with according to the power of e^{iqD} :

$$(e^{iqD})^2 + e^{iqD}[-2a_1 a_2 - b_1 c_2 - c_1 b_2] + (a_1 a_2)^2 + b_1 c_2 c_1 b_2 - a_1^2 b_2 c_2 - b_1 c_1 a_2^2 = 0$$

Furthermore, divide both sides by e^{iqD} (which is not equal to zero):

$$e^{iqD} + [-2a_1 a_2 - b_1 c_2 - c_1 b_2] + e^{-iqD}[(a_1 a_2)^2 + b_1 c_2 c_1 b_2 - a_1^2 b_2 c_2 - b_1 c_1 a_2^2] = 0$$

Now, to further simplify the equation, apply Euler's identity ($e^{iqD} = \cos(kD) + i \sin(kD)$). Additionally, separate the real and imaginary part:

$$\begin{aligned} \left(\cos(kD)[1 + (a_1 a_2)^2 + b_1 c_2 c_1 b_2 - a_1^2 b_2 c_2 - b_1 c_1 a_2^2] + [-2a_1 a_2 - b_1 c_2 - c_1 b_2] \right) \\ + i \left(\sin(kD)[1 - (a_1 a_2)^2 - b_1 c_2 c_1 b_2 + a_1^2 b_2 c_2 + b_1 c_1 a_2^2] \right) = 0 \end{aligned}$$

Compare the imaginary part of both sides of the equation. Since $\sin(kD)$ is not always equal to 0, the following condition has to hold:

$$1 = (a_1 a_2)^2 + b_1 c_2 c_1 b_2 - a_1^2 b_2 c_2 - b_1 c_1 a_2^2$$

Now, compare the real part. The equation for the real part can be further simplified by using the result above, which gives:

$$\cos(kD)[1 + 1] + [-2a_1 a_2 - b_1 c_2 - c_1 b_2] = 0$$

$$\cos(kD) = a_1 a_2 + \frac{1}{2}(b_1 c_2 + c_1 b_2)$$

Finally, the elements a_1 , a_2 , b_1 , b_2 , c_1 and c_2 can be replaced by the original terms upon comparison of equation 3.16 with equation 3.17. This results in the dispersion relation for the two-layer unit cell:

$$\boxed{\cos(qD) = C_1 C_2 - \frac{1}{2} \left(\frac{Z_1}{Z_2} + \frac{Z_2}{Z_1} \right) S_1 S_2} \quad (3.20)$$

The equation was also derived in reference [10] and [58]. The former reference used the Interface Response Theory in the derivation, while the latter reference followed similar steps in analyzing the dynamics of the phononic crystal although without going through the Transfer Matrix formalism.

To derive the dispersion relation for a three-layer unit cell is obtained using the same steps, this time setting $J = 3$. The resulting dispersion relation is given in equation 3.21.

$$\boxed{\cos(qD) = C_1 C_2 C_3 - \frac{1}{2} \left[\left(\frac{Z_1}{Z_2} + \frac{Z_2}{Z_1} \right) C_3 S_1 S_2 + \left(\frac{Z_2}{Z_3} + \frac{Z_3}{Z_2} \right) C_1 S_2 S_3 + \left(\frac{Z_1}{Z_3} + \frac{Z_3}{Z_1} \right) C_2 S_1 S_3 \right]} \quad (3.21)$$

It is noted that in the dispersion relation (equation 3.20 and 3.21) takes frequency (ω) as input, and Bloch's wavenumber (q) as output. This output can be either real or complex. The output is complex when the right-hand side of the dispersion relation is greater than one. In fact, the range of frequencies for which q is complex gives the band gap of the phononic crystal.

Now that the dispersion relations have been obtained, the analytical equation that gives the eigenfrequency that lies within the band gap shall be derived. This is done in the next section.

3.2.2 Band gap eigenfrequency of the phononic crystal

This section begins by giving a reminder: the goal for finding the eigenfrequency within the band gap of a phononic crystal is to choose f_{TS} which coincides or is very close to exciting resonance. The benefit is that the displacement of the structure interface imposes a relatively large effect on the flow. This eigenfrequency gives rise to the "surface mode" of the phononic crystal [10]. The name "surface mode" refers to the nature of wave propagation with frequencies within the band gap: that the displacements are dominant near the surface and attenuates as one travels down the layers [5].

As mentioned in the literature study of the phononic crystal (section 2.2.3), there is exactly one eigenfrequency within the band gap of the phononic crystal according to the Interface Response Theory (IRT). Additionally, this eigenfrequency does not depend on the number of unit cells.

This section gives the mathematical steps in detail in deriving the analytical formulation for finding this eigenfrequency (closely following the guidance given in chapter 3 of P. A. Deymier [10]). The reason for this extensive mathematical detail is that the final analytical formula (equation 3.27) turns out to be different than the one found in reference [10]. Hence, this

section does not discuss the Interface Response Theory, but rather uses existing results of the theory to derive a new formula for the phononic crystal analysis.

The goal is to obtain the inverse Green's function of the phononic crystal's unit cell, that is generally given in the following form [10]:

$$g^{-1}(MM) = \begin{bmatrix} a & b \\ b & c \end{bmatrix} \quad (3.22)$$

where M denotes the interface space (i.e. the boundaries of the phononic crystal). This inverse Green's function is built up from the Green's function of the layers that constitute the unit cell, which is given by [10]:

$$g_j^{-1}(MM) = \begin{bmatrix} -\omega Z_j C_j / S_j & \omega Z_j / S_j \\ \omega Z_j / S_j & -\omega Z_j C_j / S_j \end{bmatrix} \quad (3.23)$$

In the above equation, $Z_j = \rho_j c_j$ (which is different from the definition of Z_j given in the discussion of the Transfer Matrix method with the absence of ω). Similar to the Transfer Matrix discussion, the entries of $g_j^{-1}(MM)$ will be shortened as follows:

$$g_j^{-1}(MM) = \begin{bmatrix} a_j & b_j \\ b_j & a_j \end{bmatrix} \quad (3.24)$$

To obtain the inverse Green's function of the unit cell, the inverse Green's functions of the layers are linearly juxtaposed, creating a $(J + 1) \times (J + 1)$ matrix. In this report, the derivation is discussed in more detail for $J = 2$. The resulting juxtaposition of inverse Green's function is given by:

$$g_{UC}^{-1} = \begin{bmatrix} a_1 & b_1 & 0 \\ b_1 & a_1 + a_2 & b_2 \\ 0 & b_2 & a_2 \end{bmatrix}$$

Next, this matrix is inverted. This gives:

$$g_{UC} = \frac{1}{a_1 a_2 (a_1 + a_2) - a_1 b_2^2 - a_2 b_1^2} \begin{bmatrix} a_2(a_1 + a_2) - b_2^2 & -a_2 b_1 & b_1 b_2 \\ -b_1 a_2 & a_1 a_2 & -a_1 b_2 \\ b_1 b_2 & -a_1 b_2 & a_1(a_1 + a_2) - b_1^2 \end{bmatrix}$$

Now, the corner elements are taken and put into a new matrix as only the elements that belong to the interface space are necessary. This results in a 2×2 matrix:

$$g(MM) = \frac{1}{a_1 a_2 (a_1 + a_2) - a_1 b_2^2 - a_2 b_1^2} \begin{bmatrix} a_2(a_1 + a_2) - b_2^2 & b_1 b_2 \\ b_1 b_2 & a_1(a_1 + a_2) - b_1^2 \end{bmatrix}$$

Finally, this matrix is inverted again to obtain the inverse Green's function of the unit cell:

$$g^{-1}(MM) = \frac{1}{a_1 + a_2} \begin{bmatrix} a_1(a_1 + a_2) - b_1^2 & -b_1b_2 \\ -b_1b_2 & a_2(a_1 + a_2) - b_2^2 \end{bmatrix} \quad (3.25)$$

The surface mode of the phononic crystal (which corresponds to the eigenfrequency that lies within the band gap) can be obtained from the elements of the general inverse Green's function (equation 3.22) through the following equation:

$$ac - b^2 = 0 \quad (3.26)$$

The mathematical details on the derivation of the above equation was given by E. H. El Boudouti and B.Djafari-Rouhani in reference [10]. It is simply remarked here that the equation for the surface mode coincides with the determinant of the inverse Green's function.

Comparing equation 3.22 and 3.25, the equation for the surface mode simplifies into:

$$\frac{(a_1(a_1 + a_2) - b_1^2)(a_2(a_1 + a_2) - b_2^2) - (b_1b_2)^2}{a_1 + a_2} = 0$$

Expanding the terms in the numerator on the left-hand side yields:

$$\frac{a_1a_2(a_1 + a_2)^2 - a_1b_2^2(a_1 + a_2) - a_2b_1^2(a_1 + a_2) + (b_1b_2)^2 - (b_1b_2)^2}{a_1 + a_2} = 0$$

Simplifying the terms further yields:

$$a_1a_2(a_1 + a_2) - a_1b_2^2 - a_2b_1^2 = 0$$

The terms above are further re-arranged into the following:

$$a_1(a_2^2 - b_2^2) + a_2(a_1^2 - b_1^2) = 0$$

Now, drop the temporary shortened notation and put the true elements of the inverse Green's function by comparing equation 3.23 with equation 3.24. Furthermore, omit ω as it can be factored out of the equation. This yields:

$$Z_1 \frac{C_1}{S_1} \left(Z_2^2 \frac{C_2^2}{S_2^2} - \frac{Z_2^2}{S_2^2} \right) + Z_2 \frac{C_2}{S_2} \left(Z_1^2 \frac{C_1^2}{S_1^2} - \frac{Z_1^2}{S_1^2} \right) = 0$$

The above equation can be further simplified by using the trigonometric identity $C_j^2 - 1 = -S_j^2$:

$$Z_1 Z_2^2 \frac{C_1}{S_1} + Z_2 Z_1^2 \frac{C_2}{S_2}$$

Then, divide both sides by $Z_1 Z_2$

$$Z_2 \frac{C_1}{S_1} + Z_1 \frac{C_2}{S_2} = 0$$

Finally, multiply both sides by $S_1 S_2$. This gives the analytical result for the surface mode of a two-layer unit cell phononic crystal:

$$\boxed{Z_1 S_1 C_2 + Z_2 S_2 C_1 = 0} \quad (3.27)$$

It is remarked that the above equation has ω as the unknown; other variables depend on the unit cell. The zero of the equation that lies within the band gap frequency range gives the surface mode of the phononic crystal. In the results given in this thesis report, the zero is obtained numerically using the bisection method, giving the two end points of the band gap interval as inputs.

As a reminder, this result is not the same as chapter 3 of Deymier [10], although the same steps for the derivation laid down in the reference were followed.

Finally, equation 3.27 has been verified by comparison with the problem studied by Hussein et al. in reference [30]. The "truncation frequency" in the reference paper refers to the eigenfrequency in the band gap. For the phononic crystal studied in the reference paper, the truncation frequency was given to be 1685.2 Hz. Using equation 3.27, the eigenfrequency of the same phononic crystal was obtained to be 1687.5 Hz, which is very close to the one given in the aforementioned reference. This discrepancy is attributed to the fixed boundary condition, as shall be further supported by the results given in section 4.1. It is noted that using the equation given in chapter 3 of [10], the eigenfrequency is given to be 2101.6 Hz, which is far from 1687.5 Hz. The resulting equation [10] was also further verified using FEM analysis, as shall be further corroborated in section 4.1.

Performing the same analysis for $J = 3$ results in the analytical equation for three-layer unit cell phononic crystal:

$$\boxed{\begin{aligned} & (Z_1 C_1)^2 S_2 S_3 (Z_2 Z_3 C_2 C_3 - Z_3^2 S_2 S_3) \\ & + Z_1 Z_2 Z_3 C_1 C_2 C_3 C_1 (Z_2 C_2 S_3 + Z_3 C_3 S_2) \\ & \quad + Z_3^2 S_2 (Z_1^2 S_2 - Z_1 Z_2 C_1 C_2 S_1) \\ & \quad \quad - Z_1 Z_2^2 Z_3 C_1 C_3 S_1 S_1 \\ & - Z_1^2 S_2 C_3 (Z_2 Z_3 C_2 S_3 + Z_3^2 C_3 S_2) = 0 \end{aligned}} \quad (3.28)$$

Again, the above equation was verified with FEM analysis, as shall be seen in section 4.1.

3.2.3 Chosen design of the phononic crystal's unit cell

This section discusses how the unit cell is chosen using the equations developed in the two previous sections, and presents the final design of the unit cell and its relevant properties.

As mentioned in section 3.2.1, two and three unit cell designs are investigated. The reason for this is to see if it is possible to reduce the length of the unit cell (D) by adding a layer. This problem of length concerns the practicality of experimental studies for future researches; and this was indeed a feasibility problem in reference [30].

The materials to be investigated for the two unit cell design are rubber² and aluminium³. As for the three unit cell design, a layer of steel³ is added. These material properties are given in table 3.3.

	ρ (kg/m ³)	E (GPa)	ν (-)
Rubber	1300	1.04×10^{-3}	0.3
Aluminium	2710	70	0.34867
Steel	7850	200	0.3119

TABLE 3.3: Material properties for the two and three unit cell designs

The layer properties that determine the band structure and surface mode eigenfrequency (f_{SM}) are ρ_j , c_j and d_j (see equations 3.20, 3.21, 3.27 and 3.28). By choosing the material of the layers, ρ_j and c_j are specified. The only thing left to be chosen are the layer thickness (d_j). To do this, a python program was written which computes f_{SM} of different combinations of d_j for both the two and three unit cell designs. f_{SM} was calculated by finding the zero of equation 3.27 and/or 3.28 with bisection method, using the edges of the band gap as inputs. These band gap edges were found from equation 3.20 and/or 3.21. The aim of this program is to see which combinations of d_j produces f_{SM} near the chosen f_{TS} . This results in the design space. Figure 3.5 and 3.6 show the results of this program.

²Properties derived from reference [65]

³Properties derived from reference https://www.efunda.com/materials/common_matl/Common_Matl.cfm?MatlPhase=Solid&MatlProp=Acoustic#Acoustic and https://www.efunda.com/materials/common_matl/Common_Matl.cfm?MatlPhase=Solid&MatlProp=Physical#Physical (LAST ACCESSED ON 30/05/2021)

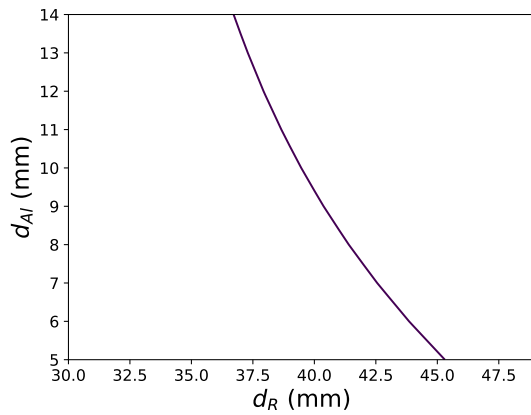


FIGURE 3.5: Design space of the two-layer unit cell phononic crystal

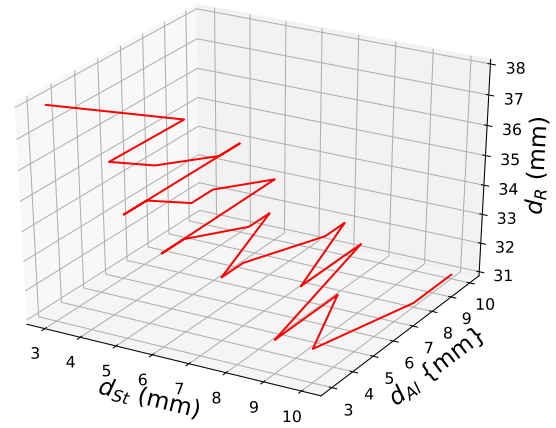


FIGURE 3.6: Design space of the three-layer unit cell phononic crystal

The combinations of d_j that yields f_{SM} near the chosen f_{TS} are those that lie within the curves in the two plots above. As a remark, layer thicknesses in the order of millimeters are sought; considering the dimension of TU Delft A-tunnel for possible future researches. Returning to the curves, the point that gives the minimum unit cell thickness D is chosen. This yielded $D = 50$ mm and $D = 43$ mm for the two and three unit cell design respectively. This shows that by adding a layer in the unit cell, it is possible to minimize the thickness of the unit cell for the purpose of obtaining a certain surface mode frequency.

With this, the unit cell for the two- and three-layer designs are chosen. Their properties are summarized in table 3.4. Furthermore, the dispersion curves are given in figure 3.7 and 3.8. In these two figures, the red dot represents the location of f_{SM} while the green-shaded region emphasizes the band gap frequencies.

	Two-layer	Three-layer
d_R (mm)	44	35
d_{Al} (mm)	6	3
d_{Steel} (mm)	-	5
D (mm)	50	43
f_{SM} (Hz)	299.13	300.76

TABLE 3.4: Two- and three-layer design unit cell properties

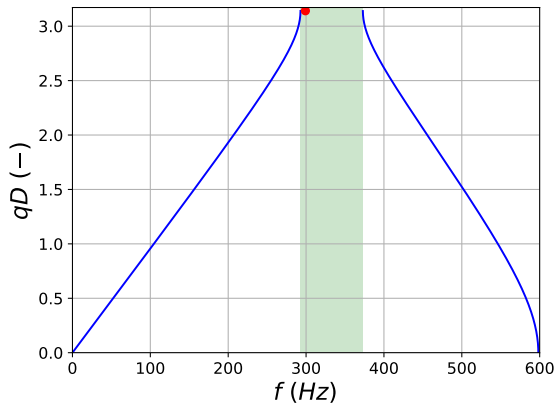


FIGURE 3.7: Dispersion curve of the two layer design (44 mm rubber and 6 mm aluminium)

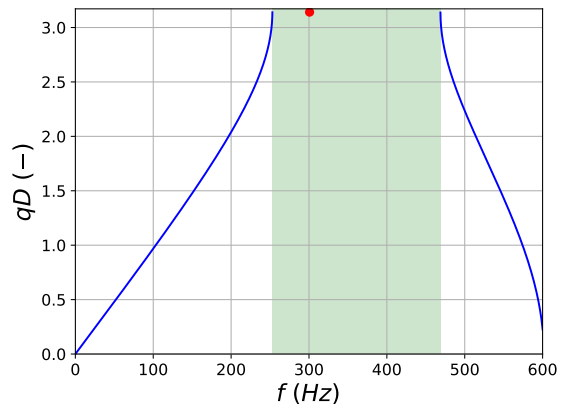


FIGURE 3.8: Dispersion curve of the three layer design (35 mm rubber, 3 mm aluminium and 5 mm steel)

The only variable to be chosen for the phononic crystal is the number of unit cells (N_{UC}). This variable could not have been chosen with the help of the methods developed in section 3.2.1 and 3.2.2. Indeed, from the two theories used so far, the resulting band structure and f_{SM} are independent of N_{UC} . The N_{UC} shall be determined with a different analysis, namely discretizing the governing partial differential equation with finite elements method (FEM) as shall be seen in section 4.1

3.3 Simulation method

The numerical simulations were performed using COMSOL Multiphysics® version 5.6[6]. This software numerically solves partial differential equations using the finite elements discretization method. In the simulations performed, only spatial discretization was relevant. Quadratic elements were used to represent the solution. In the fluid domain, quadratic Lagrange elements were used (9 nodes per quadrilateral element); whereas incomplete quadratic elements (quadratic serendipity, 8 nodes per quadrilateral element) were used in the solid domain.

Three types of simulations were performed, to be elaborated in the following paragraphs.

3.3.1 Structural analysis simulation

This simulation studied the properties of the designed phononic crystal in isolation (without the flow). The aim is to verify the properties of the phononic crystal predicted by the design method with a more accurate model. In this simulation, the structural mechanics module of COMSOL® was employed. Linear elastic material was used to model the layers of the phononic crystal. Consequently, the same constitutive properties used in the phononic crystal design (E and ν) were re-used.

However, the option of geometric non-linearity was enabled. This option was selected to account for in the case of possibly large deformations. In this geometrically non-linear case, the constitutive equation relates the second Piola-Kirchoff stress to the Green-Lagrange strain. This is different from the partial differential equation used in designing the phononic crystal, where the first Piola-Kirchoff stress is related to the infinitesimal strain. Nevertheless, in both cases the unknowns are the structural displacement field (\mathbf{u}).

The governing equations are mathematically illustrated as follows. In the absence of body force, the equation of motion for a continuum solved in the material (Lagrangian) frame (which is used to model solids) is given by:

$$\nabla \cdot \sigma = \rho \frac{\partial^2 \mathbf{u}}{\partial t^2} \quad (3.29)$$

where σ is the first Piola-Kirchoff stress tensor and \mathbf{u} is the structural displacement. This stress tensor is obtained when the Cauchy's stress tensor is transformed from the spatial (Eulerian) frame to the Lagrangian frame.

The constitutive model is obtained by relating σ to a measure of strain. As mentioned in the previous paragraph, the constitutive model is given by a linear relation between the Second Piola-Kirchoff stress (\mathbf{S}) and the Green-Lagrange strain measure (\mathbf{E}):

$$\mathbf{S} = \mathbb{C}\mathbf{E} \quad (3.30)$$

with \mathbb{C} being a fourth-order tensor, representing the generalized stiffness. The elements in this tensor are fully specified (for an isotropic solid) given a Young's modulus and Poisson's ratio. The second Piola-Kirchoff stress is related to the first Piola-Kirchoff stress through the following:

$$\sigma = \mathbf{F}\mathbf{S} \quad (3.31)$$

where F is the deformation gradient, which, by definition, is given by:

$$\mathbf{F} = \mathbf{I} + \nabla \mathbf{u} \quad (3.32)$$

with \mathbf{I} being the identity matrix.

Furthermore, the Green-Lagrange strain measure is defined in terms of the structural displacement by:

$$\mathbf{E} = \frac{1}{2}(\mathbf{F}^T \mathbf{F} - \mathbf{I}) \quad (3.33)$$

Equation 3.29 to 3.33 form a partial differential equation for the unknown structural displacement \mathbf{u} , which, in general is different from the more simple equation used in the analytical model (equation 3.1).

Two types of studies were performed in this simulation, namely an eigenfrequency and frequency domain study. The first study aims at confirming the predicted surface mode eigenfrequency. The second study investigates the amplitude and phase response of the phononic crystal as a result of a given harmonic load.

In both studies, a harmonic time dependency is assumed on the unknown variables. In this case, the unknown is the solid displacement field. Hence, any component of the solid displacement vector takes the following form (the y component is used for the following example):

$$u_y = \bar{u}_y e^{i\omega t} \quad (3.34)$$

where \bar{u}_y is the complex amplitude, ω is the angular frequency and t is time. The complex variable \bar{u}_y can also be represented in Euler form in terms of its magnitude/amplitude and phase, which transforms equation 3.34 into the following:

$$u_y = \tilde{u}_y e^{i(\omega t + \phi_{u_y})} \quad (3.35)$$

From here on, the complex amplitude is dropped and any mention of "amplitude" refers to the real amplitude denoted by $\tilde{\cdot}$.

The actual solution is the projection of the above on the real axis (also see reference [35] for a similar method of analysis):

$$u_y = \tilde{u}_y \cos(i(\omega t + \phi_{u_y})) \quad (3.36)$$

In the discussions of the results, it shall be seen that the main interest lie in the amplitude \tilde{u}_y and phase ϕ_{u_y} rather than the real solution.

3.3.2 Steady-State Fluid-Structure Interaction (FSI) simulation

The steady-state fluid-structure interaction (FSI) simulation was used to obtain the basic solution of the problem (see the decomposition of flow field in the flow stability problem, discussed in section 2.1). Unlike the restrictions imposed in studying flow stability with the the Orr-Sommerfeld equation, the stability problem performed in this simulation accounted for variations of the flow in the streamwise direction (hence no assumption of parallel flows). Thus, the result of the simulation is a better model of the real flow case.

The modules used were structural mechanics, laminar flow, heat transfer, nonisothermal flow and fluid-structure interaction multi-physics coupling.

The structural mechanics module has been explained in the structural analysis simulation.

The laminar flow module was selected to solve low Mach number compressible flow. This model essentially solves the two-dimensional Navier-Stokes equations. The heat transfer module solves

the energy balance, which complements the compressible laminar flow problem as the laminar flow module only solves the continuity and momentum equation.

The governing equations of the laminar and heat transfer modules are given by the steady balance of mass, momentum and energy; which are equations 3.37, 3.38 and 3.39 respectively. Equation 3.40 gives the constitutive model for the Cauchy's stress tensor (τ) for air.

$$\nabla \cdot (\rho \mathbf{v}) = 0 \quad (3.37)$$

$$\rho(\mathbf{v} \cdot \nabla) \mathbf{v} = \nabla \cdot \tau \quad (3.38)$$

$$\rho C_p \mathbf{v} \cdot \nabla T + \nabla \cdot (-k \nabla T) = \alpha_p T \mathbf{v} \cdot \nabla p + \tau_v : \nabla \mathbf{v} \quad (3.39)$$

$$\tau = -p \mathbf{I} + \left(\mu_a (\nabla \mathbf{v} + (\nabla \mathbf{v})^T) - \frac{2}{3} \mu_a (\nabla \cdot \mathbf{v}) \mathbf{I} \right) = -p \mathbf{I} + \tau_v \quad (3.40)$$

In equation 3.38, μ_a denotes the dynamic viscosity of air.

In equation 3.39 T is the temperature, C_p is the specific heat of air at constant pressure, k is the thermal conductivity of air, and α_p is the coefficient of thermal expansion (which is equal to $1/T$ with the ideal gas model). The three aforementioned material properties are functions of temperature and are set to the default setting of the material database. The reference temperature was taken to be 293.15 K (or 20 °C).

The two terms on the right-hand side of equation 3.39 represent the work done by pressure and viscous forces. The notation ":" in the viscous work signifies double dot product of two tensors.

The coupling between the laminar flow and heat transfer physics was done with the nonisothermal flow multiphysics module. This module simply ensures that the density of air is a function of pressure and temperature (through the ideal gas equation).

Finally, the coupling between the flow and the structure was done with the help of the fluid-structure interaction multiphysics module. This module ensured that the loading from the fluid (which originates from pressure and shear stresses) is imposed onto the structure.

3.3.3 Frequency Domain Fluid-Structure Interaction (FSI) Simulation

This simulation was performed to solve the harmonic response of the coupled fluid-structure domain with Tollmien-Schlichting waves.

The modules used were structural mechanics, linearized Navier-Stokes (frequency domain) and aeroacoustic-structure boundary multiphysics coupling.

The structural mechanics module has been explained in the structural analysis simulation.

In the frequency domain linearized navier-stokes module, the flow field is decomposed into a "background" and a "scattered" field. In fact, this is the same as the flow decomposition performed in section 2.1 (where the terminologies "basic" and "disturbance" were used instead of "background" and "scattered" respectively). The input background flow field is the solution of the non-isothermal flow, given by the second simulation.

The equations solved are the balance of mass, momentum and energy in frequency domain. (shown in equations 3.41, 3.42 and 3.43 respectively). The transformation from the time to the frequency domain was obtained by assuming a harmonic time dependency of the unknowns (see section 3.3.1). The implication of this transformation is that the time derivatives become multiplication with $i\omega$.

$$i\omega\rho + \nabla \cdot (\rho\mathbf{v}_0 + \rho_0\mathbf{v}) = 0 \quad (3.41)$$

$$\rho_0(i\omega\mathbf{v} + (\mathbf{v} \cdot \nabla)\mathbf{v}_0 + (\mathbf{v}_0 \cdot \nabla)\mathbf{v}) + \rho(\mathbf{v}_0 \cdot \nabla)\mathbf{v}_0 = \nabla \cdot \boldsymbol{\tau} + \mathbf{F} \quad (3.42)$$

$$\begin{aligned} \rho_0 C_p (i\omega T_0 + \mathbf{v} \cdot \nabla T_0 + \mathbf{v}_0 \cdot \nabla T) + \rho C_p (\mathbf{v}_0 \cdot \nabla T_0) - \alpha_p T_0 (i\omega p + \mathbf{v} \cdot \nabla p_0 + \mathbf{v}_0 \cdot \nabla p) \\ - \alpha_p T (\mathbf{v}_0 \cdot \nabla T_0) = \nabla \cdot (k \nabla T) + \Phi \end{aligned} \quad (3.43)$$

It is to be noted that the disturbance field is inside the total field (ρ , p , T and \mathbf{v}). The subscript "0" denotes the basic solution obtained from the steady-state FSI simulation. Finally, the term " Φ " denotes the linearized viscous dissipation term, given by:

$$\Phi = \nabla \mathbf{v} : \boldsymbol{\tau}_{v,0} + \nabla \mathbf{v}_0 : \boldsymbol{\tau}_v \quad (3.44)$$

As the name of the module suggests, the governing equations are linear in the disturbance flow. Furthermore, as the name also suggests frequency domain simulation, all variables are assumed to have harmonic time dependencies. This means that all time derivatives in the partial different equations become multiplication with $i\omega$. The outputs of the solver are the complex amplitudes of the disturbance flow field.

The aeroacoustic-structure boundary multiphysics coupling was used to couple the structural mechanics and frequency domain linearized navier-stokes modules. This coupling imposes continuity of velocities and stresses at the fluid-structure boundary.

In addition to the physics modules, perfectly-matched layers are placed upstream and downstream the flow domain to minimize boundary reflections.

The main advantage of performing the FSI simulation in the frequency domain (instead of the time domain) is the reduction in computational complexity. The frequency domain simulation avoids any difficulties in choosing a suitable time step that minimizes the inherent damping within the solver while maintaining stability of the solution. Furthermore, the total simulation

time has to be chosen carefully in order to balance between obtaining reliable statistics and total computational time. If the time domain simulation were chosen, only a few simulation conditions can be studied within the given time. Choosing the frequency domain simulation allows for the investigation of more cases.

Nevertheless, there are also disadvantages within the frequency domain simulation. First, the time taken for the fluid-structure system to reach the harmonic response is not known, which may become important for practical purposes. Second, as the frequency domain simulation only considers responses of a single frequency (i.e. the TS wave frequency), any interactions between solutions of different frequencies was captured. Third, the frequency domain Navier-Stokes model available in COMSOL® is linearized: non-linear phenomenon was not resolved. However, as in the frame of linear stability theory, non-linear effects can be expected to not be dominant.

3.4 Verification and Validation

In this section, the procedures to verify and validate the the numerical simulation results shall be explained in section 3.4.1 and 3.4.2 respectively.

3.4.1 Verification

Verification is necessary to ensure that the results obtained in the numerical simulation conform to what is intended to be simulated. Thus, the verification procedures are used to check whether or not the simulations yield intended results shall be explained.

In general, the verification of the results of the three numerical simulations are done in two ways. The first is to verify the boundary conditions and fluid-structure coupling where applicable. The second method is to compare the numerical results with well-established theories. The latter method shall be detailed for each type of simulation in the following paragraphs.

In the structural analysis simulation, the obtained eigenfrequencies are compared with the analytical formulae given by equations 3.27 and 3.28. This verification step is given in table 4.1. As for the frequency domain simulation, the amplitude and phase responses are compared with the well-known resonance response of a system (where the amplitude peaks at the resonance frequencies and the phase difference with respect to a forcing function is zero below resonance, and π above resonance). The results are given in figure 4.4 and 4.5.

As for the steady-state fluid-structure simulation, the velocity profile is compared with the Blasius' boundary layer solution that can be derived from the data available in reference [67]. This comparison is given in figure 4.7.

Finally, in the frequency-domain fluid-structure simulation, the shape of the velocity fluctuations are compared with data from previous studies (such as LST and experimental data given in figure 2.4 [48] for the streamwise velocity fluctuation, or Direct Numerical Simulation and Parabolized Stability Equations results given in reference [33]). Additionally, it is expected that the response

of the phononic crystal has the behaviour of a resonance response (as suggested by the results obtained in reference [30]). This resonance response is applicable to the vertical displacement, and is shown in figure 4.13.

3.4.2 Validation

The purpose of the validation step is to ensure that the simulation results obtained conform to the real physical case. Hence, the most appropriate method for validation is to compare the results of the numerical simulation with experiments. However, experimental studies are beyond the scope of this thesis.

Here, steps are taken to ensure that the numerical simulations results are as accurate as possible, given the available resources. This is done by performing sensitivity analysis with respect to the mesh refinement levels, i.e. a mesh convergence study. The results of such a study are given in appendix E.

Chapter 4

Results and Discussions

As stated in section 3.3, there are three types of simulations performed in this thesis project; namely structural analysis, steady-state FSI and frequency domain FSI simulations. The results of these simulations are given in section 4.1, 4.2 and 4.3 respectively. In all cases, the simulations are two-dimensional. Ultimately, the research questions introduced in chapter 1 were answered with the results of the last type of simulation. However, the other two simulations were necessary in order to arrive to the frequency domain FSI simulation.

4.1 Structural Analysis Simulation

This section gives the results of the structural analysis simulation. The structural analysis simulation was used to determine the optimal number of unit cells (N_{UC}) of the phononic crystal. The set-up of the structural analysis simulation is given in section 4.1.1. Two analyses were performed within the structural analysis framework: eigenfrequency and frequency response analyses. The eigenfrequency analysis was used to confirm the predicted surface mode eigenfrequency (f_{SM}); to see if there are any discrepancies between the previously discussed one-dimensional models and the two-dimensional structural analysis results. For to the eigenfrequency analysis, the boundary conditions are varied in order to see their effects. The results are given in section 4.1.2. Once the eigenfrequencies of the final design have been confirmed, a frequency response analysis was performed. This analysis is used to compare the surface displacement amplitude near the resonance frequencies between the different designs of the phononic crystal, as well as to confirm the out-of-phase response as predicted in reference [30]. The results for this analysis are given in section 4.1.3.

4.1.1 Set-up of the Structural Analysis Simulation

The set-up of the structural analysis simulation are illustrated in figure 3.4 and 4.2 for a sample case of two-layer unit cell design with $N_{UC} = 1$ and $L_{UC} = 1$ mm. The coordinate system of the simulation is the same as the one given in figure 3.1.



FIGURE 4.1: Geometry of the two-layer one unit cell phononic crystal

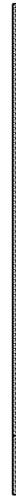


FIGURE 4.2: Mesh of the two-layer one unit cell phononic crystal design

Before the simulation can be performed in COMSOL®[®], four items have to be specified: geometry, material, boundary conditions and meshing. The geometry of the phononic crystal is relatively simple (figure 4.1), consisting of multiple rectangles where each rectangle represents a given layer of the phononic crystal. The material properties given in table 3.3 are assigned to each layer, according to the design. The boundary conditions are assigned to each sides of the phononic crystal: top, bottom, the left and the right side. The specific boundary condition to be assigned shall be discussed in more detail in section 4.1.2. Finally, for this eigenfrequency and frequency response study, the mesh used was an automatically generated mesh, choosing the "extremely fine" scale. Triangular elements were built. An example of the resulting mesh is given in figure 4.2.

There were six phononic crystal designs investigated: the two unit cell designs with varying N_{UC} , between $N_{UC} = 1, 3, 5$. In each case, the set-up are similar as described in the previous paragraph. The next sections give results of the eigenfrequency and frequency response study for these six designs.

4.1.2 Effect of boundary conditions on eigenfrequencies

There are two types of boundary conditions to be tested. The first one consisted of the following: free top and bottom sides, and constrained displacement in the x direction on the right and the left sides ($u_x = 0$). This shall be referred as "BC1". The second boundary conditions to be studied were the same as BC1, except that the bottom is fixed. This second set of boundary conditions shall be referred as "BC2". The reason for the study of BC1 is to verify the eigenfrequency predicted by IRT in section 3.2. The main difference between the phononic crystal design and simulation is that in the design, the problem was one-dimensional; whereas it is two-dimensional for the simulation. It was to be seen whether or not BC1 would give the

same result as a one-dimensional analysis. However, evidently the bottom side would have to be fixed in practice, otherwise the phononic crystal would fall. Hence the study of BC2.

This effect of difference in boundary condition was studied by computing the surface mode eigenfrequencies (f_{SM}). From the simulations, multiple eigenfrequencies were observed. The (first) surface mode was obtained by assuming that the eigenfrequencies followed the result of IRt [10]: that is, the first $N_{UC} - 1$ eigenfrequencies correspond to the bulk mode, whereas the next eigenfrequency (i.e. the N_{UC}^{th} eigenfrequency) corresponds to the surface mode. Hence, the first eigenfrequency was picked for $N_{UC} = 1$, the third for $N_{UC} = 3$ and the fifth for $N_{UC} = 5$. This was also verified by plotting the corresponding eigenmode: the displacement of surface modes are dominant near the surface, and attenuates as one travels down the layers. A sample result comparing the bulk and surface mode is given in figure 4.3.

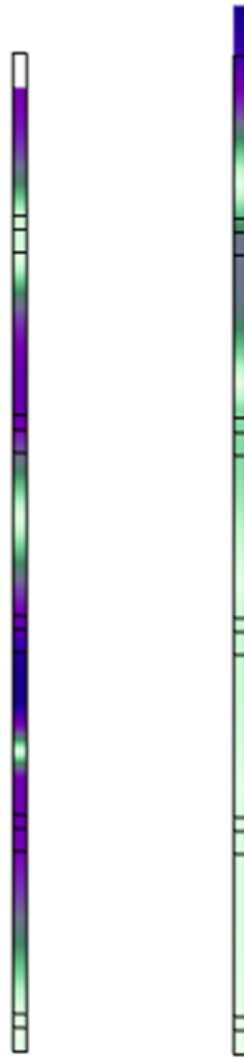


FIGURE 4.3: An example of bulk (left) and surface mode (right) of phononic crystal. (Three-layer unit cell design, $N_{UC} = 5$ and BC2 was used). The colored geometry represents the deformed configuration.

It was observed that both applications of BC1 and BC2 exhibit bulk and surface modes. With

the nature of the modes verified, f_{SM} of the different phononic crystal designs were documented. These are compared in table 4.1.

Unit cell design	N_{UC}	$f_{\text{SM, BC1}}$ (Hz)	$f_{\text{SM, BC2}}$ (Hz)	$f_{\text{SM, IRT}}$ (Hz)	Δf (%)
Two-layer	1	299.13	186.46	299.13	37.67
	3	299.13	282.06		5.70
	5	299.13	294.23		1.64
Three-layer	1	300.76	234.40	300.76	22.06
	3	300.76	299.35		0.47
	5	300.76	300.71		0.02

TABLE 4.1: Effect of boundary conditions on f_{SM} of the different phononic crystal designs

In the table above, Δf represents the percentage difference between $f_{\text{SM, IRT}}$ and $f_{\text{SM, BC2}}$, as given by the following equation:

$$\Delta f = \frac{f_{\text{SM, IRT}} - f_{\text{SM, BC2}}}{f_{\text{SM, IRT}}} \times 100 \quad (4.1)$$

Several observations can be made from table 4.1. First, the resulting f_{SM} predicted by IRT is equal to that computed with FEM, applying BC1, to two decimal places. Hence, the application of BC1 effectively renders the problem one-dimensional. This could be further observed from the eigenmodes: the displacements of the structure are only in y direction. Second, there is a difference between $f_{\text{SM, BC1}}$ and $f_{\text{SM, BC2}}$. This difference is attributed to the fixed boundary condition at the bottom of the structure. Hence, the surface mode eigenfrequency is, in fact, a property of the structure and not of the unit cell as suggested by reference [30]. Consequently, $f_{\text{SM, BC2}}$ differs from the f_{SM} of the design method ($f_{\text{SM, IRT}}$). This can be explained by the fact that derivation for the IRT equation (equation 3.27 and 3.28) did not account for boundary conditions (or that the layer interfaces are free). The third observation however, is that this difference becomes smaller as N_{UC} increases. This can be explained by the fact that the boundary condition along the direction of wave propagation (y direction) exhibits weaker influence as the structure becomes longer. Finally, the last observation to be made is that Δf of the three-layer unit cell design reduces to zero faster with increasing N_{UC} than the two-layer unit cell design (even though the total length ($N_{\text{UC}} \times D$) of the structure is smaller).

With this, it is reasonable to conclude that the three-layer design is better given the following criteria: smaller structure and quicker convergence of f_{SM} with the prediction design method. However, there is still one more thing to investigate: the surface displacement amplitude given a harmonic loading. This, as well as a verification on the phase of the surface displacement response, shall be discussed in the following section.

4.1.3 Comparison of frequency domain surface displacement

The study of the steady-state displacements of the phononic crystal was done by applying a load at its top surface ($y = 0$), along the x direction. A load per unit area with 2 N/m^2 amplitude was

semi-arbitrarily chosen (the magnitude had to be small in the order of the TS wave pressure load magnitude). The analysis was performed in the frequency domain. Hence the load is harmonic, assigned a certain frequency (f) and the steady-state response also becomes harmonic with the same frequency. The output displacements of the simulation are the complex amplitude of a harmonic function.

Applying a harmonic load and/or setting the problem to be geometrically non-linear do not change the eigenfrequencies of the structure. The mesh that was used in the eigenfrequency study was also used for the structural frequency domain study. Of interest is the displacement at the top surface of the phononic crystal, since the surface interacts with the flow.

The simulation was performed. It was found that the phase is either 0 or π . In other words, the displacements are effectively real. A phase of π signifies that the response is out-of-phase with respect to the boundary load. Furthermore, an effectively constant displacement was observed along the top surface. Nevertheless, an average was taken along the top surface (denoted by $\langle \cdot \rangle$) for comparison of the different phononic crystal designs.

The resulting average surface displacements in the y direction ($\tilde{u}_y(y=0)$) for the different designs at 0.001 Hz higher than their f_{SM} are given in table 4.2 to two decimal places.

Unit cell design	N_{UC}	$\langle \tilde{u}_y \rangle (y=0)$ (mm)
Two-layer	1	-4.75
	3	-1.54
	5	-1.17
Three-layer	1	-4.75
	3	-2.64
	5	-2.55

TABLE 4.2: Average negative surface displacements of the different phononic crystal designs around the corresponding $f_{\text{SM}, \text{BC}2}$

From the table, it can be seen that displacements very close to the resonance frequency are in the order of millimetres. Hence, choosing any of the designs should influence the flow in the same order of magnitude. Therefore, the surface displacement do not cause significant difference between the different phononic crystal designs. Hence, the criteria that weighs more is the relative error with respect to the design f_{SM} . This leads the three-layer unit cell with $N_{\text{UC}} = 5$ design as the chosen design.

Further results from the frequency domain analysis shall be presented. The benefit of choosing the surface mode eigenfrequency is that the frequency interval for out-of-phase response can be the largest when the resonance frequencies are dense (also see [30]). This is shown for the three-layer unit cell design with $N_{\text{UC}} = 5$ by plotting the surface-averaged phase response for frequencies between 10 and 600 Hz, with a step of 1 Hz, as given in figure 4.4. The corresponding real amplitudes is given in figure 4.5. The green-shaded area corresponds to the band gap of the unit cell.

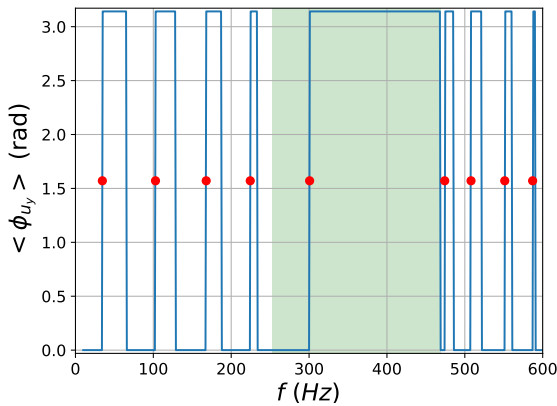


FIGURE 4.4: $\langle \phi_{u_y} \rangle$ for the three-layer unit cell, $N_{UC} = 5$ phononic crystal design

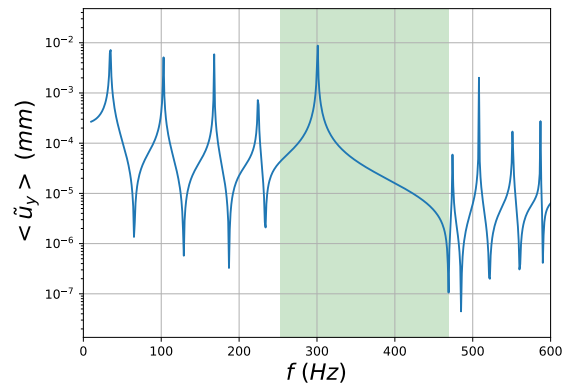


FIGURE 4.5: $\langle \tilde{u}_y \rangle$ for the three-layer unit cell, $N_{UC} = 5$ phononic crystal design

The phase plot contains jumps, where the values could either be 0 or π . This is simply due to the fact that the amplitude of \tilde{u}_y changes sign between positive and negative (although not captured in the semi-log plot of the real amplitude response). Furthermore, some of these jumps correspond to resonance frequencies. These particular jumps have been marked by red dots. The significance is that, since the distance between the surface mode eigenfrequency and the next eigenfrequency is large, the phase of π is maintained in a relatively large frequency interval.

It can be seen from the amplitudes that there are differences in order of magnitudes between the responses near the resonance frequencies and the responses away from it. Furthermore, a remark can be made that the 1 Hz frequency step is not sufficiently refined to yield the response in the order of millimetres, as was obtained in table 4.2. Hence, the size of the frequency step is important in order to obtain responses that are very close to resonance.

It is not yet clear whether or not the displacements at frequencies away from the resonance are large enough to influence the flow. With this, the three-layer unit cell design with $N_{UC} = 5$ shall be further used in the FSI simulation, discussed in detail in the following section.

4.2 Steady-State Fluid-Structure Interaction (FSI) Simulation

The steady-state fluid-structure interaction simulation was performed in order to obtain the baseline flow. As a reminder, the problem at hand is the flow over a flat plate at angle of attack of zero. In the simulation, the assumptions were limited; meaning that the full viscous, compressible conservation equations were solved for (as explained in section 3.3.2). The main goal of this non-simplifying simulation is to get close to practical situations as possible.

This section consists of two subsections. The first explains the set-up of the simulation (subsection 4.2.1). The second shows and discusses the results of the simulation (subsection 4.2.2).

Note that the basic solution was not used to answer the research questions. Rather, it was used to enable the frequency-domain fluid-structure interaction simulation, which directly dealt with the problem of flow instability.

4.2.1 Set-up of the Steady-State FSI Simulation

The set-up of the steady-state FSI simulation consisted of the same steps taken in the structural analysis simulation, namely: (1) defining the geometry, (2) assigning the appropriate material in each domain, (3) specifying the initial and boundary conditions, and (4) constructing the mesh. These steps took place before the numerical simulation. The following paragraphs discuss the steps in the given order.

Geometry and material assignment

A zoomed-out view of the geometry of the problem is given in figure 4.6.

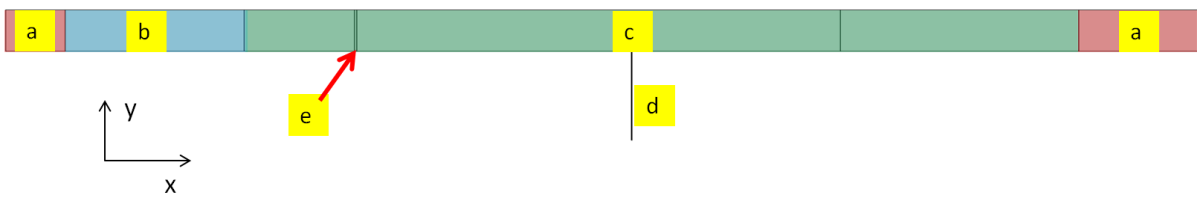


FIGURE 4.6: Geometry of the numerical simulation

The x -position and y - positions specify the horizontal and vertical coordinates respectively, the same as previously discussed geometries.

As seen from the above figure, the computational domain is divided into several parts/sub-domains given by the labels. These are explained in the following:

- a: These are the Perfectly-Matched Layers (PMLs). They are used to minimize the reflections from the boundary when the Tollmien-Schlichting waves are excited. These are not actually accounted for in the steady-state FSI.
- b: This sub-domain contains the air that flows upstream of the flat plate.
- c: This sub-domain contains the air that flows above the flat plate.
- d: This is the phononic crystal
- e: This sub-domain is a relatively small rectangle that exists within the interval $x \times y = [0.185, 0.189]m \times [0, 0.0005]m$. In this sub-domain, a distribution of body force (that oscillates in time and in the x direction) is given in order to produce TS waves. This domain does not have significance in the steady-state simulation.

In addition to the above, there are air gaps on the sides of the PC (see Appendix A for a closer view). These gaps were used because it was found that in the frequency domain FSI simulation, without the air gaps, the top corners of the PC did not exhibit displacement even though pressure was impinging. Thus, the result with air gaps were thought to be more physical. The width of these gaps were chosen to be very small in order to minimize the impact on the

numerical solutions. These air gaps did not have significant impact on the steady-state FSI simulation.

Boundary conditions

With the geometry and materials defined, the boundary conditions were specified. In the fluid domain, the boundary conditions (accounting for laminar flow and heat transfer) are as follow:

1. Left wall as inlet, with an x - velocity of 20 m/s (the freestream velocity used in section 3.1). The temperature here is specified to be 293.15 K.
2. Right wall as outlet. Here, pressure was specified, which was equal to the reference value (1 atm). Additionally, the option "suppress backflow" was selected. For heat transfer, the outflow specified zero heat transfer normal to the outlet.
3. Slip condition was assigned to the top wall. This slip specifies zero normal velocity, and neglects viscosity. Hence it represents the fact that far above the flat plate, there is no solid and that the flow must be the same as the freestream velocity. As for the heat transfer, the condition of thermal insulation was assigned.
4. Symmetry condition was assigned to the bottom wall of the rectangle upstream of the flat plate ($x = -0.3$ to $x = 0$ m). This was used as only the flow in the upper-half of the flat plate was solved for with the given geometry.
5. No-slip condition and thermal insulation along the flat plate ($x = 0$ to $x = 1.4$ m).

As for the PC, BC2 was employed (see subsection 4.1.2).

In addition to the boundary conditions, "initial conditions" were specified for the numerical simulation in order to assist convergence. Note that these initial condition do not yield physical significance in a steady-state simulation. It is solely used for convergence. Hence, initial conditions that were expected to be close to the solution were chosen.

In the fluid domain, the following initial condition was applied:

$$V_x(x, y) (m/s) = \begin{cases} V_\infty \sin\left(\frac{1}{0.002} \frac{\pi}{2} y\right) & 0 < y \leq 0.002 (m) \\ V_\infty & 0.002 < y < 0.1 (m) \end{cases}$$

where the above simply predicts a fast evolution of velocity from zero to the freestream value very close to the bottom wall (as is the case in the anticipated boundary layer). The initial temperature was set to be 293.15 K everywhere in the domain. Lastly, the initial solid displacements and velocities were set to be zero everywhere.

The multiphysics FSI coupling was used along the fluid-structure interface (which is at the top of the PC). This ensured that the fluid imposes load onto the structure and that the solid imposes velocity onto the fluid.

Meshing

For the meshing, only quadrilateral elements were used. This choice yielded an average element quality of 1.0 in terms of skewness. In the fluid domain, the mesh was made to be particularly finer along the bottom wall, and around the leading edge of the flat plate forcing domain, and above the phononic crystal. The main reason is to resolve the boundary layer, stagnation point (expected to be at the leading edge from thin-airfoil theory), the generation of TS waves (for the frequency domain FSI simulation) and finally to resolve the fluid-structure interaction. The average quality of the growth rate is 0.9161. The element sizes within the phononic crystal were chosen with the wavelength of acoustic propagation in mind, which was relevant for the frequency domain FSI simulation. In total, there are 153994 elements. Screenshots of the mesh can be found in Appendix B.

Quadratic Lagrange and serendipity elements were chosen for the discretization within the fluid and solid domain respectively. The reason for choosing the serendipity elements for the structural problem (which has one less node than the Lagrangian elements) was to reduce memory requirements. Additionally, it was found that the quadratic serendipity elements yielded very similar results as the quadratic Lagrange elements in the isolated structural analysis (for instance, the same eigenfrequencies to two decimal places). Overall, the aim was to use at least a second-order element type due to the highest order of derivative in the governing partial differential equations.

Having defined the geometry, domain material, boundary conditions and meshing defined, the numerical simulation could commence. The relative tolerance was set to 10^{-4} . The results and discussions of the steady-state FSI results are given in the following subsection.

4.2.2 Results of the Steady-State FSI Simulation

The results of the steady-state FSI are the steady flow velocity and solid displacement fields. In the framework of stability analysis, this velocity field refers to the basic flow solution (see the discussion pertaining to equation 2.2). Compared to the assumptions used in the stability analysis discussed in section 2.1, the spatial dependency of the basic flow field obtained in the numerical simulation is not limited to the y direction only (i.e. non-parallel flow).

As a side note, there is no decomposition of the structural displacement.

The fields obtained from the numerical simulation are by the contour plots of figure 4.7 to 4.9.

First, consider the zoomed-in contour plot of the velocity near the leading edge 4.7). This figure contains two sub-plots. On the left, the solution obtained from COMSOL[®] is shown. This figure is compared with the Blasius boundary layer solution, given on the right (derived from the data given in reference [67]). It can be seen that the solution obtained from COMSOL[®] also shows a boundary-layer profile: where the streamwise velocity is equal to the freestream value away from the wall, but decreases to zero near the wall. Additionally, there is the growth in the boundary-layer thickness from the leading edge.

The main difference with respect to the Blasius' profile lies at and upstream of the leading edge ($x \leq 0$ m). The Blasius' solution does not predict the solution upstream of the flat plate. Furthermore, in the Blasius' case, there is a great jump in the streamline (shown by the contour)

due to the omittance of the second derivative of the flow velocity with respect to x . Other differences can also be attributed to the inclusion of compressibility in the COMSOL® simulation. Nevertheless, the similarities outweigh the differences and thus the COMSOL® result is taken to be verified.

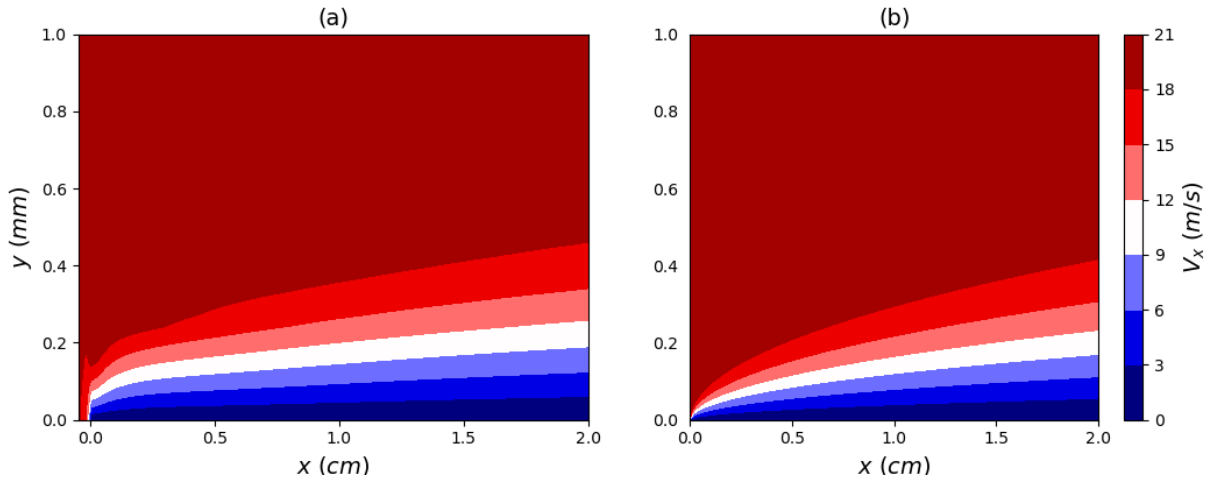


FIGURE 4.7: Comparison of basic flow velocity V_x between the results obtained from (a) steady-state FSI simulation and (b) Blasius' solution.

Now, consider the pressure near the leading edge. This is given in figure 4.8. There is a jump in pressure near the leading edge. This is also expected as illustrated by the well-known thin-airfoil theory (for instance, from standard textbook such as [1]) which is based on potential flow (which is derived from irrotationality of velocity field), with the addition of Bernoulli's equation to obtain the pressure. In this theory, the leading edge of a flat plate constitutes a stagnation point (in which the flow velocity is zero in the potential flow framework), which implies maximum pressure. Differences between the leading edge pressure of thin-airfoil theory and the numerical simulation can be attributed to the inclusion of viscosity and compressibility.

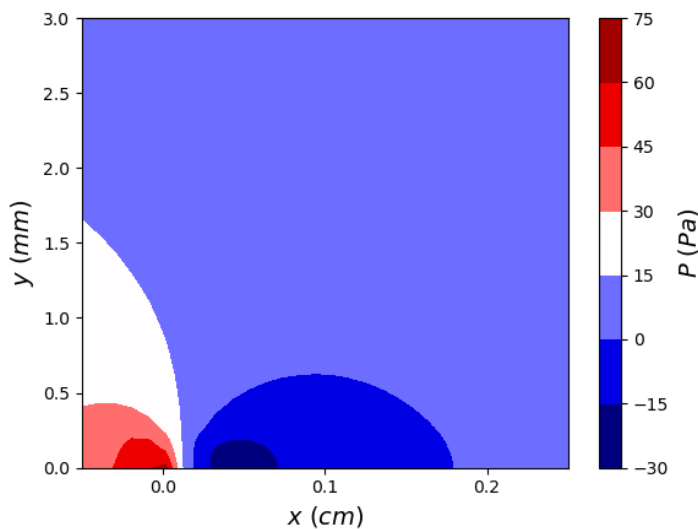


FIGURE 4.8: Gauge pressure (Pa) near the leading edge of the flat plate.

Finally, figure 4.9 shows the field of V_x and u_y near the PC. Just like in figure 4.7, there is a boundary layer structure near the wall of the flat plate. The presence of the PC has negligible effect on this structure, due to the small magnitude of displacement (10^{-7} m). To end, it can be seen from the figure that u_y is effectively constant along the x -direction of the phonic crystal. This simply verifies the boundary condition in which no restriction was put on the vertical displacement of the PC.

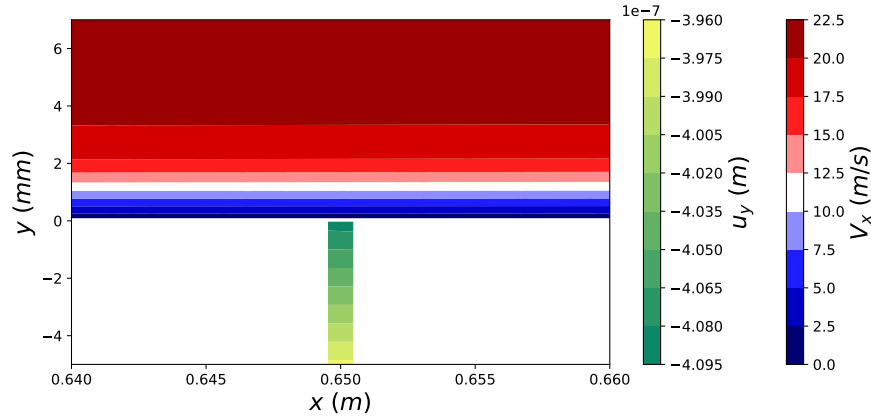


FIGURE 4.9: Contour of the streamwise component of the velocity (V_x (m/s)) and the vertical displacement of the PC (u_y (m)).

Having obtained and qualitatively investigated the basic flow field, the frequency domain FSI was performed. This shall be discussed in more detail in the following section.

4.3 Frequency Domain Fluid-Structure Interaction (FSI) Simulation

The results of the frequency domain FSI are used to answer the research questions (see chapter 1). Similar to the previous section, this section consists of two subsections. The first (subsection 4.3.1) explains the set-up of the frequency domain simulation. The second subsection (subsection 4.3) presents and discusses the results obtained from the simulation.

4.3.1 Set-up of the Frequency Domain FSI Simulation

The geometry, material and the meshing of the steady-state FSI simulation were also used in the frequency domain study (see section 4.2.1 for the details). As a reminder, two things are now relevant in the frequency domain: the perfectly-matched layers (PMLs) and the forcing domain, denoted by sub-domain (a) and (e) respectively (figure 4.6). The former items were used to minimize reflection, and the latter was used to generate the TS wave.

The forcing function applied was a two-dimensional cosine function with an amplitude of 12 N/m^3 . The cosine behaviour was chosen in order to smoothen the body force distribution in the body force domain (with the maximum at the center). This application of a forcing

distribution is able to simulate the effect of a plasma actuator on a flow [36], where the influence of a plasma actuator has also been proven to generate TS waves [7].

The boundary conditions for the frequency domain simulation were the same as the steady-state simulation, except for one: at the inlet and outlet, the disturbance velocity components were set to zero.

As for the initial conditions, the disturbance flow field was set to zero.

Finally, an extra parameter has to be assigned in the simulation, namely the excitation frequency (see equations 3.41 - 3.43 to see how the frequency is introduced in the problem). This excitation frequency also corresponds to the TS wave frequency. Following the results of reference [30], it is of interest to see the response of the PC for frequencies that lie within the band gap. Furthermore, it was also shown that the largest response occurs near the resonance frequency. With this in mind, a frequency sweep from 296 Hz to 306 Hz was performed in this frequency domain simulation (as a reminder, the predicted band gap frequency interval starts from 253.0 Hz and ends at 468.7 Hz, derived from figure 3.8; the resonance occurs at 300.76 Hz for the isolated structure). Steps of 0.04 Hz were taken for the intervals 296-299.96 Hz and 302.04-306 Hz. The remaining frequencies were swept with a step size of 0.02 Hz. These small frequency steps were chosen in order to anticipate a resonance response which is known to have very large gradients near the resonance frequency.

The results of the frequency domain FSI simulation are presented in the next section.

4.3.2 Results of the Frequency Domain FSI Simulation

A number of different physical quantities were derived from the frequency domain FSI simulation. In this section, the quantities shall be presented as follows. To start the analysis, the so-called "overall" quantities are discussed (section 4.3.2.1). These quantities are only a function of the TS wave frequency. This analysis gives a broad overview of the influence of the PC to the disturbance flow field, but obscures any details in the spatial variation. Such an analysis allows for choosing frequencies that are of interest for more detailed studies. This analysis deals with the main research question, the second and the third sub research question (see chapter 1).

The second analysis is to see quantities that vary only along the streamwise direction at some frequencies of interest (section 4.3.2.2). These quantities are expressed in terms of integrals in the wall-normal direction. This analysis primarily deals with the first and second sub research question. However, as shall be seen, it can also give a more detailed answer to the main research question.

Finally, a summary and extra remarks of the results of the frequency domain FSI simulation are given in section 4.3.2.3.

4.3.2.1 Overall quantities

Several "overall" quantities shall be presented in the ensuing paragraphs. As mentioned, these quantities are only functions of the frequency. Furthermore, these quantities can be distinguished according to the media: those pertaining to the fluid domain (disturbance flow field) and solid domain (structural displacement) separately. In the case of the fluid domain overall quantities, the first quantity that shall be discussed is the time-averaged kinetic energy. This quantity gives a general overview on the influence of PC on the TS waves. Next, the components of the kinetic energy shall be analyzed i.e. the square of the streamwise and the wall-normal velocity amplitudes. As for the solid domain quantities, the amplitude and phase response at the fluid-structure boundary shall be analyzed.

The following paragraphs present the results of the aforementioned overall quantities.

Change in the averaged kinetic energy

The kinetic energy of the disturbance flow has been used as a criterion in defining flow stability [19][53]. The advantage of this approach is the inclusion of all disturbance velocity components.

Before presenting the results, the time-averaged kinetic energy shall be derived from the frequency domain solution.

The starting point is the instantaneous kinetic energy. This physical property can be obtained from the real parts of the disturbance velocities:

$$\begin{aligned} e_{k,i} &= \frac{1}{2}((\text{Real}(v'_x))^2 + (\text{Real}(v'_y))^2) \\ &= \frac{1}{2}((\tilde{v}'_x \cos(\omega t + \phi_{v'_x}))^2 + (\tilde{v}'_y \cos(\omega t + \phi_{v'_y}))^2) \end{aligned} \quad (4.2)$$

Next, an averaging operation is performed over the time variable. The time-averaged kinetic energy is given by:

$$e_k = \lim_{t^* \rightarrow \infty} \frac{1}{t^*} \int_0^{t^*} e_{k,i} dt \quad (4.3)$$

Upon evaluating the integral analytically, one arrives at the following equation:

$$e_k = \frac{1}{4}(\tilde{v}'_x{}^2 + \tilde{v}'_y{}^2) \quad (4.4)$$

This time-averaged kinetic energy is then integrated over the fluid domain:

$$E_k = \iint_{S_f} e_k dS \quad (4.5)$$

Finally, to evaluate the effect of PC on the TS waves, the difference with the reference is taken:

$$\Delta E_k = \frac{E_k - E_{k,\text{ref}}}{E_{k,\text{ref}}} \quad (4.6)$$

It is noted that ΔE_k is now only a function of frequency, as the time and spatial variations have been eliminated through averaging and integration respectively.

The variation of ΔE_k with frequency is shown through the plot given in figure 4.10.

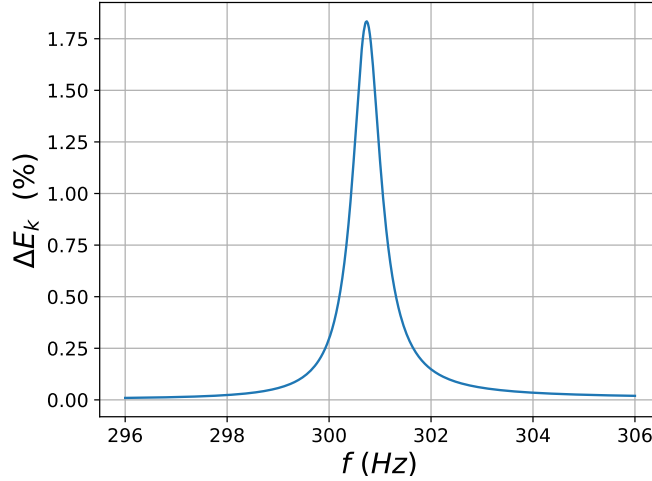


FIGURE 4.10: Variation of ΔE_k with TS wave frequency

A number of important observations can be made from figure 4.10. The first and the most important observation is that there is only an increase in the overall kinetic energy of the disturbance flow field at all of the simulated frequencies, which may imply that there is no stabilization at all. This observation indicates a contrast to the numerical result obtained in reference [30] in two ways. One is the fact that there is no stabilization at all by the kinetic energy criteria. The other thing is that the effect of the phononic crystal on the disturbance field is the same regardless whether the frequency is above or below resonance (i.e. regardless of the phase response of the phononic crystal surface; the actual resonance frequency and the PC response studied in the study given here is around 300.72. This shall be motivated in one of the upcoming paragraphs, with the use of figure 4.13).

The second observation made by looking at figure 4.10 is that the influence of PC on the disturbance flow field is relatively small. This is directly seen from the small change of magnitude of the overall disturbance kinetic energy with respect to the reference configuration, where the maximum ΔE_k lies slightly above 1.83 %. The frequency of this maximum lies slightly above the resonance frequency, at 300.74 Hz.

Yet another important observation of figure 4.10 is the narrowband PC response to TS wave excitation. The effect on the disturbance flow tends to zero relatively quickly. A 1 Hz increase in the frequency from 300.74 Hz yields a change in kinetic energy of approximately 11.8 % of the maximum value.

Nevertheless, this small magnitude of ΔE_k does not necessarily mean that there is no effect of the PC on the flow. This is because a surface integral was taken over the whole fluid domain. This small magnitude implies that the PC exerts its influence on the flow locally, rather than globally. This shall be made clearer in section 4.3.2.2.

The final remark to be made here is that the resonance obtained from the isolated structure is a good prediction for the frequency of that yields the largest influence on the disturbance flow field. The implication is that the structural analysis (which is much more efficient than the full fluid-structure interaction) can be used effectively to design the operating frequencies of the phononic crystal.

Change in the amplitudes of the perturbation velocities

More details of the overall performance of the PC can be analysed. The components of the kinetic energy, i.e. the amplitude of the streamwise and wall-normal velocities, can be compared with respect to the reference configuration. This analysis is used to analyze where the contributions to the change in kinetic energy come from. The plot of the surface-integrated change in velocity amplitudes w.r.t. the reference (denoted as $\Delta \tilde{V}'_x$ and $\Delta \tilde{V}'_y$) against TS wave frequencies is given in figure 4.11. Just like the case for the kinetic energy, the integration was performed over the whole fluid domain.

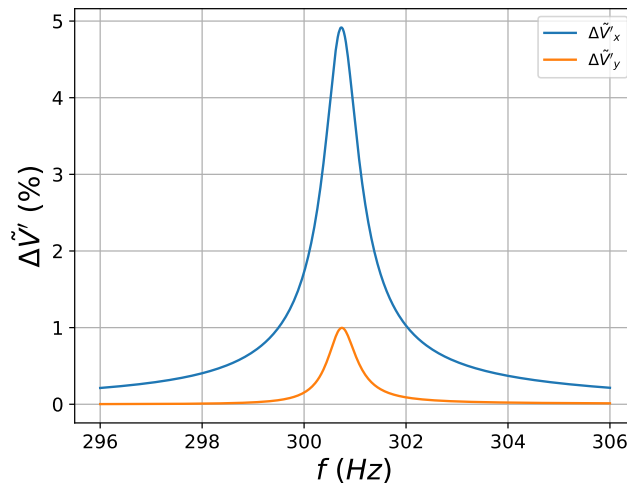


FIGURE 4.11: Variation of $\Delta \tilde{V}'_x$ and $\Delta \tilde{V}'_y$ with TS wave frequency

Several remarks can be made from this figure. The first is that there is only an increase in both the velocity component amplitudes ($\Delta \tilde{V}'_x, \Delta \tilde{V}'_y > 0$) at all the simulated frequencies. This means that globally, none of the velocity components were damped with the PC. Furthermore, the frequency of the maximum of $\Delta \tilde{V}'_x$ and $\Delta \tilde{V}'_y$ coincide with the maximum of ΔE_k at 300.74 Hz.

A more interesting remark is that the increase of the streamwise disturbance velocity amplitude is larger than its wall-normal counterpart, both in relative and absolute value (while the relative increase was shown in figure 4.11, and example of comparison between the magnitudes of the

two disturbance flow velocity components can be found in Appendix C). The maximum of $\Delta\tilde{V}'_x$ is approximately 4.93 times of the maximum of $\Delta\tilde{V}'_y$.

This is a very interesting finding since the PC was designed with the vertical displacement as the displacement component that would influence the flow field, and was not designed with the horizontal displacement in mind. One may suggest that there is an unexpected effect of the PC's horizontal displacement. This shall be further investigated in the upcoming paragraphs.

PC's surface displacements

After looking at the fluid side's overall performances, the performance of the phononic crystal shall be evaluated. Here, the "overall" properties were obtained by taking the performances at the mid-point of the PC's top boundary ($x, y = (0.65, 0)$ m), denoted by $(\cdot)_m$. This operation was chosen as it was found that there are very little variations in the complex displacements over the PC's top surface for the vertical displacement in particular (see Appendix D). With this, the performances are only a function of TS wave frequency.

As with the analysis performed in the isolated structure frequency response (section 4.1.3), the magnitude of the complex amplitude and its phase can be used as analysis tools.

The plot of the average horizontal displacement's amplitudes ($(\tilde{u}_x)_m$) is given in figure 4.12. The plot of the average vertical displacement amplitudes ($(\tilde{u}_y)_m$) and phase differences ($(\Delta\phi_{u_y})_m$) are given in figure 4.13. The pointwise phase difference is defined as follows:

$$\Delta\phi_{u_y} = |\phi_{p'} - \phi_{u_y}| \quad (4.7)$$

where $\phi_{p'}$ and ϕ_{u_y} are the arguments of the complex amplitudes of the pressure fluctuation and PC's vertical displacement. For $(\Delta\phi_{u_y})_m > \pi$, the value is replaced by the difference between 2π and the old value. This is to ensure that the phase has a maximum of π (becomes π -periodic).

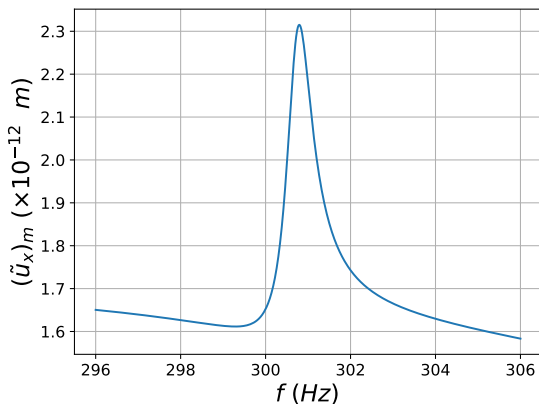


FIGURE 4.12: Overall amplitude response of the phononic crystal's x -displacement for various excitation response

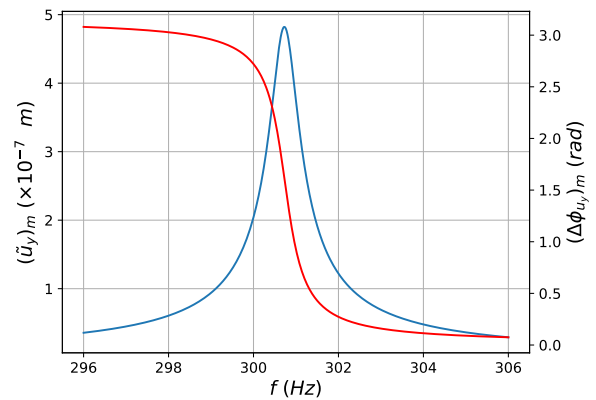


FIGURE 4.13: Overall amplitude (blue curve) and phase (red curve) responses of the phononic crystal's x -displacement for various excitation response

A number of observations can be made from the two figures. The first is the magnitude of $(\tilde{u}_x)_m$, which has the order of 10^{-12} m. Alternatively, one could also look at the surface velocity, as it the velocity (and not the displacement) that is imposed on to the fluid. The velocity of the PC can be easily derived from the displacement through multiplication by $i2\pi f$. With the range of simulated frequencies, the magnitude of the complex velocity would become 3 to 4 orders higher than the magnitude of the complex displacement. This means that, at best, the horizontal velocity would be in the order of 10^{-8} m/s. This order of magnitude is far too small in comparison to the magnitude of the streamwise velocity fluctuation of 10^{-2} m. Hence, it can be concluded that the horizontal displacement does not affect the flow in the simulation.

On the other hand, one could observe the magnitude of $(\tilde{u}_y)_m$. It is in the order of 10^{-7} m. This yields vertical velocities with magnitudes of 10^{-3} to 10^{-4} m/s. This is very much comparable to the magnitude of the wall-normal disturbance velocity of 10^{-3} m/s. Therefore, it was concluded that the influence of the PC on the flow effectively only comes from its vertical displacement.

A small observation can be made on the frequency that yields the peak of the PC displacements. The maximum $(\tilde{u}_x)_m$ and $(\tilde{u}_y)_m$ occur at 300.8 and 300.72 Hz respectively. The latter frequency was used to define the resonance frequency for the discussion, which also coincides with the frequency of maximum ΔE_k .

Finally, from figure 4.13, it can be observed that the behaviour of the amplitude and phase of the vertical displacement is similar to that of a resonance behaviour: where there is a clear peak in the displacement followed by a phase change. However, there are two differences with respect to the isolated structural analysis (section 4.1.3). The first is that the phase differences are flipped: in figure 4.13, the phase difference tends towards π below the resonance and goes to zero above it (while the opposite is true in figure 4.4). This is because of the definition of the forcing function. In obtaining figure 4.4, the function was defined to be positive upwards. In the case of figure 4.13, the forcing function is the fluid's pressure which acts downwards for positive pressure. This difference in the definition of positive force direction caused a flip in the phase differences.

The other difference is that the resonance response given in figure 4.13 is similar to the damped case. This can be derived from the fact that the phase jump does not occur instantaneously (as is the case of figure 4.4). This means that there is a damping in the vibrational energy within the PC structure. However, no damping was applied in the solid mechanics model. Hence, the damping can only happen due to the transfer of energy from the PC onto the flow, where this energy is then dissipated as heat.

This concludes the discussions on the overall performance of the PC in stabilizing TS waves. In the next section, quantities that only vary in x shall be further investigated for three sample frequencies that are far below, around and far above resonance.

4.3.2.2 x -varying quantities

In this section, quantities that vary along the streamwise direction (i.e. x - direction) shall be investigated. The aim of studying such quantities is to understand the streamwise evolution of

the TS wave as it passes through the phononic crystal. The nature of the evolution may also give insight on how the PC influences the TS wave.

The flow quantities of interests are the same as before: disturbance kinetic energy and the magnitude of the disturbance velocity components. However, in this section, the quantities shall be integrated along the y - direction; such that once a frequency has been chosen, the resulting quantities are only functions of x . To be more specific, the quantities to be studied are $\int_0^H e_k dy$, $\int_0^H \tilde{v}'_y dy$, $\int_0^H \tilde{v}'_x dy$, and $\int_0^H (\tilde{v}'_x)^2 dy$. In the integration limits, H is the height of the computational domain (it is to note that the disturbance vanishes quickly with y). The first and the last of the aforementioned integral are the same or similar to quantities which have been used to determine the growth rate of TS waves [19].

The choice of the frequencies to be studied are based on the performance of the phononic crystal (figure 4.13). Three distinct performances can be studied by selecting frequencies far below, around and far above the resonance. These corresponds to three different phases $\Delta\phi_{u_y}$ of π , $\pi/2$ and 0 rad. As previously discussed, the phase π actually corresponds to "in-phase" response while the phase "0" corresponds to the "out-of-phase" response (because positive pressure causes downward displacement). This definition shall be carried in the following discussion. Nevertheless, with this in mind, frequencies of 298, 300.72, and 304 Hz were chosen to be further studied in detail.

Time-averaged kinetic energy

The streamwise variation of y -integrated time-averaged kinetic energy ($\int_0^H e_k dy$) at $f = 298$, 300.72 and 304 Hz are given in figure 4.14. In the figure, the region shaded by magenta denotes the location of the PC. As a reminder, the "reference" simulation refers to the simulation without PC.

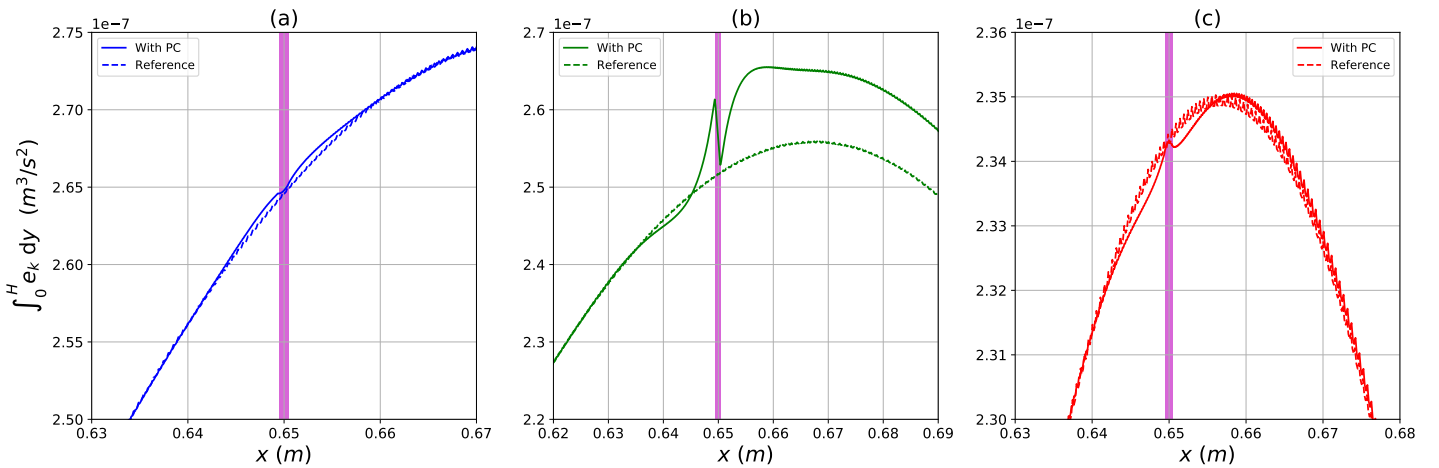


FIGURE 4.14: $\int_0^H e_k dy$ vs x for $f = 298$ ("in-phase"), 300.72 ("resonance") and 304 Hz ("out-of-phase") (subplot (a), (b) and (c) respectively). In each subplot, the location of the phononic crystal is given by the region shaded in magenta.

The trends in the three figures above are as follows. For the frequency below resonance ($f = 298$ Hz), there is an increase of kinetic energy integral around the PC. However, as the flow reaches

the PC, there is a drop. The opposite can be observed for the frequency above resonance ($f = 304$ Hz). The peak of kinetic energy integral that appears very close to the PC is surrounded by a dip. This opposing response happens simultaneously with a change in phase difference ($\Delta\phi_{u_y}$, see equation 4.7 and figure 4.13). This behaviour shall be further analyzed with the study of the velocity component integrals. Nevertheless, from this decrease in kinetic energy integral, one could deduce that there is indeed some stabilization when $\Delta\phi_{u_y}$ tends towards zero (i.e. when positive pressure fluctuation yields a positive (upwards) vertical displacement of the PC's top surface). Nevertheless, there is an addition phenomenon that happens at $f = 304$ Hz, namely the increase in kinetic energy for some part downstream of the PC (around $x = 0.66$ m), which compromises the stabilization.

As for the response around the resonance ($f = 300.72$ Hz), it can be seen that there is an overall increase in the kinetic energy integral. Furthermore, the influence around the resonance is much larger than at the other two frequencies, as can be seen by the huge relative difference of the kinetic energy integral. There is a trend to be noted: starting from upstream, the kinetic energy decreases slightly, then experiences a sharp increase just in front of the PC. At the PC, the kinetic energy decreases sharply, and then increases again downstream. At this frequency, the downstream influence of the PC extends further than at $f = 304$ Hz.

Wall-normal disturbance flow velocity

The wall-normal disturbance flow velocity is the velocity that is directly affected by the motion of the PC, as it was found that the PC's vertical displacements are of 5 orders of magnitudes larger than its horizontal displacement (figure 4.12 and 4.13). Hence, the analysis of \tilde{v}'_y shall give the most direct insight on the effect of PC on TS waves.

The streamwise variation of y-integrated amplitude of the wall-normal velocity ($\int_0^H \tilde{v}'_y dy$) for $f = 298$, 300.72 and 304 Hz are given in figure 4.15.

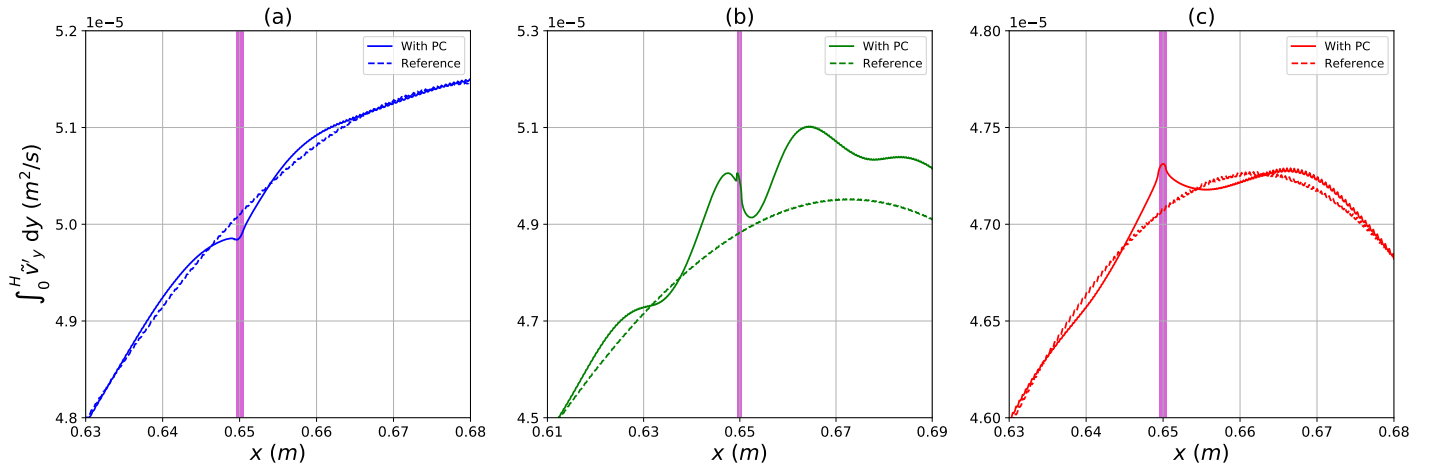


FIGURE 4.15: $\int_0^H \tilde{v}'_y dy$ vs x for $f = 298$ ("in-phase"), 300.72 ("resonance") and 304 Hz ("out-of-phase") (subplot (a), (b) and (c) respectively). In each subplot, the location of the phonic crystal is given by the region shaded in magenta.

The first and foremost is observation to be made from the figures above is that, there is a drop of \tilde{v}'_y integral at the PC for $f = 298$ Hz while an increase is observed for $f = 304$ Hz. The behaviours are opposite when the phase differences are opposite. In fact, this shows that when the pressure and the vertical displacement are "in-phase" (i.e. positive pressure yields downwards vertical displacement, as in when $f = 298$ Hz), there is a stabilizing effect in \tilde{v}'_y . On the other hand, there is an destabilizing effect in \tilde{v}'_y when the PC's surface vertical displacements are "out-of-phase".

Another observation regards the behaviour near the resonance frequency ($f = 300.72$ Hz). Just like the previously studied quantities, there is a significant increase in the \tilde{v}'_y integral along a relatively large part of the domain. In particular, the increase in \tilde{v}'_y integral is more prominent downstream of the PC. However, again, just like the previous quantities, it can be observed that there is a sharp drop of \tilde{v}'_y integral at the PC, which is then followed by an increase further downstream.

Streamwise disturbance flow velocity

In addition to the wall-normal velocity, the streamwise disturbance velocity is also worth analyzing as it has been used to define stability in experimental simulations ([55] and [51], as mentioned in [19]). Furthermore, it was found that the magnitudes of the streamwise disturbance velocity was larger than its wall-normal counterpart. Hence, it contains more of the energy of the TS waves and so influencing this velocity component is desirable.

The streamwise variation of y-integrated amplitude of the streamwise velocity ($\int_0^H \tilde{v}'_x dy$) for $f = 298, 300.72$ and 304 Hz are given in figure 4.16.

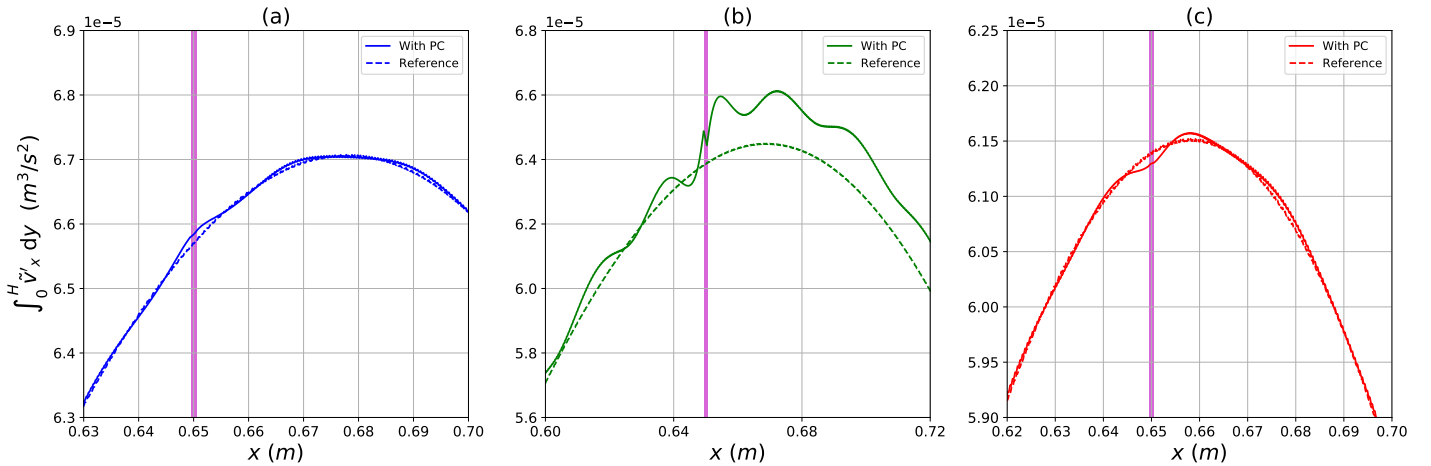


FIGURE 4.16: $\int_0^H \tilde{v}'_x dy$ vs x for $f = 298$ ("in-phase"), 300.72 ("resonance") and 304 Hz ("out-of-phase") (subplot (a), (b) and (c) respectively). In each subplot, the location of the phononic crystal is given by the region shaded in magenta.

The above figures show striking contrasts with respect to the wall-normal velocity. When the PC's vertical displacement is "in-phase" ($f = 298$ Hz), an increase in \tilde{v}'_x integral is observed at the PC. The opposite is true for the "out-of-phase" response i.e. an increase at the PC for $f =$

304 Hz. Hence, in fact, the out-of-phase response benefits stabilization when \tilde{v}'_x is used as the stability criterion.

The other contrasting result is the sharp increase of \tilde{v}'_x integral at resonance at the PC. Otherwise, the same significant increase can be observed elsewhere. Indeed, downstream of the PC, both \tilde{v}'_y and \tilde{v}'_x integrals become larger than the reference simulations.

Square of streamwise disturbance flow velocity

The y -integrated square of the amplitude of the streamwise disturbance flow velocity shall also be analyzed. This term also signifies the streamwise component of the kinetic energy.

The streamwise variation of y -integrated amplitude of the streamwise velocity ($\int_0^H (\tilde{v}'_x)^2 dy$) for $f = 298, 300.72$ and 304 Hz are given in figure 4.17.

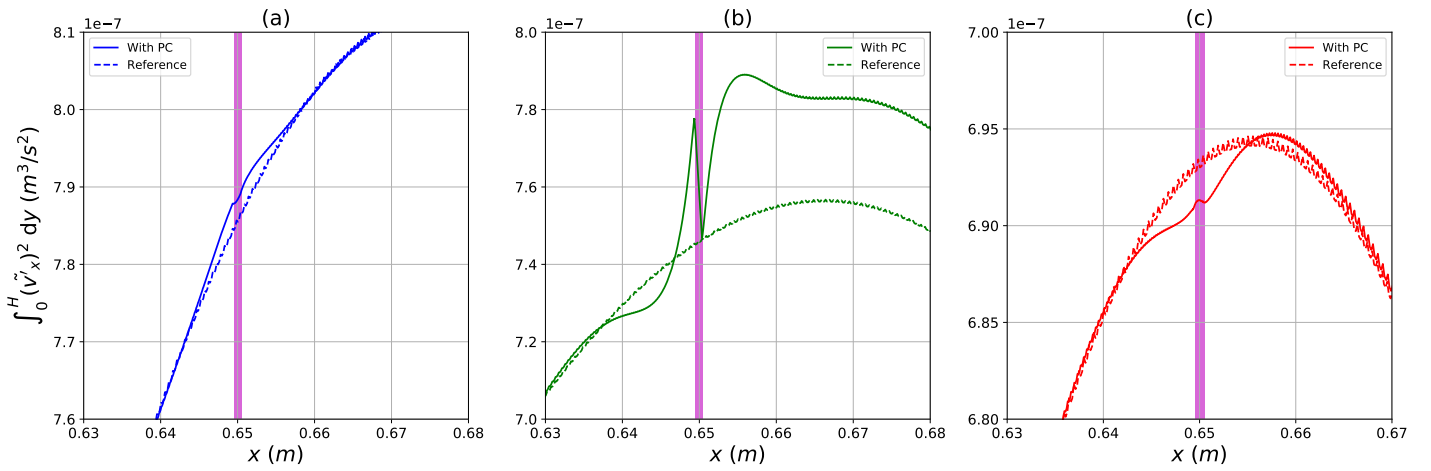


FIGURE 4.17: $\int_0^H (\tilde{v}'_x)^2 dy$ vs x $f = 298$ ("in-phase"), 300.72 ("resonance") and 304 Hz ("out-of-phase") (subplot (a), (b) and (c) respectively). In each subplot, the location of the phonic crystal is given by the region shaded in magenta.

It can be seen from the above figures that squaring the velocity results in vanishing oscillatory behaviours that can be seen in the analysis of \tilde{v}'_x integral far away from the PC. Furthermore, the $(\tilde{v}'_x)^2$ integral shows more-pronounced increase (for $f = 298$ Hz) and decrease (for $f = 304$ Hz) at the PC.

The behaviour of $(\tilde{v}'_x)^2$ integral is very similar to the behaviour of the kinetic energy integral (figure 4.14).

Additionally, when comparing with the kinetic energy integral, it can now be concluded that for the two frequencies away from the resonance, the influence around the PC (not at the PC) are dominated by the streamwise component while the influence at the PC is dominated by the wall-normal velocity component.

4.3.2.3 Summary and further remarks

In summary, overall and x -varying quantities were derived from the solutions of the frequency domain FSI numerical simulation. In the overall properties, it was observed that stabilization could not be obtained if the disturbance flow properties were integrated fully. None of the disturbance flow velocity component integrals were attenuated. However, it was shown that the streamwise component had a bigger relative and absolute change with respect to the simulation without PC. Furthermore, the maximum influence of the PC was observed for frequency near the peak of the vertical displacement amplitude.

The magnitude of the horizontal displacement of the phononic crystal was five orders of magnitudes smaller than the vertical displacement, and hence it was concluded that the horizontal displacement played negligible influence. This meant that the pressure was a major contributor to the stress in the structure, while the shear stresses were insignificant. Additionally, the vertical displacement was found to have a damped resonance behaviour, as shown by the smooth jump of phase around the maximum amplitude. The resonant behaviour was as expected, in the sense that "in-phase" response was observed below the resonance and "out-of-phase" response above.

Having verified the nature of the response of the PC to the TS waves and the frequencies of interest, x -varying quantities were investigated at three distinct frequencies: one for the "in-phase", another near resonance and the final one in the "out-of-phase" regime. The kinetic energy and streamwise velocity amplitude integrals showed attenuations in the vicinity of the PC for the "out-of-phase" response. As for the "in-phase" response, these x -varying quantities were increased. However, the opposite behaviour was found for the wall-normal velocity amplitude integral.

Around the resonance, major increases were found in the flow variables, in particular downstream the PC. Attenuation exists upstream the PC, however, it was negligible compared to the increase.

With this, it can be concluded that stabilization can occur to a certain extent in the case of "out-of-phase" response.

It is also interesting to see the variation of stabilization with frequency. This is because although the "out-of-phase" response is desirable, a large amplitude response ensures a larger influence in the flow (as derived from the discussion of the overall quantities). However, the largest amplitude response does not yield the best phase response. Hence, there is a trade-off, where it is thought there is an optimum frequency for a balance between amplitude and phase responses.

An attempt at finding this optimum frequency is given by the plot showing the maximum decrease (shown by "minimum increase") of the kinetic energy integral as a function of Ts wave frequency (figure 4.18).

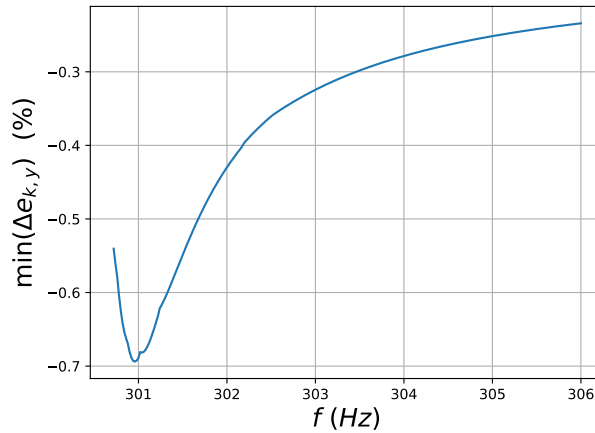


FIGURE 4.18: Variation of the maximum decrease of the kinetic energy integral as a function of frequency

The above plot is given for frequencies above the resonance. It can be seen that as the frequency increases, this decrease increases and peaks at $f = 300.96$ Hz. However, it was also found that the behaviour at this peak is similar to the resonance behaviour, with severe increases downstream the PC (figure 4.14).

Hence, in addition to observing the plot of maximum decrease in kinetic energy, it is also necessary to consult with the plot of maximum increase in kinetic energy. This is given in figure 4.19.

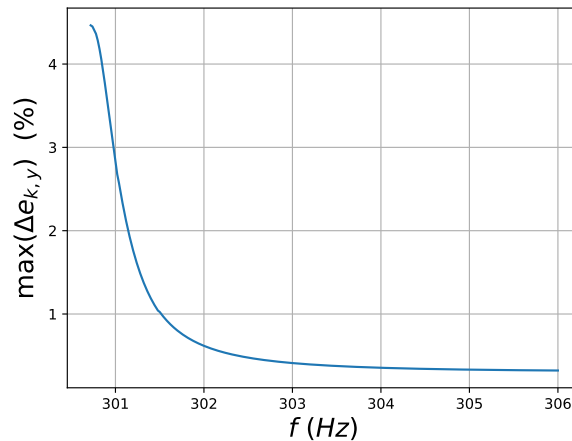


FIGURE 4.19: Variation of the maximum increase of the kinetic energy integral as a function of frequency

Nevertheless, once this peak is passed (or valley as given in figure 4.18), there is a continuous decrease in the stabilization of the kinetic energy. This is as expected, since the phase response cannot get better than "out-of-phase" (or by the convention, $\Delta\phi_{u_y} = 0$) while the amplitude continuously decreases as the frequency becomes further from the resonance.

Another interesting performance was derived from the simulation of multiple identical phononic crystals. It was found that stabilization can be further enhanced by placing multiple identical phononic crystals in the streamwise direction. An example of this enhancement is shown by the plot of the kinetic energy integral for five PCs given in figure 4.20 for $f = 304$ Hz.

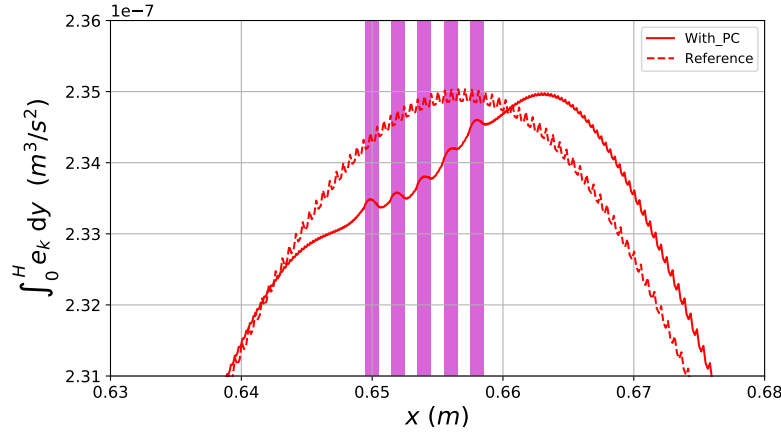


FIGURE 4.20: $\int_0^H \tilde{v}'_y dy$ vs x for $f = 304$ Hz with five identical PCs

In the above plot, the maximum decrease in the kinetic energy is found to be approximately 0.554 % at $x \approx 0.653$ m. Furthermore, it can be seen that the downstream increase in the kinetic energy can be shifted by placing phononic crystals. Ultimately, if the whole flat plate's surface is covered with PC structures, it may be possible to completely eliminate the increase in the kinetic energy.

This ends the presentation of the results of the frequency domain FSI simulation. In the next chapter, the research questions are going to be answered more explicitly, along with the conclusions derived from the whole thesis report and recommendations for improvements.

Chapter 5

Conclusions and Recommendations

This chapter is divided into two sections. In section 5.1, the conclusions of this thesis report shall be given. The tasks performed in this thesis project shall be summarised and the research questions are to be clearly answered. In section 5.2, recommendations for improvements of the current study shall be outlined.

5.1 Conclusions

This thesis project was motivated by the need to reduce drag over an aircraft. One way is to maintain laminar flow throughout aircraft body parts (for instance, a wing). In order to achieve this, the mechanism for laminar-turbulent transition had to be understood. A number of mechanisms can be identified. The one dealt in this thesis project was the growth of small disturbances in the form of a wave, also known as Tollmien-Schlichting waves. This "wave" is not the same as classical waves (such as acoustic or electromagnetic waves), because of the differing form governing equations. The physical implication of the model describing TS waves is that the wave is being convected with the flow, whereas in classical waves convection is not necessary in order for the wave to propagate.

With this in mind, there is a newly emerging class of materials called "metamaterials", which have been used traditionally to alter the properties of classical waves. This thesis aims at investigating whether or not these metamaterials can be used to alter the properties of TS waves, with the desire to attenuate TS waves in order to maintain laminar flow. In order to set this project focused, research questions were formulated.

Several acoustic metamaterials were investigated in the literature study (chapter 2), namely the Helmholtz resonators, membrane and phononic crystals. The working principles of these metamaterial were identified. On the basis of the metamaterial's likelihood in successfully achieving stabilization of TS waves, the phononic crystal was chosen to be further studied.

The choice of the type of study was a two-dimensional numerical simulation. In order to design this numerical simulation, one had to find the conditions for which the flow became unstable. A linear stability analysis was performed in which the Orr-Sommerfeld equation was solved

numerically. This led to the choice of the freestream velocity, the unstable TS wave frequencies and wavenumber. The properties of the TS waves were then used to design the phononic crystal constituents and dimensions in order to ensure that the working range of the phononic crystal lies within the unstable TS wave frequency range. The phononic crystal design procedure employed relatively simple analysis, where analytical equations were derived.

Having chosen the flow conditions and designed the phononic crystal, numerical analysis was performed using COMSOL®. Three types of simulation was performed: namely the structural analysis, steady-state FSI and frequency domain FSI. The first analysis was performed in order to verify and finalize the design of the phononic crystal. The second analysis was used to enable the third. The research questions can be answered using the data derived from the third simulation. The word "metamaterial" in the research question shall now be replaced with "phononic crystal", as this was the metamaterial chosen to be studied in detail. The answers are the focus of the following paragraphs.

Main RQ: Can TS waves in a laminar boundary layer flow be attenuated using a phononic crystal?

When the disturbance field (i.e. its kinetic energy or velocity components) is integrated over the fluid domain, the phononic crystal destabilizes the basic flow. This was shown in the analysis of the "overall" quantities. However, when looking at the spatial variation of the disturbance field, there is a region in which the flow is stabilized i.e. reduction in the kinetic energy or the velocity disturbance component. This region is found to be in the vicinity of the phononic crystal. Destabilization occurs further downstream. Hence, to a certain extent, the boundary layer can be stabilized with the phononic crystal.

Sub-RQ 1: What are the changes imparted on the TS waves when approaching the phononic crystal?

This answer is dealt using the results of the x -varying quantities. Depending on the frequencies and the disturbance physical quantities being considered, stabilization (decreases) and destabilization (increases) can occur. The frequencies were categorized into three regions, namely the "in-phase", "near resonance" and "out-of-phase" frequencies. The phase was by the difference between the phase of the pressure fluctuation and PC's surface vertical displacement. In the case of the "in-phase" frequency, the wall-normal velocity disturbance amplitude decreases. Simultaneously, the streamwise velocity disturbance increases. The effect on the streamwise disturbance was found to be larger than that of its wall-normal counterpart. Consequently, an increase of the kinetic energy was found in the vicinity of the PC. The opposite behaviour was found in the case of the "out-of-phase" frequency. As for the "near resonance" frequency, severe increases in all the disturbance flow velocity can be found slightly upstream and downstream the PC.

Sub-RQ 2: What is the physical mechanism that drives the attenuation of the TS waves (if any attenuation takes place)?

The range of frequencies simulated in the frequency domain FSI simulation covered the frequency range in the predicted band gap of the PC's unit cell. However, it was found that the band gap did not play a direct role in the behaviour of the response of the phononic crystal. Rather, a damped resonance behaviour was found. This is because destabilization can occur within the band gap itself, for the frequencies below resonance. Hence, the mechanism that the phononic crystal uses in order to attenuate TS waves is the resonance. Consequently, any resonating structure could also replace the phononic crystal.

This resonance response was found for the vertical displacement of the phononic crystal. The horizontal displacement was found to be five orders of magnitudes smaller than the vertical displacement, and hence can be concluded to have played negligible effect on influencing the TS waves.

The stabilization of the TS wave can occur within the "out-of-phase" response of the resonance behaviour. A suggestion for how the "out-of-phase" response stabilizes the phononic crystal is given as follows. The interaction between the disturbance flow and the phononic crystal is compared to a forced spring system, where the flow represents the driving force and the structure represents the spring. Under the normal case ("in-phase" behaviour), the flow drives the vibration of the spring by transfer of energy (or performing work). However, in the "out-of-phase" case, it is suggested that the driver-driven role of the fluid-structure case is swapped. That is, the structure transfers energy into the flow. As a direct consequence, the amplitude wall-normal disturbance flow component is increased.

In turn, the streamwise disturbance flow decreases. This can be understood mathematically from the conservation of mass of the disturbance flow, given by equation 2.5a. This equation can also be interpreted as follows (by divergence theorem): the net flux of the disturbance flow velocity has to equal zero. This means that due to the increase in the wall-normal velocity flux, the streamwise velocity flux has to decrease.

An analogy for this phenomenon suggested. The wall-normal velocity is thought to be an "obstacle", where due to its increase, the streamwise component has to decrease in order for the flow to pass (much like how a person has to decrease its ground velocity in order to climb a vertical obstacle or that a car should decrease its speed when encountering a speed bump).

Sub-RQ 3: How large is the attenuation (if any)? What is the sensitivity of the attenuation with respect to the TS wave's characteristics?

From the plots of the derived physical quantities, it is clear that the attenuations attained by the phononic crystal are very small. Furthermore, it was indeed found that the attenuation depends on the frequency of the TS wave (figure 4.18, the figure also gives the magnitude of the decrease numerically). This can be explained by the variation of the vertical amplitude and phase response of the phononic crystal as functions of frequency. It was found that, for frequencies sufficiently away from the resonance, there is a continuous decrease in stabilization (which correlates with the decrease in amplitude of the vertical displacement). Finally, it is remarked that the role of the material constituents and the dimensions of the phononic crystal are embedded within its frequency response. Hence, the design of the phononic crystal can be used to optimize the response at certain frequencies.

These conclusions derived from answering the research questions were formulated using data derived from the numerical simulations. It is clear that numerical simulations had limitations. Therefore, in the next section, recommendations in order to improve the study of stabilization of TS waves with metamaterials shall be outlined.

5.2 Recommendations

This section gives the recommendations that can be used to improve the study. These are outlined in the following list:

- **Perform an experimental study.** Numerous benefits can be derived from such a study such as: validation of the current numerical simulation, looking at the effect of the boundary conditions of the structure on the working frequency range and understanding the effect and the lifetime of the transients.
- **Perform a time-dependent simulation.** This study provides an alternative to the experimental study in order to see the time for the transient to disappear and its effects.
- **Include non-linear terms in the numerical model.** This study can be used to verify the assumption that the non-linear terms in the disturbance flow equations stay negligible when there is influence from the phononic crystal.
- **Introduce a wavepacket rather than single frequency disturbances.** Such a study can be used to understand if the response of the single frequency simulation can be used to predict the response to simultaneous multiple frequency excitations.
- **Study the performance of the phononic crystal for TS waves at oblique angles.** This study is aimed at investigating the directionality of the phononic crystals. Furthermore, this study may extend the application of the phononic crystal to stabilizing cross-flow instabilities.
- **Choose a different phononic crystal design.** For instance, one may think of higher dimensional phononic crystals in order to directly affect the streamwise disturbance flow velocity. Another option is to choose a one-dimensional phononic crystal with solid-fluid constituents, to see if the PC's response can be further improved in affecting the flow.
- **Study the effect of wall curvature and pressure gradient.** In this report, the study was on a flat plate. It is important to also study the response of the phononic crystal when curvature of the surface cannot be avoided, which is the case for real airfoils. Such studies would also give insights to the effect of pressure gradients.

Appendix A

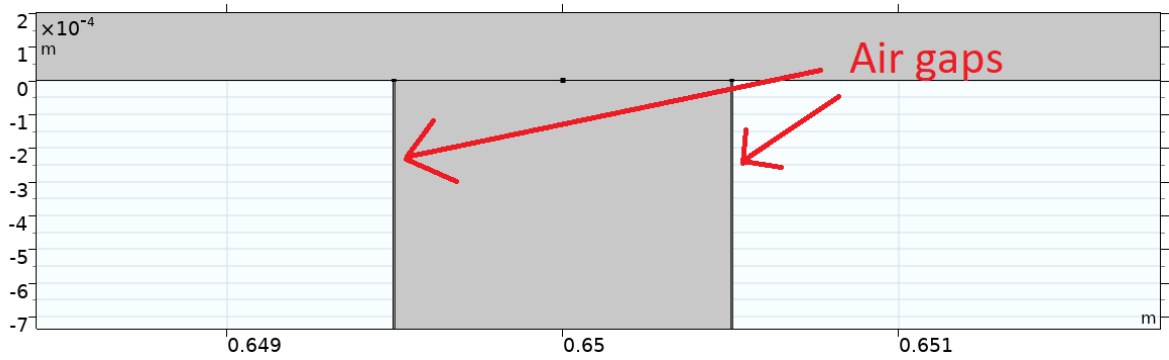


FIGURE A.1: Narrow air gaps used to allow for displacements at the top corners of the PC in the frequency domain FSI simulation. The widths are $5 \mu\text{m}$.

Appendix B

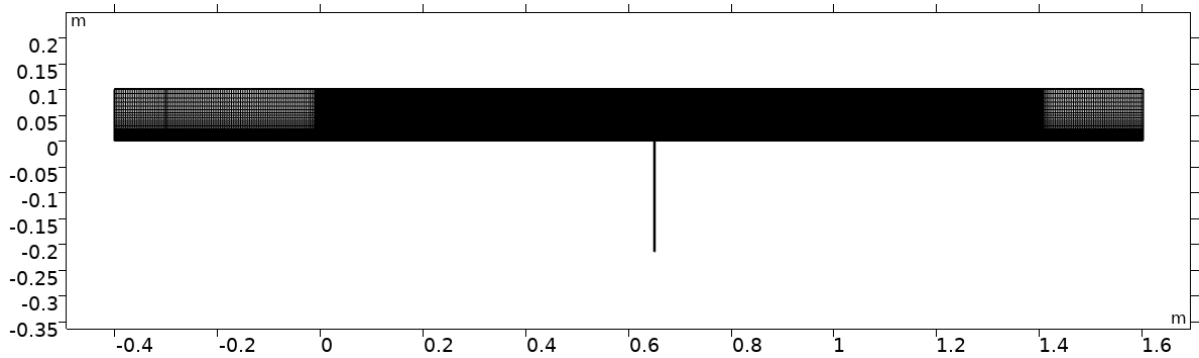


FIGURE B.1: Zoomed-out view of the mesh used to perform the steady-state and frequency domain FSI simulations

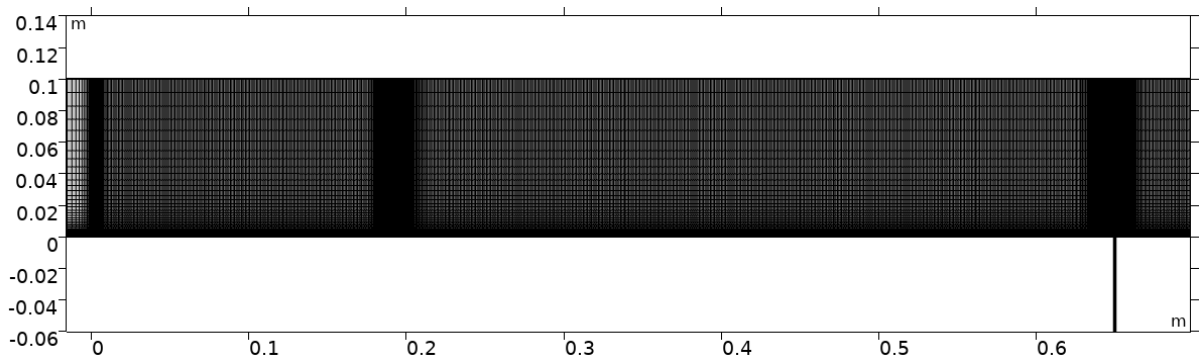


FIGURE B.2: Zoomed-in view of the mesh used to perform the steady-state and frequency domain FSI simulations. The focus is on the refinement around the leading edge ($x = 0$ m), forcing domain ($x \approx 0.185$ m) and the phononic crystal region ($x \approx 0.65$ m).

Appendix C

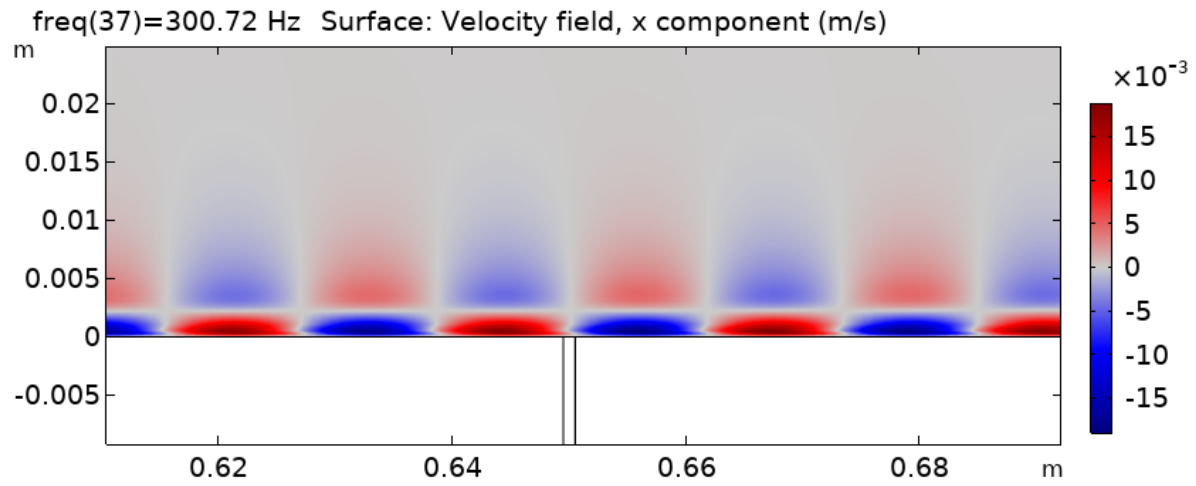


FIGURE C.1: An example of the contour plot of $\tilde{v}'_x e^{i\phi_{v'_x}}$.

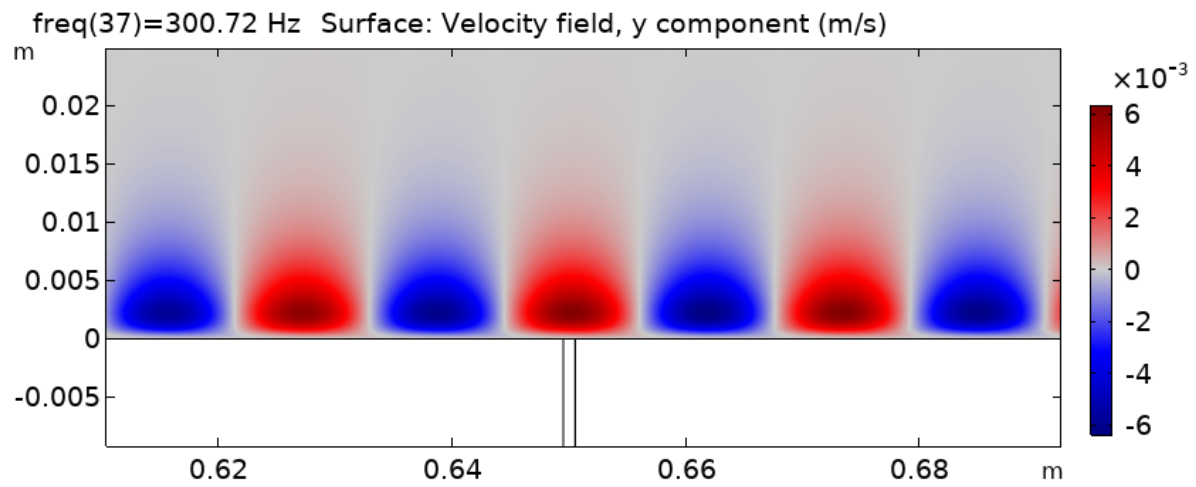


FIGURE C.2: An example of the contour plot of $\tilde{v}'_y e^{i\phi_{v'_y}}$.

Appendix D

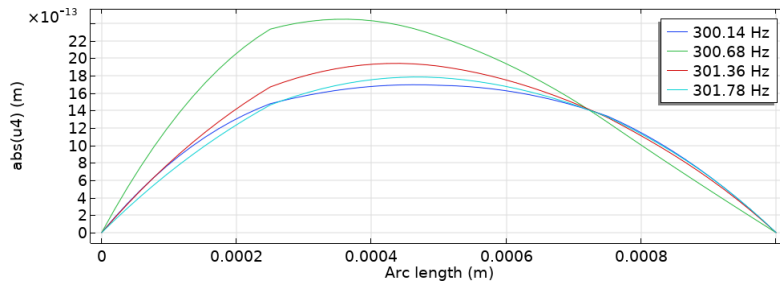


FIGURE D.1: Examples of distribution of \tilde{u}_x along the top boundary of the phononic crystal. In the plot, "abs(u4)" refers to \tilde{u}_x .

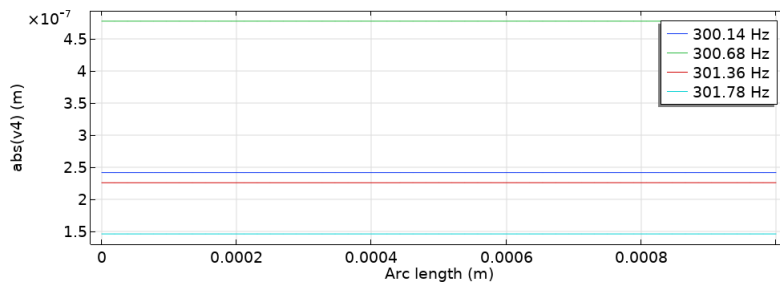


FIGURE D.2: Examples of distribution of \tilde{u}_y along the top boundary of the phononic crystal. In the plot, "abs(v4)" refers to \tilde{u}_y .

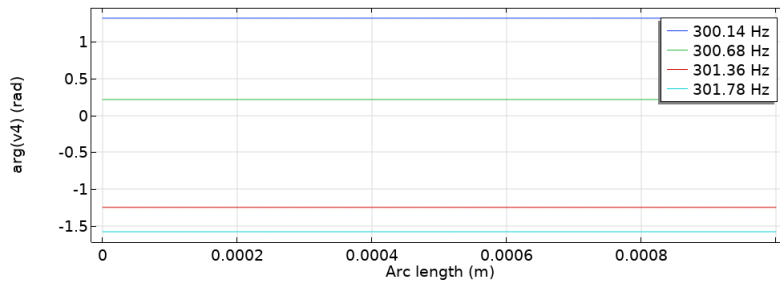


FIGURE D.3: Examples of distribution of ϕ_{u_y} along the top boundary of the phononic crystal. In the plot, "arg(v4)" refers to ϕ_{u_y} .

Appendix E

This appendix documents the mesh convergence study of the steady-state and frequency domain FSI simulations. The structural analysis simulation is omitted as its numerical solution is deemed to be sufficiently converged, as suggested by the predicted surface mode eigenfrequency.

The method is explained as follows. Three different mesh refinement levels were used, referred to as "Coarse", "Medium" and "Fine" levels. Convergence is accepted when there is a "small" deviation between the mesh levels. It should also be noted that the mesh refinement levels had to be compensated with the available memory.

In the two FSI simulations, the mesh elements are defined to be inversely proportional to a certain number denoted as N_{mesh} . The mesh sizes are thus represented as follows: $\Delta x, \Delta y \tilde{1}/N_{\text{mesh}}$. A larger value of N_{mesh} yields finer mesh. The specifications of the mesh refinement levels for the two FSI simulations are given in table E.2.

Mesh refinement level	N_{mesh}	Number of elements
Coarse	0.70	118895
Medium	0.80	144455
Fine	0.85	153994

TABLE E.2: Mesh refinement level specifications for the steady-state and frequency domain FSI simulations.

The simulations were performed. For the steady-state simulation, the velocity profiles are deemed to be the best representation of the numerical simulations. Plots of V_x and V_y against y for the different mesh levels are plotted in figure E.3 and E.4. Each figure contains two sub-figures corresponding to different x -locations: near the leading edge (subfigures (a), taken as $x = 2 \times 10^{-4} \text{m}$) and at the PC (subfigures (b), taken as $x = 0.65 \text{ m}$).

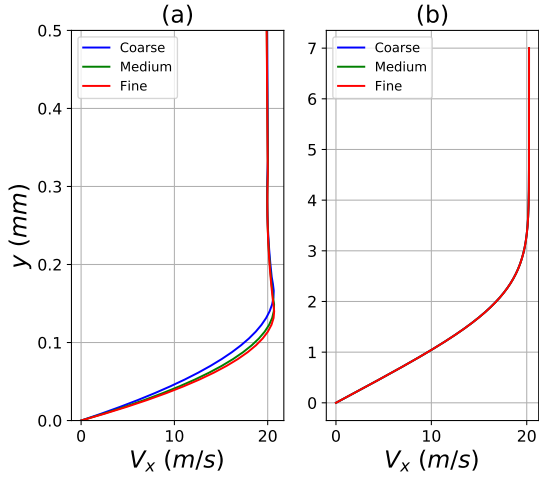


FIGURE E.3: Profiles of V_x for $x = 2 \times 10^{-4}$ m (subfigure (a)) and $x = 0.65$ m (subfigure (b)) for the different mesh refinement levels.

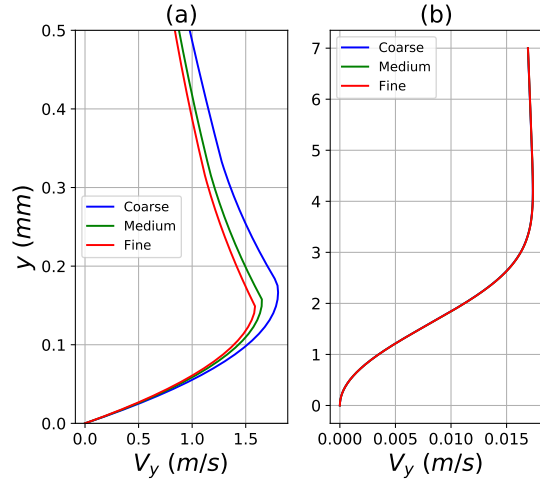


FIGURE E.4: Profiles of V_y for $x = 2 \times 10^{-4}$ m (subfigure (a)) and $x = 0.65$ m (subfigure (b)) for the different mesh refinement levels.

For the station $x = 0.65$ m, it can be seen that there are no significant changes to the velocity profiles. As for the V_x profile near the leading edge, small deviations in the Coarse level can be seen. The largest difference between the Coarse and the Fine levels is approximately 10.3%, occurring at $y \approx 0.0788$ mm. Nevertheless, it can be seen that the profiles for the Medium and the Fine levels effectively overlap.

In the case of the V_y profile, a larger discrepancy can be seen. The largest discrepancy between the Coarse and the Fine levels is 20.8% at $y \approx 0.184$ mm. This maximum discrepancy reduces to 6.12% (at $y \approx 0.158$ mm) when comparing the Medium and the Fine mesh levels. For this thesis, the discrepancies between the Medium and the Fine levels are deemed to be small enough to consider the solutions of the Fine mesh to have converged.

In the frequency domain FSI simulation, the plots of the velocity fluctuation profiles at the PC ($x = 0.65$ m) are deemed to be the representative variable of the numerical solution. The real part of the velocity fluctuations are given in figure E.5 and E.5 for the different mesh levels at three different frequencies: 298, 300.72 and 304 Hz, where each frequency represents in-phase, resonance and out-of-phase response respectively (see section 4.3).

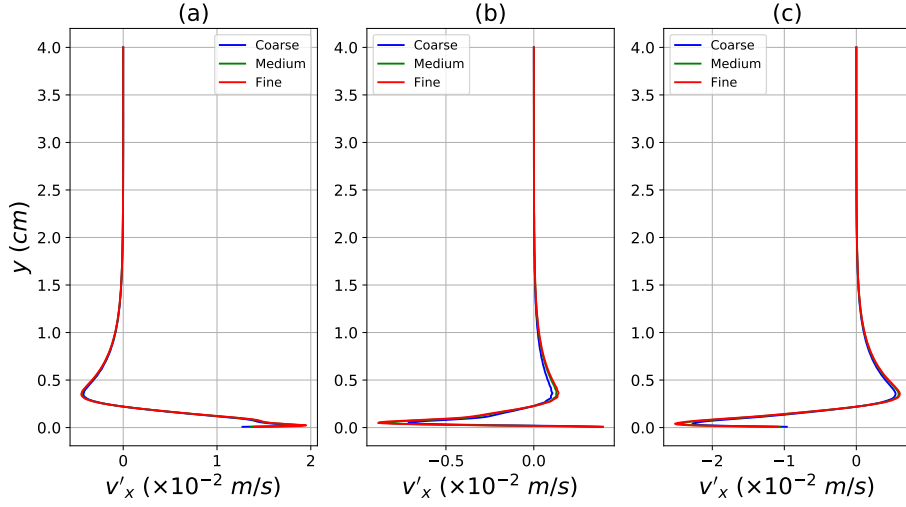


FIGURE E.5: Plots of v'_x profile for the different mesh levels at $f = 298$ (a), 300.72 (b) and 304 (c) Hz.

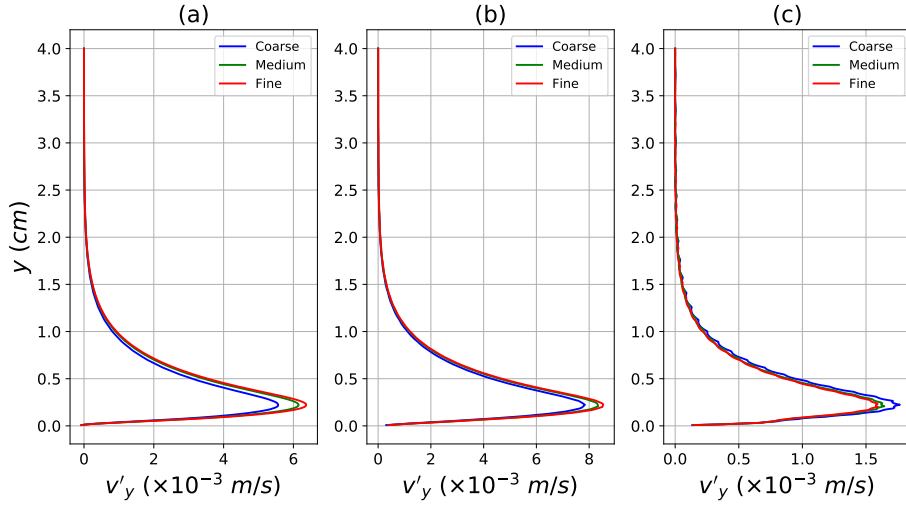


FIGURE E.5: Plots of v'_y profile for the different mesh levels at $f = 298$ (a), 300.72 (b) and 304 (c) Hz.

From figure E.5, it can be seen that small deviations exist primarily for the Coarse mesh level at $f = 300.72$ and 304 Hz. Otherwise, the plots of v'_x are effectively overlapping.

As for the v'_y profiles, there are relatively larger discrepancies between the Coarse and the Fine levels and smaller discrepancies between the Medium and Fine levels. In all of these cases, the largest discrepancies occur around the y -location of maximum v'_y ($y \approx 0.2$ cm). The maximum magnitude of relative discrepancies between the Medium and the Fine levels are approximately 3.46, 2.55 and 3.94 % for $f = 298$, 300.72 and 304 Hz respectively. Again, these discrepancies are deemed to be small enough to consider the solution of the Fine mesh refinement level to have sufficiently converged.

Bibliography

- [1] J. D. Anderson Jr. *Fundamentals of aerodynamics*. Tata McGraw-Hill Education, 2010.
- [2] L. Y. L. Ang, Y. K. Koh, and H. P. Lee. Broadband sound transmission loss of a large-scale membrane-type acoustic metamaterial for low-frequency noise control. *Applied Physics Letters*, 111(4):041903, 2017.
- [3] H. Blasius. The boundary layers in fluids with little friction. 1950.
- [4] G. S. Brennan, J. S. Gajjar, and R. E. Hewitt. Cancellation of tollmien–schlichting waves with surface heating. *Journal of Engineering Mathematics*, 128(1):1–23, 2021.
- [5] R. Camley, B. Djafari-Rouhani, L. Dobrzynski, and A. Maradudin. Transverse elastic waves in periodically layered infinite and semi-infinite media. *Physical Review B*, 27(12):7318, 1983.
- [6] COMSOL Multiphysics® v. 5.6. www.comsol.com. COMSOL AB, Stockholm, Sweden.
- [7] G. Correale, T. Michelis, D. Ragni, M. Kotsonis, and F. Scarano. Nanosecond-pulsed plasma actuation in quiescent air and laminar boundary layer. *Journal of Physics D: Applied Physics*, 47(10):105201, 2014.
- [8] C. Davies and P. W. Carpenter. Numerical simulation of the evolution of tollmien–schlichting waves over finite compliant panels. *Journal of Fluid Mechanics*, 335:361–392, 1997.
- [9] F. M. De Espinosa, E. Jimenez, and M. Torres. Ultrasonic band gap in a periodic two-dimensional composite. *Physical Review Letters*, 80(6):1208, 1998.
- [10] P. A. Deymier. *Acoustic metamaterials and phononic crystals*, volume 173. Springer Science & Business Media, 2013.
- [11] B. Djafari-Rouhani, L. Dobrzynski, O. H. Duparc, R. Camley, and A. Maradudin. Sagittal elastic waves in infinite and semi-infinite superlattices. *Physical Review B*, 28(4):1711, 1983.
- [12] L. Dobrzynski and H. Puzzkarski. Eigenvectors of composite systems. i. general theory. *Journal of Physics: Condensed Matter*, 1(7):1239, 1989.
- [13] E. El Boudouti, B. Djafari-Rouhani, A. Akjouj, and L. Dobrzynski. Acoustic waves in solid and fluid layered materials. *Surface Science Reports*, 64(11):471–594, 2009.
- [14] R. Esquivel-Sirvent and G. Coccoletzi. Band structure for the propagation of elastic waves in superlattices. *The Journal of the Acoustical Society of America*, 95(1):86–90, 1994.

- [15] N. Fang, D. Xi, J. Xu, M. Ambati, W. Srituravanich, C. Sun, and X. Zhang. Ultrasonic metamaterials with negative modulus. *Nature materials*, 5(6):452–456, 2006.
- [16] J. Fey and W. M. Robertson. Compact acoustic bandgap material based on a subwavelength collection of detuned helmholtz resonators. *Journal of Applied Physics*, 109(11):114903, 2011.
- [17] G. Floquet. Sur les équations différentielles linéaires à coefficients périodiques. In *Annales scientifiques de l'École normale supérieure*, volume 12, pages 47–88, 1883.
- [18] J. Gao, X.-Y. Zou, J.-C. Cheng, and B. Li. Band gaps of lower-order lamb wave in thin plate with one-dimensional phononic crystal layer: Effect of substrate. *Applied Physics Letters*, 92(2):023510, 2008.
- [19] M. Gaster. On the effects of boundary-layer growth on flow stability. *Journal of Fluid Mechanics*, 66(3):465–480, 1974.
- [20] C. J. Gedney. The cancellation of a sound-excited tollmien–schlichting wave with plate vibration. *The Physics of Fluids*, 26(5):1158–1160, 1983.
- [21] B. Graczykowski, F. Alzina, J. Gomis-Bresco, and C. Sotomayor Torres. Finite element analysis of true and pseudo surface acoustic waves in one-dimensional phononic crystals. *Journal of Applied Physics*, 119(2):025308, 2016.
- [22] B. Graczykowski, M. Sledzinska, N. Kehagias, F. Alzina, J. S. Reparaz, and C. M. Sotomayor Torres. Hypersonic phonon propagation in one-dimensional surface phononic crystal. *Applied Physics Letters*, 104(12):123108, 2014.
- [23] S. Grundmann and C. Tropea. Active cancellation of artificially introduced tollmien–schlichting waves using plasma actuators. *Experiments in Fluids*, 44(5):795–806, 2008.
- [24] D. Guan, J. H. Wu, L. Jing, N. Gao, and M. Hou. Application of a helmholtz structure for low frequency noise reduction. *Noise Control Engineering Journal*, 63(1):20–35, 2015.
- [25] N. A. Haskell. The dispersion of surface waves on multilayered media. *Bulletin of the seismological Society of America*, 43(1):17–34, 1953.
- [26] J. Healey. On the neutral curve of the flat-plate boundary layer: comparison between experiment, orr–sommerfeld theory and asymptotic theory. *Journal of Fluid Mechanics*, 288:59–73, 1995.
- [27] T. Herbert. Parabolized stability equations. *Annual Review of Fluid Mechanics*, 29(1):245–283, 1997.
- [28] A.-C. Hladky-Hennion and M. d. Billy. Experimental validation of band gaps and localization in a one-dimensional diatomic phononic crystal. *The Journal of the Acoustical Society of America*, 122(5):2594–2600, 2007.
- [29] Z. Hou and B. M. Assouar. Numerical investigation of the propagation of elastic wave modes in a one-dimensional phononic crystal plate coated on a uniform substrate. *Journal of Physics D: Applied Physics*, 42(8):085103, 2009.

- [30] M. I. Hussein, S. Biringen, O. R. Bilal, and A. Kucala. Flow stabilization by subsurface phonons. *Proceedings of the Royal Society A: Mathematical, Physical and Engineering Sciences*, 471(2177):20140928, 2015.
- [31] M. I. Hussein, G. M. Hulbert, and R. A. Scott. Dispersive elastodynamics of 1d banded materials and structures: analysis. *Journal of sound and vibration*, 289(4-5):779–806, 2006.
- [32] S. John. Strong localization of photons in certain disordered dielectric superlattices. *Physical review letters*, 58(23):2486, 1987.
- [33] R. Joslin, C. Streett, and C.-L. Chang. Spatial direct numerical simulation of boundary-layer transition mechanisms: Validation of pse theory. *Theoretical and Computational Fluid Dynamics*, 4(6):271–288, 1993.
- [34] Y. S. Kachanov. Physical mechanisms of laminar-boundary-layer transition. *Annual review of fluid mechanics*, 26(1):411–482, 1994.
- [35] L. E. Kinsler, A. R. Frey, A. B. Coppens, and J. V. Sanders. *Fundamentals of acoustics*. John wiley & sons, 2000.
- [36] M. Kotsonis, R. Giepmans, S. Hulshoff, and L. Veldhuis. Numerical study of the control of tollmien–schlichting waves using plasma actuators. *AIAA journal*, 51(10):2353–2364, 2013.
- [37] M. S. Kushwaha, P. Halevi, L. Dobrzynski, and B. Djafari-Rouhani. Acoustic band structure of periodic elastic composites. *Physical review letters*, 71(13):2022, 1993.
- [38] M. S. Kushwaha, P. Halevi, G. Martinez, L. Dobrzynski, and B. Djafari-Rouhani. Theory of acoustic band structure of periodic elastic composites. *Physical Review B*, 49(4):2313, 1994.
- [39] B. Liu and L. Yang. Transmission of low-frequency acoustic waves in seawater piping systems with periodical and adjustable helmholtz resonator. *Journal of Marine Science and Engineering*, 5(4):56, 2017.
- [40] M. J. Lowe. Matrix techniques for modeling ultrasonic waves in multilayered media. *IEEE transactions on ultrasonics, ferroelectrics, and frequency control*, 42(4):525–542, 1995.
- [41] J.-H. Lu, C.-C. Kuo, F.-L. Hsiao, and C.-C. Chen. Acoustic filter based on helmholtz resonator array. *Applied Physics Letters*, 101(5):051907, 2012.
- [42] G. Ma and P. Sheng. Acoustic metamaterials: From local resonances to broad horizons. *Science advances*, 2(2):e1501595, 2016.
- [43] J. Mei, G. Ma, M. Yang, Z. Yang, W. Wen, and P. Sheng. Dark acoustic metamaterials as super absorbers for low-frequency sound. *Nature communications*, 3(1):1–7, 2012.
- [44] R. W. Milling. Tollmien–schlichting wave cancellation. *The Physics of Fluids*, 24(5):979–981, 1981.
- [45] M. V. Morkovin. Critical evaluation of transition from laminar to turbulent shear layers with emphasis on hypersonically traveling bodies. Technical report, MARTIN MARIETTA CORP BALTIMORE MD RESEARCH INST FOR ADVANCED STUDIES, 1969.

- [46] C. J. Naify, C.-M. Chang, G. McKnight, and S. Nutt. Transmission loss and dynamic response of membrane-type locally resonant acoustic metamaterials. *Journal of Applied Physics*, 108(11):114905, 2010.
- [47] W. M. Orr. The stability or instability of the steady motions of a perfect liquid and of a viscous liquid. part ii: A viscous liquid. In *Proceedings of the Royal Irish Academy. Section A: Mathematical and Physical Sciences*, volume 27, pages 69–138. JSTOR, 1907.
- [48] H. L. Reed, W. S. Saric, and D. Arnal. Linear stability theory applied to boundary layers. *Annual review of fluid mechanics*, 28(1):389–428, 1996.
- [49] G. A. Reynolds and W. Saric. Experiments on the stability of the flat-plate boundary layer with suction. *AIAA journal*, 24(2):202–207, 1986.
- [50] O. Reynolds. Xxix. an experimental investigation of the circumstances which determine whether the motion of water shall be direct or sinuous, and of the law of resistance in parallel channels. *Philosophical Transactions of the Royal society of London*, (174):935–982, 1883.
- [51] J. Ross, F. Barnes, J. Burns, and M. Ross. The flat plate boundary layer. part 3. comparison of theory with experiment. *journal of fluid mechanics*, 43(4):819–832, 1970.
- [52] J. Sapriel and B. D. Rouhani. Vibrations in superlattices. *Surface science reports*, 10(4-5):189–275, 1989.
- [53] W. S. Saric and A. H. Nayfeh. Nonparallel stability of boundary-layer flows. *The physics of Fluids*, 18(8):945–950, 1975.
- [54] H. Schlichting. *Boundary-layer theory*. McGraw-Hill, 1979.
- [55] G. B. Schubauer and H. K. Skramstad. Laminar boundary-layer oscillations and transition on. *Journal of research of the National Bureau of Standards*, 38:251, 1947.
- [56] F. T. Smith. On the non-parallel flow stability of the blasius boundary layer. *Proceedings of the Royal Society of London. A. Mathematical and Physical Sciences*, 366(1724):91–109, 1979.
- [57] A. Sommerfeld. *Ein beitrage zur hydrodynamischen erklarung der turbulenten fluessigkeitsbewegungen*. 1909.
- [58] D. Sotiropoulos. Dispersion of elastic waves in periodically inhomogeneous media. *Computational mechanics*, 12(3):134–146, 1993.
- [59] N. Sugimoto and T. Horioka. Dispersion characteristics of sound waves in a tunnel with an array of helmholtz resonators. *The Journal of the Acoustical Society of America*, 97(3):1446–1459, 1995.
- [60] B. Sylla, L. Dobrzynski, and H. Puzkarski. Eigenvectors of composite systems. ii. phonon eigenvectors in some layered materials. *Journal of Physics: Condensed Matter*, 1(7):1247, 1989.
- [61] W. T. Thomson. Transmission of elastic waves through a stratified solid medium. *Journal of applied Physics*, 21(2):89–93, 1950.

-
- [62] J. Van Ingen. A suggested semi-empirical method for the calculation of the boundary layer transition region. *Technische Hogeschool Delft, Vliegtuigbouwkunde, Rapport VTH-74*, 1956.
- [63] I. A. Veres and T. Berer. Complexity of band structures: Semi-analytical finite element analysis of one-dimensional surface phononic crystals. *Physical Review B*, 86(10):104304, 2012.
- [64] S. Walther, C. Airiau, and A. Bottaro. Optimal control of tollmien-schlichting waves in a developing boundary layer. *Physics of Fluids*, 13(7):2087–2096, 2001.
- [65] G. Wang, D. Yu, J. Wen, Y. Liu, and X. Wen. One-dimensional phononic crystals with locally resonant structures. *Physics Letters A*, 327(5-6):512–521, 2004.
- [66] Z. G. Wang, S. H. Lee, C. K. Kim, C. M. Park, K. Nahm, and S. Nikitov. Acoustic wave propagation in one-dimensional phononic crystals containing helmholtz resonators. *Journal of Applied Physics*, 103(6):064907, 2008.
- [67] F. M. White and I. Corfield. *Viscous fluid flow*, volume 3. McGraw-Hill New York, 2006.
- [68] Z. Xue-Feng, L. Sheng-Chun, X. Tao, W. Tie-Hai, and C. Jian-Chun. Investigation of a silicon-based one-dimensional phononic crystal plate via the super-cell plane wave expansion method. *Chinese Physics B*, 19(4):044301, 2010.
- [69] Z. Yang, H. Dai, N. Chan, G. Ma, and P. Sheng. Acoustic metamaterial panels for sound attenuation in the 50–1000 hz regime. *Applied Physics Letters*, 96(4):041906, 2010.
- [70] Z. Yang, J. Mei, M. Yang, N. Chan, and P. Sheng. Membrane-type acoustic metamaterial with negative dynamic mass. *Physical review letters*, 101(20):204301, 2008.